Synthesis and Development of a Series of Peptide Based Zwitterionic Cross-Linkers

A Dissertation

Presented in Partial Fulfillment of the Requirements for the

Degree of Doctor of Philosophy

with a

Major in Chemistry

in the

College of Graduate Studies

University of Idaho

By

Moubani Chakraborty

Major Professor: Kristopher V. Waynant, Ph.D.

Committee Members: Matthew Bernards, Ph.D.; Patrick Hrdlicka, Ph.D.

Darren Thompson, Ph.D.

Department Administrator: Ray von Wandruszka, Ph.D.

August 2022

Abstract

Zwitterionic polymeric hydrogels (polyampholytes) have shown promise as functional biomaterial platforms with resistance to nonspecific protein adsorption (non-biofouling) and as controlled release drug delivery materials. However, there are few zwitterionic cross-linkers to complement these materials and provide a fully zwitterionic material. To date, available zwitterionic cross-linkers have been limited to carboxybetaine or sulfobetaine acrylate/methacrylates and only one of these has been tested *in vivo*. Peptides offer a highly adaptable zwitterionic scaffold to imbed a series of desired functions. To investigate this hypothesis a simple N-Ser-Ser-C dimethacrylate cross-linker was synthesized. This novel cross-linker was incorporated into a polyampholyte hydrogel, and its physical properties and biocompatibility were compared against a polyampholyte hydrogel synthesized with an EG-based cross-linker to reveal increased non-fouling performance, while promoting enhanced cellular adhesion to fibrinogen delivered from the hydrogel over commercial polyethylene glycol (PEG) cross-linkers. Therefore, these results suggest that the S-S cross-linker will demonstrate superior future performance for *in vivo* applications Continuing, a library of serine and lysine based zwitterionic dimethacrylamide and mixed methacrylate/ methacrylamide zwitterionic dipeptide cross-linkers (Lys-Lys, Ser-Lys, Lys-Ser) have been developed to provide a tunable polymer platform that retains the desired non-fouling properties. Moreover, this strategy was employed to build tripeptide zwitterionic cross-linkers as to extend the distance between the zwitterionic components, another key feature not amenable in the carboxy- or sulfobetaine based cross-linkers. Peptide-based cross-linkers can be synthesized following an ‘outside-in’ approach and key to this route is selective protection strategy of both

N and C termini, peptide coupling, and chemo-selective protection and deprotection strategy. It has been hypothesized that molecular-level control over the length, charge spacing, charge density, and sidechains will lead to fully tunable polymer hydrogels for directed biomaterial scaffolds.

Acknowledgement

Undertaking this Ph.D. has been a life changing experience for me, and it would not have been possible without the support and guidance I received from many people along the way.

First and most of all, I would like to thank to my supervisor, Dr. Kris Waynant for his continuous guidance, patience and support that carried me through all different stages of my Ph.D. journey. This thesis would never be possible without his expertise and help. I would like to thank my committee members Dr. Matthew Bernards, Dr. Darren Thompson, Dr. Patrick Hrdlicka for their valuable suggestions and encouragement. I offer my sincere appreciation to my committee for providing me the learning opportunities along the way. I would like to thank Dr. Lee Deobald for always offering many generous and helpful suggestions regarding HPLC-MS and Dr. Alexander Blumenfeld for his guidance in analyzing NMRs. I would also like to thank our department chair Dr. Ray Von Wandruszka for helping me with the lyophilizer.

Last but not the least, I would like to extend my deepest gratitude to my lab mates and colleagues for all the fun and emotional support- I am lucky to have made such great friends. Rabina, Skyler, Akeem, Jeremy, Megan, Connor, Laxme thank you all for making the long hours in the lab equally engaging and exciting and for sharing this academic journey with me.

Finally, I wish to acknowledge all the faculty and staff of the Department of Chemistry at the University of Idaho for a friendly and productive graduate experience and University of Idaho start-up fund for funding this project.

Dedication

I would like to dedicate this Ph.D. to my beloved mother Bandana Chakraborty, who has been my source of inspiration and faith. This work is a fruit of countless sacrifices she made. She gave me all the strength, emotional and moral support along my Ph.D. journey. I hope that this achievement will complete the vision she had for me many years ago when she chose to provide me the best education, she possibly could so that I can be the best version of myself.

Table of Content

List of Figures

List of Schemes

List of Abbreviations

ANOVA	One-way analysis of variance
APS	Ammonium persulfate
Aq.	Aqueous
Boc	tert-butyloxycarbonyl
br	Broad singlet
CAA	2-Carboxyethyl acrylate
d	Doublet
DCM	Dichloromethane
dd	Doublet of doublets
DEG	Diethylene glycol
DIPEA	N, N'-Diisopropylethylamine
DMF	N, N'-dimethylformamide
dq	Doublet of quartets
dsep	Doublet of septets
ECM	Extra Cellular Matrix

EDC	N-(3-dimethylaminopropyl)-N'-ethylcarbodiimide
EDTA	Ethylenediaminetetraacetic acid
Equiv	Equivalents
FBG	Fibrinogen from human plasma
FBS	Fetal bovine serum
FDA	Food and Drug Administration
FITC BSA	Bovine serum albumin-fluorescein isothiocyanate conjugate
FTIR	Fourier transform infrared
h	Hour(s)
HBTU	2-(1H-benzotriazol-1-yl)-1,1,3,3-tetramethyluronium hexafluorophosphate
HRMS	High resolution mass spectrometry
IPN	Interpenetrating polymer networks
m	Multiplet
NHS	N-hydroxysuccinimide
PBS	Phosphate buffered saline
PEG	Poly (ethylene glycol)

PG	Protecting Group
PGA	Poly Glycolic acid
pHEMA	Poly (2-hydroxyethyl methacrylate)
PMB	Paramethoxybenzoic acid
PMEA	Poly 2-methoxyethylacrylate
PNVP	Poly(vinylpyrrolidone)
q	Quartet
RES	Reticuloendothelial system
SMS	Sodium metabisulfite
t	Triplet
TEA	Triethyl Amine
TFA	Trifluoroacetic acid
TLC	Thin layer chromatography
TMA	2-(Acryloyloxy ethyl)trimethyl ammonium chloride
tt	Triplet of triplets
α-MEM	Alpha-minimum essential medium

Chapter 1: Introduction to Peptide-Based Zwitterionic Cross-linkers as Elements of Biomaterials

A biomaterial is a substance that has been engineered to interact with biological-systems.[1] By definition, a biomaterial is a non-viable material used in a medical device, intended to interact with a biological system *(Williams, 1987)*.[2] The first biomaterials were applied in medicine in the late 1940s and early 1950s and since then biomaterials have evolved in the past 70 years (as of this writing) from improvised materials to a systematic multidisciplinary field represented by many researchers in the scientific community, and with numerous applications.[3]

The first-generation biomaterials were composed largely of off-the-shelf and widely available industrial materials. Even though they were bioinert, they were not well suited for medical use. The widely used elastomeric polymer, silicone rubber is an example of these types of biomaterials.[4] Silicone rubber is superior in terms of its heat and abrasion resistance capabilities as well as chemical stability compared to organic rubbers and because of these unique features, silicone rubber has been widely used to replace petrochemical products in various industries like aerospace, automobile, construction, electric and electronics, medical and food processing industry. Second-generation biomaterials emerged from the early predecessors and were designed to induce the intended therapeutic effects by a controlled reaction with the tissues.[5] These second-generation biomaterials also included the development of biodegradability, the rate of which could be tailored to its desired application. Biodegradable polyglycolic (PGA) acid, for example, has been introduced for clinical applications since the 1960s and has been used extensively for its strength, flexibility, and chemical composition, which is conducive to tissue development. The third generation of biomaterial has been

designed for supporting and stimulating the regeneration of functional tissue.[6–8] Biomaterials play an important role in the field of regenerative therapeutics; with the help of biomaterial true replacement of living tissue was made possible for tissue engineering purposes. In the most frequently used protocol, the cells are seeded on a scaffold composed of synthetic polymer or natural material and a tissue is matured *in vitro*. The construct is then implanted in the appropriate location. A typical scaffold is capable of being absorbed into living tissue over time and has a porous configuration in the desired geometry.[9] The biomaterial community has made major contribution in understanding the interplay between physiological environment and external materials. Nowadays, a wide variety of biomaterials are commercially available, and many others are under investigation to both maintain and restore bodily functions. In the past two decades the growth of this field has been exceptional and there is a growing appreciation of the importance of their topological and mechanical properties in guiding biological responses. For example, antibacterial biomaterials, such biomaterials are characterized by antifouling coatings, exhibiting low adhesion or even repellent properties towards certain microorganisms, or they can also be used as antimicrobial coatings and are able to kill certain microbes approaching the surface.[10] These biomaterials not only allow targeted delivery of multiple agents but also provides sustained release at the infection site, thereby reducing potential harmful effects of bacterial infection. The number of FDA-approved anti-infective biomaterials has significantly increased in the past decade which indicates the need for alternatives to systemically administer antibiotics that often encounter difficulty in penetrating the cell wall and reaching the bacteria. Most of these biomaterials have been strategically synthesized to provide antimicrobial activity by drug-releasing or non-releasing approaches.[11] Biomaterials have also been used as drug carrier systems which are defined as

substrates used in the process of drug delivery and are primarily used to control the release of drugs into systemic circulation. The mode of drug delivery affects numerous factors that contribute to therapeutic efficacy, including pharmacokinetics, distribution, cellular uptake as well as toxicity and excretion. Moreover, certain drugs lose their actionable properties due to changes in environmental factors such as moisture, temperature, and pH, which can occur inside the body.[11] Biomaterials have shown to effectively deliver a range of pharmaceutical compounds including antibodies, peptides, vaccines, drugs, and enzymes, and help improve the selectivity, effectiveness, and safety of drug administration. In 1989, the U.S. Food and Drug Administration (FDA) approved the first system to slowly release a peptide.[3] These are polymer microspheres that slowly release luteinizing hormone-releasing hormone (LHRH) analogues, which are of about 1200 Da molecular weight. This molecule, if given orally or injected in unencapsulated form, is rapidly destroyed. However, when placed in a polymer matrix, release occurs over four months.[11]

Over the past fifty years biomaterials have been developed as a science with various forms of implants/medical devices and have been studied and developed for multiple applications in the human body. Implants are defined as objects that do not require any power source to carry out their expected functions whereas devices are objects that require a form of power, which may be chemical or electrical.[12] Examples of implants include knee or breast implants, whereas examples of devices include pacemakers and defibrillators. Biomaterials are a critical platform technology used in tissue regeneration, and they play a critical role in the foreign body response and the induction of healing upon implantation. The aim of regenerative medicine and tissue engineering is to make structural and functional biological replacements that maintain, improve, or repair tissue functions by using scaffolds, cells, and bioactive

molecules.[13] They range from manmade objects that provide physical support, such as bone plates, and joint replacement to applications that improve functionality of human organs, such as the pacemaker, artificial heart, and blood vessel.[14] They have also been used as scaffolds which are 3D polymeric network that mimics ECM (extracellular matrix) with the aspect of morphological, biochemical, and mechanical characteristics to improve cell adhesion, proliferation, and differentiation to provide the structural support for cell attachment and subsequent tissue development.[15] Different natural and synthetic polymers are used alone or in combination for tissue engineering purposes. Synthetic polymer-based scaffolds can be fabricated in a manner that provides structural and mechanical characteristics of native tissue ECM.

Polymeric materials have been frequently used as biomaterial because of the ease of synthesis, flexibility, as well as their wide range of mechanical, electrical, chemical, and thermal behaviors. One of the earliest examples of biomedical application of polymers is the use of poly(hydroxyethyl methacrylate), pHEMA, in contact lens. The first commercialized contact lens material was synthesized using pHEMA with an equilibrium water content (EWC, percentage of water by weight) of approximately 40%, and was introduced by Wichterle and Lim in 1959.[16] pHEMA is a biocompatible, optically transparent, hydrophilic, non-degradable polymer and is stable under different physiological pH. Polymeric materials are particularly useful as contact lenses because of their relatively good mechanical stability and favorable refractive index.[17] More recently, extended wear contact lenses have been fabricated from an IPN (interpenetrating polymer networks) composed of PNVP Poly(vinylpyrrolidone) chains entrapped within a silicone hydrogel network. In this system silicone monomers and cross-linkers are polymerized in a solution containing PNVP, and an IPN hydrogel is formed. The

PNVP helps lubricate the surface of lens against the cornea, and the silicone hydrogel provides high oxygen transport to the cornea, as well as enhanced permeability of small nutrient molecules and ions. Contact lenses are also classified as hard and soft based on their material. Soft contact lenses (pHEMA) are flexible and permeable that allow oxygen to pass through the cornea whereas hard contact lenses (PMMA) are made of rigid gas permeable materials. pHEMA is synthesized from methacrylic acid and ethylene oxide (**Figure 1.2**) and then thermally or photochemically polymerized to give pHEMA.[18] pHEMA microparticles have also been used for controlled protein delivery and for the release of peptide drugs.[19]

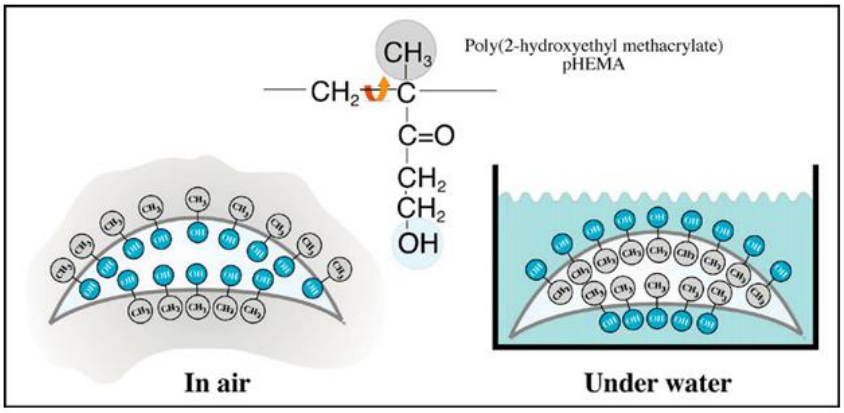

Figure 1. 1 pHEMA exhibits a surface rich in methyl groups (from the polymer chain backbone) in air, and a surface rich in hydroxyl groups under water [18]

Another polymer that has been utilized frequently as a biomaterial is PMEA, (**Figure 1.2**) it is used as a coating on the circuits and tubes implemented in bypass surgery because it reduces protein and platelet adsorption. PMEA is one of the first polymers that was approved by the FDA for in vivo applications.

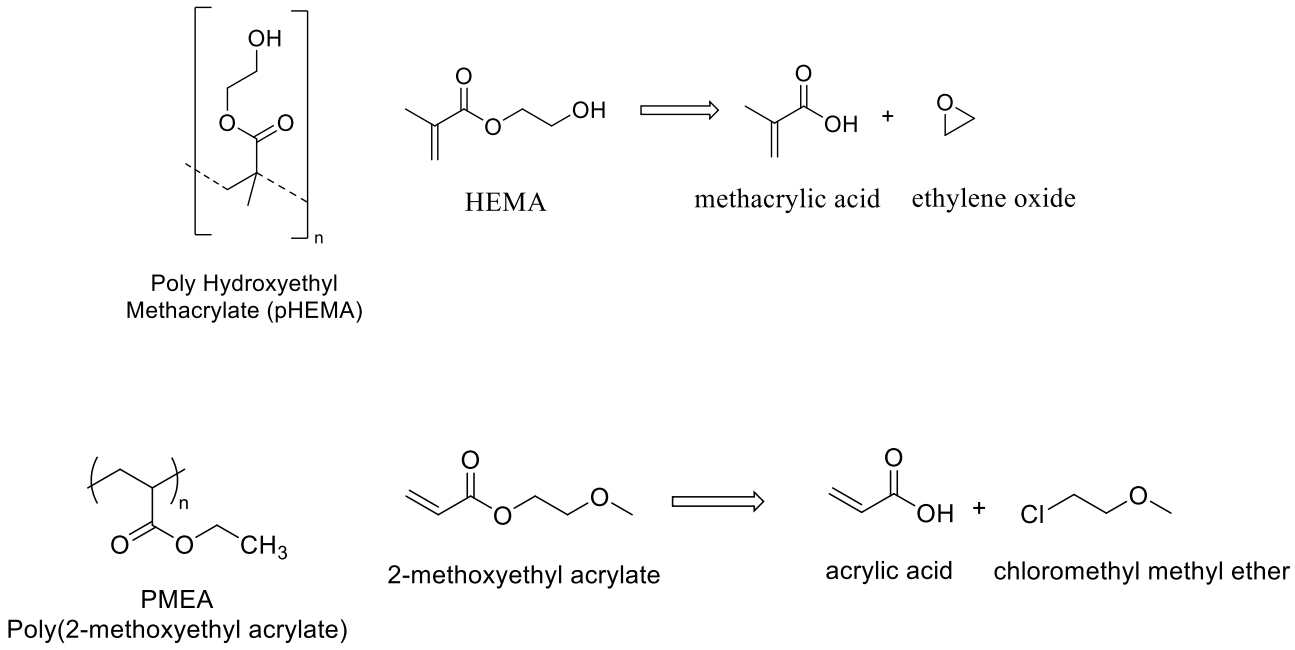

Figure 1. 2: Structures and synthesis of pHEMA and PMEA

One of the main criteria for the successful design of a biomaterial is biocompatibility.[13] By definition biocompatibility is the ability of a material to perform appropriate host response in a specific application.[2] Examples of "appropriate host responses" include resistance to blood clotting, bacterial colonization, and normal, uncomplicated healing. Biocompatibility assessment is aimed to verify the capacity of a given material to correctly perform the intended function when in contact with the biological environment without producing any toxic, immunological or any adverse reaction. Nowadays, a wide variety of materials are commercially available, and many others are under investigation, to both maintain and restore bodily functions. Different parameters of polymeric biomaterials can affect the cellular behavior in a controlled manner. Studies have shown that both molecular weight and conformational flexibility of the polymer influence biocompatibility.[20] For example, lower molecular weight poly(ethylene glycol) (PEG) coated surfaces show minimal

protein adsorption, whereas polymers with a more linear or branched and flexible structure, for example, poly(lysine), showed a higher cell damaging effect.[12,14,15] It is also desirable that the physical characteristic of a implanted biomaterial matches with that of extracellular matrix (ECM). Although the underlying mechanisms for the biocompatibility of polymers at the molecular level are complex and have not been clearly illustrated, controlling the interfacial interactions of the polymeric biomaterials with biological elements is the key to understanding the biocompatibility of biopolymer and therefore can provide necessary information towards their successful implementation in biomedical applications.[13]

Surface potential of biomaterial influences cell proliferation, differentiation, attachment, and adhesion therefore the right balance between the positive and negative charges is very important for biomaterial design and by manipulation of these fixed charges or ligand density within a biomaterial, cellular attachment can be altered.[18] One way to control the surface potential and thereby the hydrophilicity/hydrophobicity is by modifying the chemical structure of sidechains. Studies have shown that blood compatibility increases by utilizing vinyl polymers having hydrophilic functional groups.[21] A popular way to modify the side-chain structure is by tuning the number of ethylene glycol (EG) units and the chain-end terminal group. The hydrophilicity of the polymer increases with the number of EG units with increase in the number of methylene units, as the polymers have longer sidechains, the polymers become soluble in water.[22]

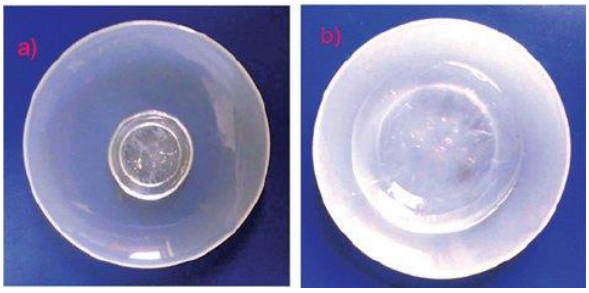

Figure 1. 3: Poly (AM-AMPS) hydrogel (DAMPS3) photographs a) dry hydrogel and b) swollen hydrogel.

Hydrogels have been used frequently as biomaterials. Hydrogels are water-swollen polymeric materials that maintain a distinct three-dimensional structure. They have received significant attention because of their high-water content and the related potential for many biomedical applications[23,24] (**Figure 1.3)** Hydrogels are held together as water-swollen gels by: (1) primary covalent cross-links; (2) ionic forces; (3) hydrogen bonds; (4) affinity or "bio-recognition" interactions; (5) hydrophobic interactions; (6) polymer crystallites; (7) physical entanglements of individual polymer chains; and/or (8) a combination of two or more of the above interactions.[12,25] According to their method of preparation, hydrogels are characterized by 3 different categories. (1) homopolymer hydrogels; (2) copolymer hydrogels; (3) multi-polymer hydrogels. (**Figure1.4**) Homopolymer hydrogels contains hydrophilic monomer units, whereas copolymer hydrogels are produced by cross-linking of chains composed of two comonomer units, at least one of which is hydrophilic and multi-polymer hydrogels are produced from three or more comonomers units respectively.[26,27] The presence of chemical or physical crosslinking points within the network helps in maintaining the three-dimensional integrity of hydrogel in swollen state. Covalently cross-linked hydrogels are usually

synthesized from small multifunctional molecules such as monomers or oligomers. Such cross-linking may be achieved by reaction of two chemical groups on two different molecules, which can be initiated by catalysts, by photo-polymerization or by radiation cross-linking.[28]

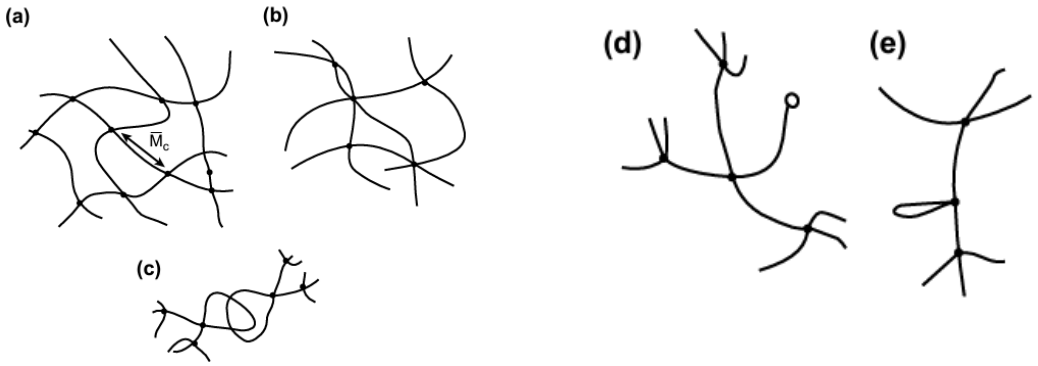

Figure 1. 4: (a) Ideal macromolecular network of a hydrogel; (b) Network with multifunctional junctions; (c) Physical entanglements in a hydrogel; (d) Unreacted functionality in a hydrogel; (e) Chain loops in a hydrogel. This Figure has been reproduced from Pappes et al, Hydrogels in Medicine and Pharmacy.[29]

Polyampholytes are polymeric systems comprised of both positively and negatively charged monomeric subunits and contain both anionic and cationic functional groups. The strengths of these functional groups are often divided into four categories, that include both weak anionic and cationic groups, weak anionic and strong cationic groups, strong anionic and weak cationic groups, and lastly, both strong anionic and cationic groups.[30] Polyampholytes appear in their most compact conformation at their isoelectric point (IEP) or pH level when the overall charge is zero, since the electrostatic attractions between the oppositely charged functional groups are balanced. As pH deviates from the IEP, the overall charge of the polyampholyte will move further from neutral, causing electrostatic repulsive forces between

like-charged regions, to increase and expand the polyampholyte. Similarly, when salt ions are present, the ions disrupt the electrostatic interactions between oppositely charged regions of the subunits (**Figure 1.5**).[31] This also causes the polyampholyte to swell. Formulation of polyampholyte by manipulating these unique electrostatic interactions and system responses has spurred investigation into using these materials as a tissue scaffold. Furthermore, polyampholyte hydrogels can deliver covalently attached biomolecules for targeted interactions with native tissue.[32]

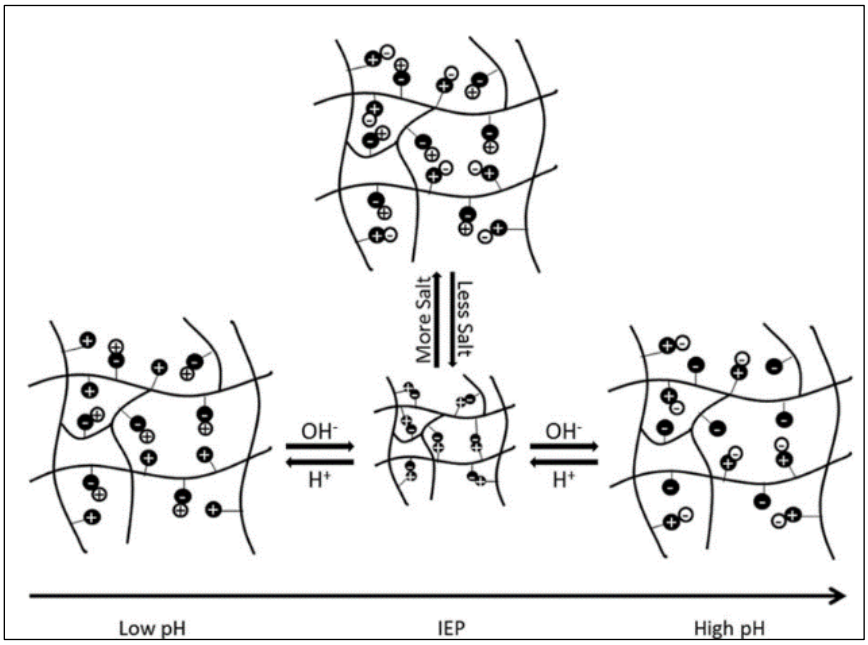

Figure 1. 5: Effect of pH on polyampholyte

Out of the many materials that have been investigated as a tissue scaffold, PEG polymers are the most commonly used material for reducing nonspecific protein adsorption which happens as a result of nonspecific protein adsorption on bio-implants that leads to the recognition of the implant by macrophages as a foreign object.[14] The ethylene glycol units of PEG bind to the water molecules, with the formation of a strong hydration layer, which creates steric hindrance to proteins, therefore preventing non-specific protein absorption. For example,

PEG has been conjugated to a phospholipid known as phosphatidylethanolamine, which inserts into a liposome's lipid bilayer. This is called "PEGylating" the liposome which essentially forms water-retaining coating around the liposome and prevents recognition by the reticuloendothelial system (RES).[33] Although PEG shows potential as a non-fouling material, there are several disadvantages of using PEG as a biomaterial. For example, PEG is susceptible to oxidation and has shown encapsulation in collagenous scar tissue via the foreign body response when used in vivo in a number of cases.[34] Additionally, research has shown that some human produce antibodies to PEG.[28,35] Therefore, alternate chemistries are desired for tissue engineering purposes.

Significant efforts have been placed on the development of polymer-based materials to improve the clinical outcomes of regenerative therapies based on biomaterials.[36] A major challenge in design of these biomaterial is the limited number of material-based approaches for delivering the combinatorial biochemical and mechanical factors that regulate the biological response and subsequent tissue regeneration.[30] Furthermore, nonspecific biological interactions with implanted biomaterials induces foreign body response rather than a regenerative healing response.[21,37] Foreign body response is defined as the phenomenon of recognition of implanted biomaterial as not only foreign but potentially harmful by body's immune system. Zwitterionic polyampholyte polymer systems have seen increasing interest in the biomaterials community because of their strong demonstrated resistance to nonspecific protein adsorption and cell adhesion. For example, poly (2-methacryloyloxyethyl phosphorylcholine) (PPBMA): poly(phosphobetaine methacrylate), generally known as PMPC (**Figure 1.6)** is a biomimetic material containing phosphorylcholine group for resisting nonspecific protein adsorption and platelet adhesion. Recently, synthetic polymers containing

zwitterionic structures similar to PPBMA, such as poly{[2-(methacryloyloxy)ethyl]dimethyl-(3-sulfopropyl)ammonium hydroxide} (poly (sulfobetaine methacrylate), and poly(1-carboxy-N,N-dimethylN-(2'-methacryloyloxyethyl)methanaminium) (poly(carboxybetaine methacrylate), bearing sulfo- and carboxy- betaine group, respectively **(Figure 1.6)**, are also reported as blood-compatible polymers, which show good plasma protein-fouling resistance.[38–42]

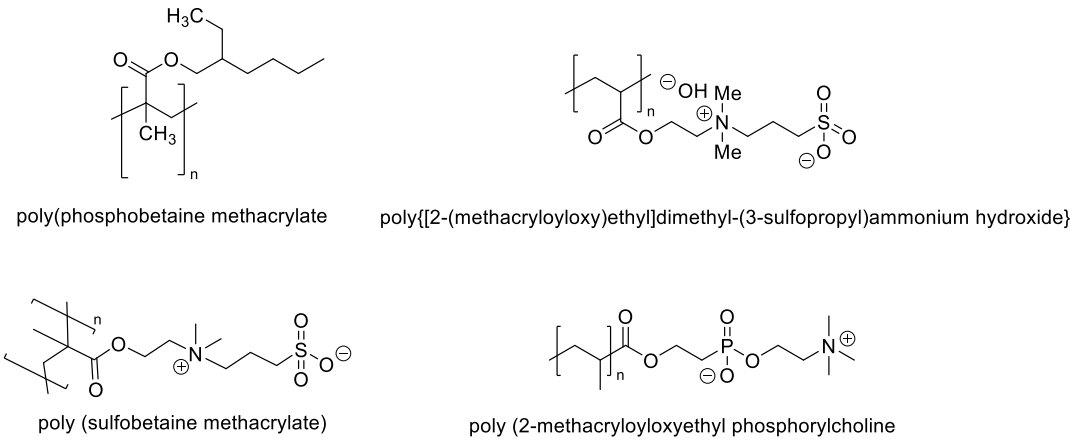

Figure 1. 6: Examples of zwitterionic polyampholyte polymers

Zwitterionic cross-linkers have existed in literature before. Shaoyi Jiang and coworkers created poly(carboxybetaine) (PCB) hydrogels cross-linked with a zwitterionic carboxybetaine disulfide cross-linker **(Figure 1.7)** (CBX-SS).[34] Another recent study was published in 2020 from Li's group where they synthesized Z-hydrogel cross-linked via thiol−ene reaction between poly(SBMA-co-HDSMA)-T and divinyl-functionalized sulfobetaine (BMSAB) **(Figure 1.8)**.[43] However, the current limitation to the advanced development of these polymers is the lack of structural diversity and an understanding of the structure-property relationships that guide their adaptations.[44,45] The goal for this project was to use a rational design strategy to synthesize a library of peptide-based zwitterionic cross-linker species for incorporation into

polyampholyte hydrogels, in order to develop structure-property relationships between the cross-linker species and the resulting polymer hydrogels.[46] This will lead to a non-fouling polymeric platform with tunable biochemical and mechanical design features. Molecular-level control over the length, charge spacing, charge density, and pendant side-chain presentation could also lead to enhanced performance of polyampholyte hydrogels, and this hypothesis was tested through paired synthesis and characterization objectives.[47]

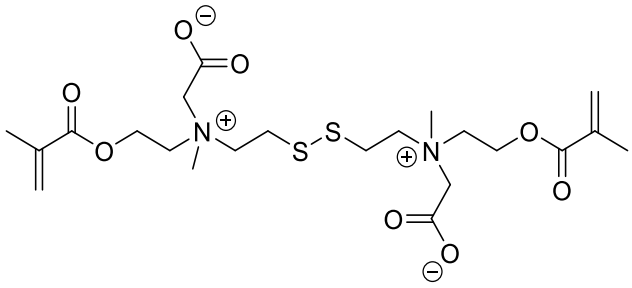

Figure 1. 7: poly(carboxybetaine) (PCB) hydrogels cross-linked with a zwitterionic carboxybetaine disulfide cross-linker (CBX-SS)

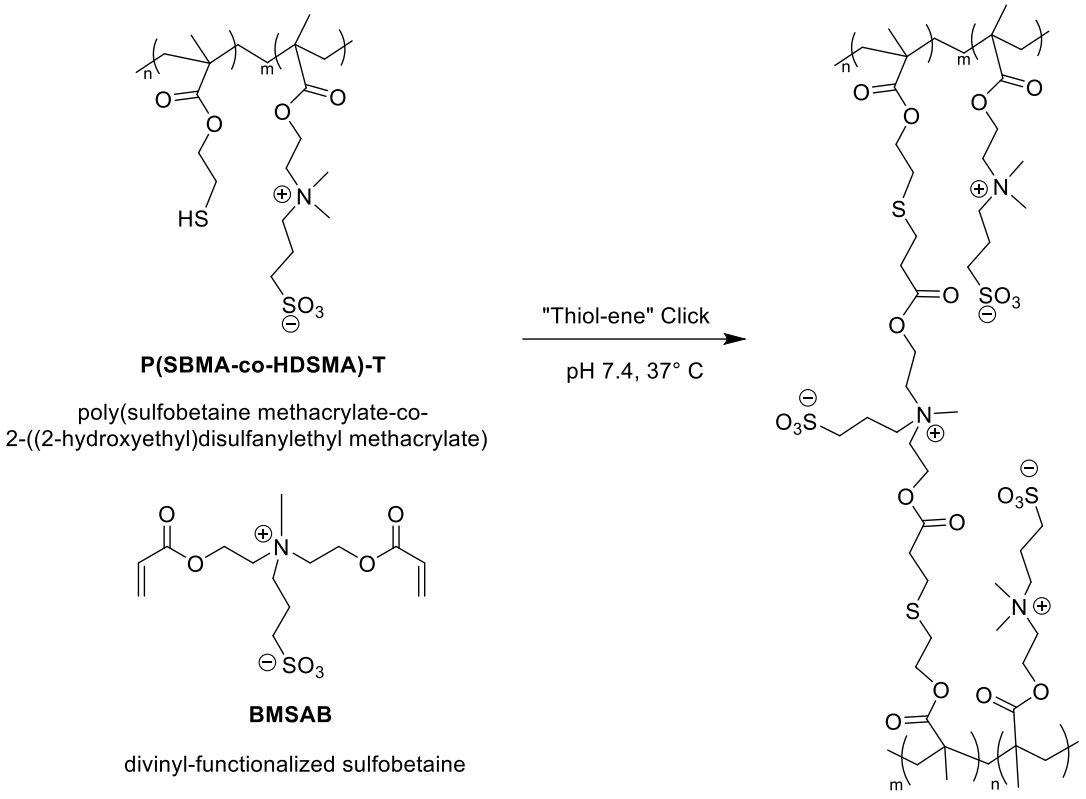

Figure 1. 8: Zwitterionic hydrogel cross-linked via thiol−ene reaction between poly(SBMA-co-HDSMA)-T and divinyl-functionalized sulfobetaine (BMSAB)

The key to synthesizing these cross linkers have involved three major steps, the first one being peptide coupling which connects the two amino acids together, the second step is methacrylation which attaches the two polymerizable entities together and the last one is selective protection and deprotection of the C and N termini. Peptide-coupling strategies will allow for critical variations in cross-linker molecular structure. Therefore, the objectives are to synthesize cross-linkers with 1) controlled overall length and fixed charge spacing[48] , 2) controlled spacing between the charged groups and with varied charge density[48] , and 3) with biochemical-signaling pendant side chain presentation. The results will be a novel library of zwitterionic cross-linker species that will subsequently be fully evaluated for their impact on

the biochemical and mechanical properties of polyampholyte hydrogels to develop structure-property relationships for each molecular variation.[49]

The four critical properties for future biomedical applications that will be assessed include: 1) the non-fouling properties of the hydrogel[50] ; 2) the ability to deliver biochemical signaling molecules from the hydrogel[51] ; 3) the mechanical properties under compression and tension, and 4) the degradation behavior. The results will be a fundamental evaluation and correlation of the structure-property relationships of critical polyampholyte hydrogel performance metrics to structural variations in the library of zwitterionic cross-linkers.

Chapter 2: Synthesis and Evaluation of Ser-Ser bis(methacrylate) cross-linker

Chapter 2 is a more detailed adaptation of a published manuscript

Chakraborty, M.; Haag, S. L.; Bernards, M. T.; Waynant, K. V. Synthesis of a zwitterionic N-Ser Ser-C dimethacrylate cross-linker and evaluation in polyampholyte hydrogels. *Biomaterials Science* **2021**, *9* (16), 5508-5518.

Section **2.2.1-2.2.6** were contributed by Stephanie Haag from the Department of Chemical Engineering, University of Idaho.

2.1 Introduction:

Significant efforts have been placed on the development of polymer-based materials to improve the clinical outcomes of regenerative therapies based on biomaterials.[52] Zwitterionic polymer (polyampholytes) have been found to be one the promising family of polymeric materials under development for regenerative therapies because of their strong demonstrated resistance to nonspecific protein adsorption and cell adhesion, commonly being referred to as non-fouling.[48] A major challenge to the advancement of these polymers is the lack of diversity and understanding of the structure-property relationships that guide their tailoring.[49] Based on these needs a rational design strategy of a dipeptide-based zwitterionic cross-linker, N-Ser-Ser-C dimethacrylate (S-S) from N-Boc-L-serine is presented. The strategy utilized a convergent coupling of methacrylated N- and C-protected serine partners followed by chemo-selective global deprotection to yield the zwitterionic cross-linker with good overall yields. This novel cross-linker was incorporated into a polyampholyte hydrogel, and its physical properties and biocompatibility were compared against a polyampholyte hydrogel synthesized with an EG-based cross-linker. The S-S cross-linked hydrogel demonstrated excellent non-

fouling performance while promoting enhanced cellular adhesion to fibrinogen delivered from the hydrogel. Therefore, the results suggest that the S-S cross-linker will demonstrate superior future performance for *in vivo* applications.

The most recent NSF Biomaterials Workshop Report recommended future investments to further improve the performance and longevity of polymers in this field.[53] Another major limitation to the fruitful design of biomaterials for these fields is their nonspecific biological interactions which eventually leads to confounding biochemical signals that induce the foreign body response rather than a regenerative healing response.[48,49] In order to address the unwanted foreign body response while maintaining the non-fouling properties of a biomaterial, a series of naturally biocompatible materials have been employed. Poly(ethylene glycol) (PEG) based hydrogels have been developed and used in a large number of biomedical applications[28,32,34,54,55] and while PEG has been widely used in the biomedical field and is approved for use by the Federal Drug Administration (FDA) in several applications, there is increasing evidence that some humans produce antibodies to PEG, suggesting that it cannot be universally used[56,57]. Further, hydrogels formed entirely from PEG-based chemistries still produce a foreign body capsule upon implantation.[58] This suggests a need for better candidates as biocompatible polymeric systems for use in tissue regeneration applications as opposed to PEG.

Polyampholytes have been found to be excellent biomaterial systems providing the needed charges to repel non-specific adhesion and yet neutrally balanced to be compatible. Many of these polyampholyte structure utilize PEG based cross-linkers which provide the structural uniformity of the polyampholyte yet are not completely zwitterionic.[36] Hydrogels formed with zwitterionic cross-linkers have demonstrated no measurable foreign body

response utilizing *in vitro* assessment techniques.[30,59] The accelerated compatibility has been reasoned to be due to the ionic solvation interactions throughout the 3D structure. These ionic solvation interactions lead to the formation of a tightly bound hydration layer that is critical for maintaining the non-fouling performance in complex environments. As a result, even a slight disruption to the hydration layer result in impacts on the non-fouling performance when these systems are evaluated in highly complex media like the *in vivo* environment.[36] This is demonstrated by a work from the Jiang lab, where they synthesized PCB poly(carboxybetaine) hydrogels cross-linked with a zwitterionic carboxybetaine disulfide cross-linker and it was evaluated across a range of monomer to cross-linker ratios.[60] The resulting hydrogels resisted the foreign body response over three months of implantation in mice,[50] (**Figure 2.1**) while also resisting encapsulation and facilitating enhanced levels of blood vessel formation at shorter evaluation time points.

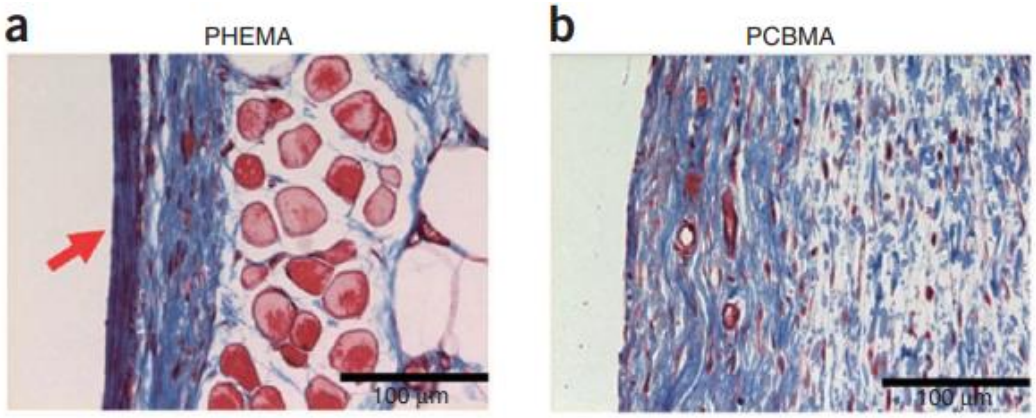

Figure 2. 1:[50] Collagen and blood vessel formation in tissues near subcutaneously implanted PCBMA and PHEMA hydrogels. (a, b) Three months after subcutaneous implantation of hydrogels, tissues were stained with Masson's trichome. Blue staining indicates collagen capsule surrounding PHEMA hydrogel with 5% cross-linking density (a) and PCBMA

hydrogel with 5% cross-linking density (b). Hydrogels are located on the left side of the images. The collagen capsule is indicated by the red arrow. Scale bars, 100 μm.

Another study published from the Li lab demonstrates the synthesis of purely zwitterionic hydrogels (Z-hydrogel) that are developed using thiolated poly (SBMA-co-HDSMA) as the network backbone and divinyl-functionalized sulfobetaine (BMSAB) as zwitterionic cross-linker via the "thiol-ene" click reaction. In *in-vivo* studies, this cross-linker not only exhibited excellent resistance to protein and fibroblast adhesion, but also showed good biocompatibility and hemocompatibility. Based on these studies, it can be concluded that the use of a zwitterionic cross-linker is a promising component for the successful prevention of the foreign body response. However, there are very few examples of zwitterionic cross-linker species that have ever been detailed in the literature and only the one example of *in vivo* experiment.[36,61]

Amino acids and peptides, both natural and non-natural, create zwitterions in biological systems and are biocompatible and biodegradable.[62] Based on the type of peptide (combination of two or more amino acids) and the homogenous distribution of charges, it can achieve overall charge neutrality at various pH's common to biological systems (pH 6-8).[63] Peptide chemistry is also well-established with decades of literature to support their construction. As a result, utilizing well-established literature on various peptide protections and coupling strategies functionalized peptides can be made with a promising approach for synthesizing zwitterionic cross-linkers.[50,64] Once key material property is established with peptide-based cross-linkers, those properties should be maintained in the switch of L-amino acids for D-amino acids if a foreign body response is found. However due to the high prevalence of peptide-based

monomers in hydrogel synthesis, a foreign body response from these materials is not expected.[65,66]

In this work, a strategy for synthesizing peptide-based N-Ser-Ser-C dimethacrylate (S-S) zwitterionic cross-linkers has been demonstrated through two different convergent strategies 1) the “inside-out” strategy, and the 2) the “outside-in” strategy as described below. After synthesizing the monomers, the cross-linker was successfully integrated into a polyampholyte hydrogel platform to test its feasibility as a biomaterial. N-Ser-Ser-C dimethacrylate (S-S) was synthesized from N-Boc-L-Serine using a convergent coupling strategy as outlined in the retrosynthesis in **Scheme 2.1**.[67] Our initial approach towards making serine based zwitterionic cross-linkers involves two different strategies.

1) ‘Outside in’ where the selectively protected serine amino acids can be first methacrylated and then coupled together.

2) ‘Inside out’ where methacrylation follows peptide coupling.

The “inside-out” method was more preferred than “outside-in” and the reason being the feasibility of peptide coupling is comparatively better, more adaptable, and commercializable in solid phase than in the liquid phase and during the first step of synthesis both liquid and solid phase synthetic strategies can be used. The first step of the inside-out strategy was the coupling of an amine and carboxylic acid with the formation of amide bond using a coupling agent such as HBTU/HATU in presence of Hünig's base and DMF as a solvent. Even though the first step was very straightforward, the following step of methacrylation was proven difficult. The reaction was screened with several equivalents (ranging from 1 equivalent to 5 equivalent) of methacrylic acid yet mono methacrylation was

found to be the only major product. The reason for this could be the higher reactivity of the starting material as opposed to the initial monomethacrylation product which could prevent the primary alcohol of the initially formed product to react with the activated ester to form the dimethacrylated product. Monomethacrylated product was isolated and treated with another 4 equivalents of methacrylic acid and dimethacrylated product was isolated with very low yield (<20%) Whereas, during the "outside-in" approach N and C protected Serine species were separately methacrylated followed by peptide coupling in liquid phase chemistry using HBTU as a coupling agent. Moving forward, the "outside-in" strategy was then leveraged for a series of cross-linkers as discussed in Chapter 3.

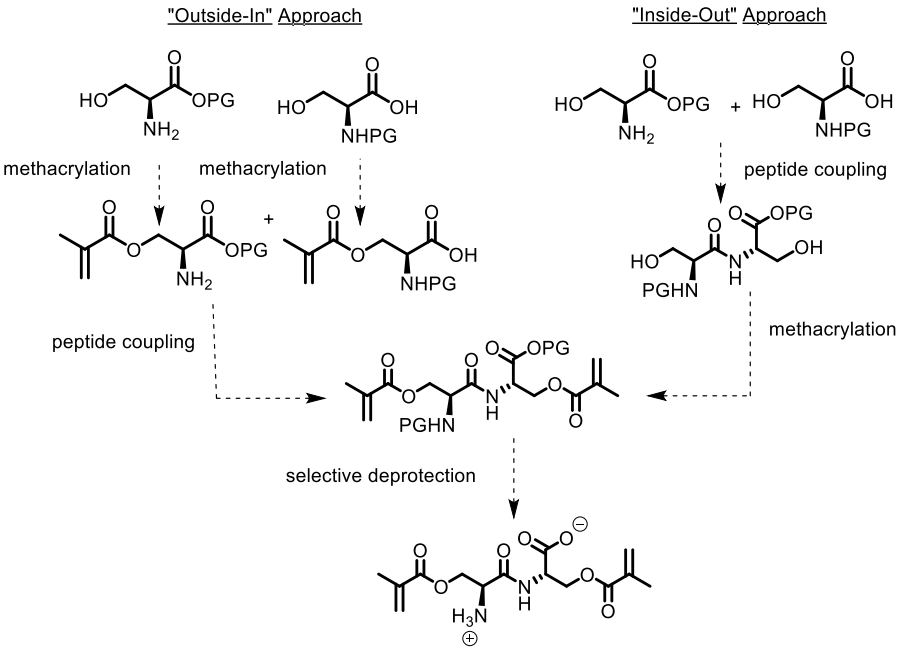

Scheme 2. 1: Retrosynthetic Approaches for synthesizing N-Ser-Ser-C Cross-linker

The synthesis of N-Ser-Ser-C cross-linker involves the three synthetic strategies consisting of selective protection/deprotection, methacrylation, and peptide coupling. Each step is described below.

1.Peptide Coupling:

Two serine precursors are coupled together using a carbodiimide based peptide coupling agent. Five different peptide coupling agents were screened (DCC (dicyclohexyl carbodiimide), EDC (1-Ethyl-3-(3-dimethylaminopropyl)carbodiimide), DIC (N, N′-Diisopropylcarbodiimide) and uronium based coupling agents (i.e., HBTU and HATU). Among the coupling strategies, HBTU had comparatively higher yields therefore HBTU was used as a peptide coupling agent for most of the coupling steps. The mechanism for HBTU coupling is as follows (**Figure 2.2**). HBTU activates carboxylic acids with the formation of a stabilized HOBt (Hydroxybenzotriazole) leaving group. In order to make the HOBt ester, the carboxylic anion of the acid attacks the imide carbonyl carbon of HBTU. Next the displaced anionic benzotriazole N-oxide attacks the acid carbonyl, forming the tetramethyl urea byproduct and the activated ester. The activated intermediate species get attacked by the amine during aminolysis with the formation of a dipeptide.

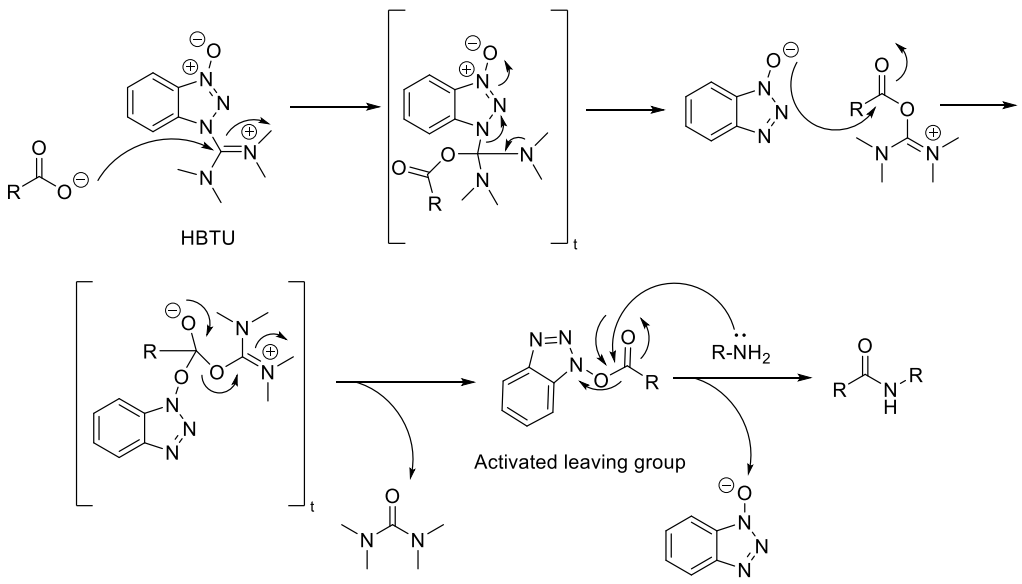

Figure 2. 2: HBTU coupling mechanism

II. Methacrylation:

The methacrylation step was realized by two different methacrylation strategies. One includes methacroloyl chloride in triethyl amine and the other one comprises of methacrylic acid in presence of Hünig's base and a coupling agent. (**Scheme 2.2**). The first one uses methacryloyl chloride in triethyl amine where there is a nucleophilic attack from the oxygen in the primary alcohol of serine **(2-1)** to the carbonyl carbon of methacryloyl chloride with the elimination of HCl which is then neutralized in situ via triethyl amine. The second strategy comprises of methacrylic acid in presence of Hünig's base and a coupling agent. In this method the coupling agent activates the methacrylic acid first with the formation of an "active ester" which could then act as a better leaving group when the primary alcohol of the serine attacks the carbonyl carbon of the activated ester. The mode of action of HBTU as a coupling agent has been described above.

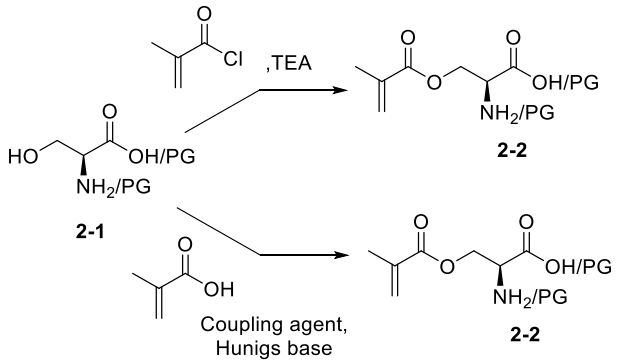

Scheme 2. 2: Two different Methcrylation strategies starting with N-Boc-L-Serine

III. Selective protection and Deprotection of C and N termini:

For the N and C protection strategy, the anticipation was to introduce an orthogonal protection and deprotection method which is a strategy that allows the specific deprotection of

one protective group in a multi-protected structure without affecting the others. In order to do so the C termini of serine was protected with the formation of an ester. Several synthetic strategies were introduced for ester formation. For example, benzyl ester was synthesized using benzyl bromide and TEA (triethyl amine), methyl ester from methanol and H_2SO_4 and PMB (para methoxy benzyl bromide) ester from PMB chloride and TEA respectively. The forward reaction was straightforward but during the reverse reaction which includes deprotection of C termini, it was found that along with deprotecting the C-termini, the methacrylate on the primary alcohol of serine had been impaired. After several trial and error with different protection and deprotection strategies the C termini of N-Boc-L-serine (**2-3**) was protected with addition of *t*-butyl-*N,N'*-diisopropylcarbamimidate in DCM which afforded the *t*-butyl protected serine (**2-4**) with 55% yield.[68] Next, (**2-4**) was treated with methacryloyl chloride in the presence of triethylamine in DCM to give (**2-5**) in an excellent 93% yield.[69] While TFA can globally deprotect both Boc and the *t*-butyl ester, the reaction rate is much faster for the Boc removal, and this was utilized to selectively cleave the Boc group from doubly protected (**2-5**), to give the first coupling component **(2-6)** as a TFA salt as shown in **Figure 2.3**[70].

The carboxylate coupling partner, N-Boc-L-serine (**2-3**) was methacrylated under Steglich-type esterification conditions, albeit in low yield, to give **(2-8)** which quickly supplies the N-protected termini for peptide coupling.[57] HBTU coupling of **(2-8)** and **(2-6)** produced the protected zwitterionic cross-linker **(2-9)** which underwent extensive TFA deprotection to provide the desired cross-linker as a TFA salt. Initially, TFA deprotection was run in $CDCl_3$ in order to monitor the deprotections via ^{1}H NMR, but it can also be run at scale in more conventional, non-deuterated solvents (i.e., DCM). While the Boc group was removed within minutes of TFA addition (as monitored by ^{1}H NMR), the reaction took 24 hours in a 1:1 DCM:

TFA solution to fully remove the *t*-butyl protecting group. The isolated TFA salt was then lyophilized in the presence of 25 mM HCl to afford the S-S cross-linker **(2-10)** as an HCl salt, ready for hydrogel incorporation. HCl was selected as the counter ion source for uniformity with the counter ions found with the TMA (2-(Acryloyloxy)ethyl) trimethylammonium chloride) and CAA (2-carboxyethyl acrylate) monomers.

Even though this strategy did not lead up to our initial expectation of orthogonal protection and deprotection, a chemo-selective protection and deprotection mechanism was introduced for synthesizing this cross-linker. Therefore, the synthesis of dipeptide based zwitterionic cross-linker, N-Ser-Ser-C dimethacrylate, **2-10,** was conducted from N-Boc-L-serine (**2-3**), utilizing a convergent "Outside-in" coupling strategy of pre-methacrylated coupling partners (**2-6** and **2-8**) followed by careful global deprotection as seen in **Scheme 2.3.**

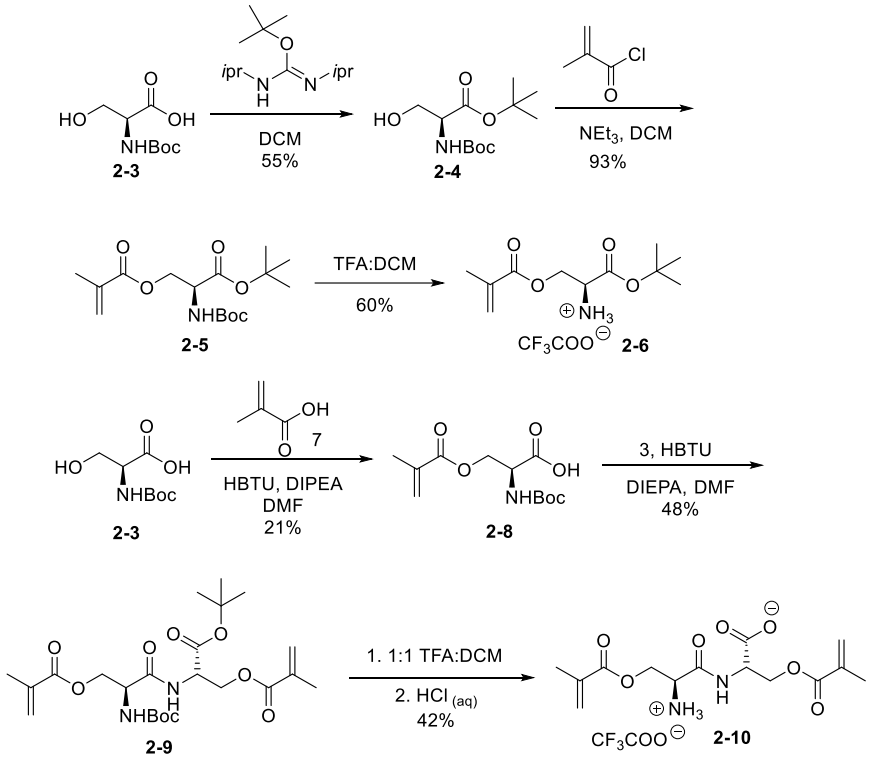

Scheme 2. 3: Synthesis of the S-S zwitterionic cross-linker from N-Boc-L-serine

After successfully synthesizing the cross-linker the product was incorporated into a polyampholyte hydrogel (**Figure 2.3**) composed of an equimolar mixture of [2-(acryloyloxy) ethyl] trimethyl ammonium chloride (TMA) and 2-carboxyethyl acrylate (CAA). The TMA: CAA formulation has previously been reported to be resistant to nonspecific protein adsorption, while also being capable of facilitating cell attachment and growth through by covalently attaching itself to proteins present in the ECM (Extra Cellular Matrix) like fibrinogen. S-S cross-linked TMA: CAA hydrogels were evaluated to determine their physical, non-fouling and biocompatibility characteristics. The performance of the S-S cross-linked hydrogel was directly compared to a TMA: CAA hydrogel formed with a diethylene glycol dimethacrylate (DEG) cross-linker due to similarities in the overall cross-linker lengths (10 versus 9 backbone atoms, respectively). Comparative study of these two cross linkers demonstrate similarity in the overall cross-linker length, the physical characteristics of the two hydrogels showed no significant differences, and the S-S cross-linked hydrogel exhibited identical non-fouling performance while demonstrating greater biocompatibility when compared to DEG based cross-linked hydrogels (**Figure 2.3**). These results suggest that an extensive family of peptide-based zwitterionic cross-linkers could easily address the limitations of ethylene glycol-based cross-linkers for *in vivo* applications.

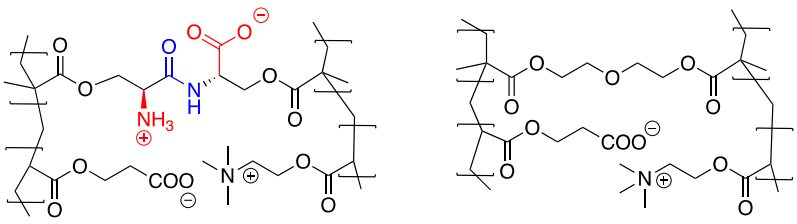

Figure 2. 3: Polyampholyte hydrogel formulations tested on the zwitterionic S-S cross-linker (left) and DEG cross-linker (right).

2.2. Experimental:

2.2.1 Materials:

Boc-L-Serine, *tert*-butyl N, N'-diisopropylcarbamimidate, trifluoroacetic acid (TFA), and 2-(1H-benzotriazol-1-yl)-1,1,3,3-tetramethyluronium hexafluorophosphate (HBTU) were purchased from AK Scientific (Union City, CA). N, N'-Diisopropylethylamine (DIPEA) and methacryloyl chloride were purchased from Acros Organics (Fair Lawn, NJ). Methacrylic acid was purchased from Alfa Aesar (Tewksbury, MA). Triethylamine was purchased from EMD Millipore (Burlington, MA). Ethyl acetate (EtOAc), hexanes, dichloromethane (DCM), N, N'-dimethylformamide (DMF), and concentrated hydrochloric acid (HCl) were purchased from Thermo Fisher (Waltham, MA). Deuterated solvents, chloroform ($CDCl_3$), and methanol-d_4 (CD_3OD) were purchased from Cambridge Isotopes (Tewksbury, MA). Fibrinogen from human plasma (FBG), ethylene glycol, phosphate buffered saline (PBS), DEG, TMA, CAA, ammonium persulfate (APS), sodium metabisulfite (SMS), N-(3-dimethylaminopropyl)-N'-ethylcarbodiimide hydrochloride (EDC), N-hydroxysuccinimide (NHS), bovine serum albumin-fluorescein isothiocyanate conjugate (FITC BSA), and sodium hydroxide (NaOH) were purchased from Sigma-Aldrich (St. Louis, MO). Alpha-minimum essential medium (α-MEM) with nucleosides, fetal bovine serum (FBS), sodium chloride (NaCl), and a live/dead cytotoxicity kit for mammalian cells were purchased from Thermo Fisher Scientific (Hampton, NH). Penicillin-streptomycin, tris hydrochloride, trypan blue, trypsin (0.25%) ethylenediaminetetraacetic acid (EDTA) (1x), trypsin soybean inhibitor, and paraformaldehyde were purchased from VWR (Radnor, PA). Ethanol was purchased from Greenfield Global (Toronto, Canada). MC3T3-E1 subclone 14 cells (batch number 61723894)

were purchased from the American Type Culture Collection (ATCC; CRL-2594) (Manassas, VA).

2.2.2 Characterization of molecules **2-4** to **2-10**:

All reaction products were fully characterized using ^{1}H and ^{13}C NMR experiments on either a Bruker AVANCE 300 or AVANCE 500 MHz instrument and results were obtained in $CDCl_3$ (referenced to 7.26 ppm for ^{1}H and 77.16 ppm for ^{13}C) or methanol-d_4 (referenced to 3.31 ppm for ^{1}H and 49.15 ppm for ^{13}C). Coupling constants (*J*) are provided in Hz. The multiplicities of the signals are described using the following abbreviations: s = singlet, br s = broad singlet, d = doublet, t = triplet, q = quartet, dd = doublet of doublets, dq = doublet of quartets, dsep = doublet of septets; tt = triplet of triplets, m = multiplet, app = apparent. All ^{1}H and ^{13}C NMR spectra can be found in Appendix A. Reaction progress was monitored by thin-layer chromatography on silica gel plates (60-F254), observed under UV light. Column chromatography was performed using silica gel (particle size 40–63 μm). High resolution mass spectrometry (HRMS) was performed on a Waters Q-Tof Premier Quadrupole-Time of Flight Mass Spectrometer.

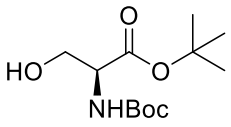

2-4

tert-butyl (tert-butoxycarbonyl)-L-serine **(2-4)**: A solution of commercially available Boc-*L*-serine (**2-3**) (1.00 g, 6.2 mmol) in DCM (100 mL) was added to t*ert*-butyl N, N'-diisopropylcarbamimidate (2.48 g, 12.4 mmol). The mixture was stirred in an ice bath for 30 min, and then allowed to warm to room temperature (RT) overnight with continual stirring. Hexanes (10 mL) were added, and the reaction was stirred for 15 min. The suspension was

filtered through a pad of celite to remove the diisopropylurea byproduct, and the filtrate was concentrated in vacuo. The resulting residue was purified by column chromatography (4:1 hexanes : EtOAc, R_f = 0.55) and concentrated in vacuo to yield 700 mg (55%) of a white solid. ^{1}H NMR (500 MHz, Methanol-d_4) δ 4.08 (t, *J* = 4.6 Hz, 1H), 3.81 (dd, *J* = 11.2, 5.0 Hz, 1H), 3.76 (dd, *J* = 11.1, 4.1 Hz, 2H), 1.48 (s, 9H), 1.45 (s, 9H). ^{13}C NMR (126 MHz, Methanol-d_4) δ 171.6, 157.9, 82.90, 80.6, 63.2, 58.0, 28.7, 28.3.

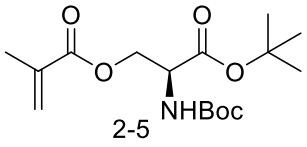

2-5

(S)-3-(tert-butoxy)-2-((tert-butoxycarbonyl)amino)-3-oxopropyl methacrylate **(2-5)**: Triethylamine (209.12 mg, 2.06 mmol) was added to a solution of *tert*-Butyl (*tert*-butoxycarbonyl)-*L*-serine (180 mg, 0.68 mmol) in DCM (5 mL), followed by dropwise addition of methacryloyl chloride (215.97 mg, 2.06 mmol) at 0 °C. The reaction mixture was slowly warmed to RT and stirred until TLC analysis (80% EtOAc/hexanes) indicated complete consumption of the starting material. Saturated aqueous $NaHCO_3$ was added to the crude mixture and the aqueous phase was extracted with EtOAc (3 x 10 mL), then the combined organic phases were washed with brine (10 mL), dried over $MgSO_4$, filtered, and concentrated in vacuo. The resulting residue was purified by column chromatography (7:3 hexanes: EtOAc, R_f = 0.5) to yield 172 mg (93% yield) of a yellow oil. ^{1}H NMR (300 MHz, Methanol-d_4) δ 6.11 (d, *J* = 1.8 Hz, 1H), 5.64 (d, *J* = 1.8 Hz, 1H), 4.43 – 4.37 (m, 3H), 1.92 (d, *J* = 1.4 Hz, 3H), 1.50 – 1.41 (m, 18H). ^{13}C NMR (126 MHz, Methanol-d_4) δ 170.9, 141.0, 126.7, 120.9, 83.2, 62.8, 57.1, 28.3, 28.2, 18.6.

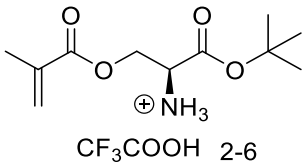

2-6

(S)-2-amino-3-(tert-butoxy)-3-oxopropyl methacrylate • *TFA* (**2-6**): tert-Butyl (tert-butoxycarbonyl)-*L*-serine methacrylate (2-6) (57.33 mg, 0.214 mmol) was dissolved in 1 mL DCM and 150 µl TFA was added at RT and stirred for 3 hours. The solvent was removed in vacuo to give a yellow oil and the material was used for the next step without any further purification. Yield: 44.13 mg of yellow oil (60%). HRMS-ESI (*m / z*): $[M+H]^+$ calcd for $C_{11}H_{19}NO_4$ 230.1392; found 230.1393.

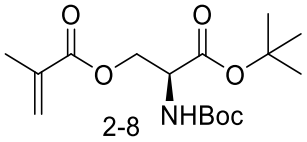

2-8

(tert-butoxycarbonyl)-L-serine methacrylate (**2-8**): A solution of methacrylic acid (258.27 mg, 3.0 mmol) in DMF (10 mL) was cooled to 0 °C to which HBTU (912.55 mg, 2.4 mmol) was added. The reaction mixture was warmed up to RT and stirred for an additional 1 hr. Boc-*L*-serine (**2-3**) (500 mg, 2.4 mmol) was then added to the reaction mixture followed by DIPEA (801.35 mg, 6.2 mmol) and stirred until the TLC indicated complete disappearance of the starting material. The reaction mixture was added to water and extracted with ethyl acetate (10 mL x 5), dried over $MgSO_4$ and purified using column chromatography (7:3 hexanes: EtOAc, R_f = 0.5) to give 140 mg (21% yield) of a yellow oil. ^{1}H NMR (300 MHz, Methanol-d_4) δ 6.12 (d, *J* = 1.6, 3.3 Hz, 1H), 5.63 (d, *J* = 1.6, 3.3 Hz, 1H), 4.48 (d, *J* = 8.5 Hz, 2H), 4.42 – 4.33 (m, 1H), 1.96 – 1.89 (m, 3H), 1.45 (d, *J* = 2.8 Hz, 9H). ^{13}C NMR (75 MHz, Methanol-d_4) δ 172.7, 168.3, 157.6, 137.3, 126.7, 80.8, 65.2, 54.1, 28.6, 18.3.

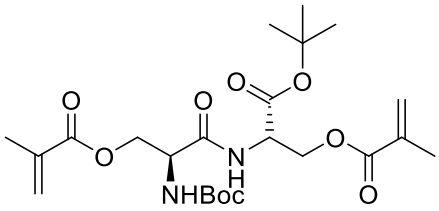

2-9

(S)-3-(tert-butoxy)-2-((tert-butoxycarbonyl)amino)-3-oxopropyl methacrylate **(2-9)**: **2-3** (71.45 mg, 0.261 mmol) was dissolved in DMF to which HBTU (99.50 mg, 0.261 mmol) was added in one portion. The reaction mixture was stirred for an hour before adding **2-8** (50 mg, 0.218 mmol) and DIPEA (87.36 mg, 0.676 mmol). The mixture was stirred for an additional three hours and then added to 10 mL of water and extracted with ethyl acetate (5 x 10 mL). The crude was then subjected to column chromatography (4:1 hexanes: EtOAc, R_f = 0.40) to yield 40 mg of a light-yellow oil (48% yield, telescopic over 2 steps). ^{1}H NMR (500 MHz, Methanol-d_4) δ 6.12 (dt, *J* = 2.0, 0.9 Hz, 2H), 5.65 (dt, *J* =2.0, 0.9 Hz, 2H), 5.62 – 5.61 (m, 1H), 4.68 (dd, *J* = 5.1, 3.9 Hz, 1H), 4.51 (d, *J* = 5.8 Hz, 1H), 4.46 (dd, *J* = 11.4, 5.2 Hz, 1H), 4.44 – 4.37 (m, 2H), 4.31 (dd, *J* = 11.2, 6.9 Hz, 1H), 1.92 (dd, *J* = 1.6, 1.0 Hz, 3H), 1.92 (dd, *J* = 1.6, 1.0 Hz, 3H), 1.46 (s, 9H), 1.45 (s, 9H). ^{13}C NMR (126 MHz, Methanol-d_4) δ 171.7, 169.3, 168.3, 168.1, 137.2, 126.9, 83.8, 81.0, 65.3, 65.0, 54.9, 53.9, 28.6, 28.2, 18.3.

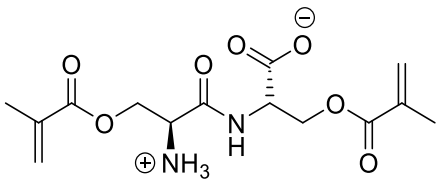

CF_3COOH **2-10**

O-methacryloyl-N-(O-methacryloyl-L-seryl)-L-serine HCl **(2-10)**: **2-9** (40 mg, 0.08 mmol) was dissolved in 4 mL of a 1:1 DCM: TFA solution and stirred at RT until all the starting material was consumed (24 h). The solvent was removed in vacuo and the TFA-salt was isolated as a

sticky oil. Yield: 19 mg (70%). ^{1}H NMR (500 MHz, Methanol-d_4) δ 6.18 (d, J =2.0, 1.2 Hz, 2H), 6.12 (d, J =2.0, 1.2 Hz, 2H), 5.64 (s, 1H), 4.81 (t, J = 4.4 Hz, 1H), 4.57 (d, J = 4.6 Hz, 2H), 4.50 (d, J = 4.5 Hz, 2H), 4.37 (t, J = 4.5 Hz, 1H), 1.92 (d, J = 6.5 Hz, 6H). ^{13}C NMR (126 MHz, Methanol-d_4) δ 171.5, 168.3, 167.9, 167.4, 162.2 (q, $J_{C\text{-}F}$ = 30 Hz, C=O), 137.1, 136.7, 127.7, 127.0, 116.6 (q, $J_{C\text{-}F}$ = 286 Hz, -CF_3), 64.8, 63.8, 53.5, 18.2.

The TFA salt (60 mg, 0.135 mmol**)** was suspended in 25 mL of 25 mM HCl and lyophilized for 16 hours two times to reveal 31 mg of the HCl salt (**2-10**) as a white solid (63% yield). ^{13}C NMR (126 MHz, MeOD) δ 171.4, 168.4, 167.9, 167.4, 137.3, 136.8, 127.9, 127.1, 64.9, 63.9, 53.6, 18.4. HRMS-ESI (*m / z*): $[M + H]^+$ calcd for $C_{14}H_{20}N_2O_7$ 329.13; found 329.135.

^{1}H and ^{13}C NMRs for these compounds can be found in **Appendix A**.

2.2.3 Hydrogel Synthesis:

Two different hydrogels were synthesized utilizing similar protocols and are referenced by DEG and S-S; (**Figure 2.3**) accordingly to which cross-linker species was used in the hydrogel. The DEG hydrogels were synthesized by mixing 4 mmol of TMA and 4 mmol of CAA monomers on a stir plate. Then 2 mL of a buffer solution composed of ethanol, ethylene glycol, and 6.7 M NaOH in a 1:1.5:1.5 ratio, respectively, was added to the monomer mixture. Next, 0.152 mmol of DEG cross-linker was added, resulting in a monomer to cross-linker ratio of 52.6 to 1. The solution was mixed well and then degassed with a vacuum pump for 30 seconds. Following degas, 32 µL of 40% (w/w) APS and 32 µL of 15% (w/w) SMS were added to initiate the polymerization reaction. The solution was gently mixed and then pipetted into a mold consisting of a 1/8’’ polytetrafluorethylene spacer clamped between two microscope

slides. The reaction proceeded for one hour at 60 °C. Following polymerization, the gel was removed from the mold and used in subsequent tests.

For the S-S hydrogels, a stock solution was created by mixing 8 mmol of TMA, 8 mmol of CAA, 4 mL of buffer solution (ethanol: ethylene glycol:6.7M NaOH in a 1:1.5:1.5 ratio) and 0.304 mmol of the S-S cross-linker. Again, the final monomer to cross-linker ratio was 52.6 to 1. The stock solution was continuously stirred on a stir plate until aliquots were removed for polymerization. For each hydrogel, 1/6 of the stock solution was mixed with 10.7 µL of 40% (w/w) APS and 10.7 µL of 15% (w/w) SMS to polymerize. The solution was mixed gently, then pipetted into the same hydrogel mold as described above and the polymerization reaction proceeded for one hour at 60°C. Following polymerization, the gel was removed from the mold and used in subsequent tests.

2.2.4 Hydrogel Characterizations

2.2.4.1 Swelling: Immediately following polymerization, length and width measurements of the hydrogels were collected using a caliper. All gels were then placed in petri dishes with pH 7.4 PBS for 24 hours. The hydrogels were remeasured after 24 hours of soaking. One set of samples continued to soak in pH 7.4 PBS for an additional 48 hours with additional measurements collected every 24 hours. Following data collection, the gels were used for the surface hardness and percent water weight experiments described below. Each experiment was completed in duplicate at a minimum and the experiment was repeated thrice (n=11).

2.2.4.2 Surface Hardness: After the hydrogels had soaked for 24 hours in pH 7.4, the gels were removed, and 00 shore hardness measurements were taken for each gel with a durometer. A minimum of two replicate samples were evaluated in each experiment and the experiment was repeated thrice (n=7).

2.2.4.3 Percent Weight: Following 24 hours soaking in pH 7.4 PBS, hydrogels were then soaked in DI water for an additional 48 hours. Afterwards, the gels were removed, patted dry, and weighed. The samples were then placed into a desiccator and monitored until they were no longer visibly shrinking. At this point, samples were weighed daily until their weight remained consistent. The wet and dry weights were then used to calculate the weight percent of water in the hydrogels. A minimum of two replicate samples were evaluated in each experiment and the experiment was repeated four times (n=9).

2.2.4.4 BSA Non fouling and Conjugation: After the hydrogels soaked in pH 7.4 PBS for 24 hours as described above, they were punched into 8 mm disks with a biopsy punch and each punch was placed into a single well of a 24-well plate. For the protein non-fouling assessment, the hydrogel samples were exposed to a 30 µL droplet of 1 mg/mL FITC BSA for 15 minutes. Then the samples were rinsed 5 times with pH 7.4 PBS followed by imaging with a Nikon Eclipse Ti-U light and fluorescent microscope with a 10x objective and NIS Elements BR 3.1 software.

Additional 8 mm samples were used for protein conjugation evaluation in a 24-well plate. Hydrogels were first exposed to 1 mL of pH 4.5 PBS for 15 minutes. After 15 minutes, the pH 4.5 PBS was removed, and 1 mL of 0.05 M EDC and 0.2 M NHS was added to each well for 7 minutes. Following the removal of the EDC/NHS solution, a 30 µL droplet of 1 mg/mL FITC BSA was placed on the top of each hydrogel for 15 minutes. Afterwards, each well received 1 mL of pH 8.9 PBS for 30 minutes followed by 1 mL of pH 7.4 PBS for 40 minutes. The resulting hydrogels were then imaged as described above. Three samples were run in each experiment and tests were run in triplicate for both the non-fouling and conjugation studies (n=9).

2.2.5 MC3T3-E1 Cell Studies:

2.2.5.1 Adhesion : MC3T3-E1 Cells were cultured as previously reported[71,72]. S-S and DEG hydrogels were synthesized and soaked in pH 7.4 PBS for 24 hours, as described above. Then 8 mm disks were punched with a biopsy punch and each sample was placed into a single well of a 24 well plate. One set of hydrogels underwent conjugation with FBG, using the procedures described above with 1 mL of 1 mg/mL FBG in place of the 30 µL droplet of 1 mg/mL FITC BSA.

As the conjugation procedure was occurring, three wells of TCPS were exposed to 1 mg/mL FBG for 30 minutes as a positive control surface. In addition, cells were prepared for seeding as done previously[72,73]. Briefly, confluent cells were rinsed twice with 10 mL tris buffer and then detached from the surface with 2 mL trypsin EDTA. The trypsin EDTA was then gently removed, and the cells were suspended in 5 mL of 5 mg/mL soybean trypsin inhibitor in PBS. The cell suspension was then centrifuged for 5 minutes at 1000 rpm. Next, the cells were washed twice with 8 mL of 1 mg/mL BSA in non-supplemented α-MEM, and then resuspended in 5 mL of non-supplemented α-MEM. Cells were counted with a hemocytometer and then diluted into two suspensions of $1x10^5$ cells/mL: one with non-supplemented α-MEM, and the other in media supplemented with 10% FBS.

Following conjugation and FBG adsorption, all the hydrogels and FBG adsorbed TCPS surfaces were rinsed trice with tris buffer. One mL of non-supplemented media with $1x10^5$ cells/mL was seeded into wells with FBG containing samples (conjugated and adsorbed). One mL of supplemented media (10% FBS) with $1x10^5$ cells/mL was seeded into wells with blank hydrogels (no prior protein) and onto blank TCPS surfaces (control). The well plate was placed

in an incubator for 2 hours, after which the cell solution was removed, and the cells were stained and imaged as described below.

2.2.5.2 Fluorescent Staining/Imaging: After 2 hours of incubation, the α-MEM was removed from all the wells. The cells were then stained with a fluorescent live-dead stain by adding 100 µL of 0.5 µM ethidium homodimer-1 and 1.5 µM calcein AM in PBS to each well. The well plate was returned to the incubator for 20 minutes, after which the samples were removed. Paraformaldehyde (4%; 0.5 mL) was added to each of the TCPS control conditions to fix the cells in those wells. The hydrogel samples were immediately imaged on a Nikon Spinning Disk Confocal Microscope with a 20x objective. After the hydrogels were imaged, the TCPS conditions were imaged on a Nikon Eclipse Ti-U light and fluorescent microscope with a 10x objective and NIS Elements BR 3.1 software. A minimum of 3 images were taken for each well, 3 samples were evaluated in each experiment, and the experiments were repeated in triplicate (n = 27).

2.2.6 Data Analysis:

Each experiment had a minimum of 2 independent samples in each experimental group and experiments were performed at least in triplicate. All measurements were compiled, and the mean and standard deviations are given throughout the results. Statistical analysis was completed with OriginPro 2017 using a one-way analysis of variance (ANOVA) and a Tukey post-hoc test. Statistical significance was determined at a probability value less than 0.05 ($p<0.05$).

2.3. Results and Discussion:

TMA: CAA hydrogels were synthesized with either DEG or S-S as the cross-linker species. While much of the literature on TMA: CAA hydrogels is based on triethylene glycol dimethacrylate[59,73–75], DEG has been used as it more closely mimics the overall length of the S-S cross-linker, so it was used as the ethylene glycol control cross-linker [21]. First, the physical properties of hydrogels formed with each cross-linker species were compared. Following hydrogel formation, samples were measured and then were allowed to soak for 24 hours in PBS to determine their extent of swelling. The DEG cross-linked hydrogels swelled ~70% larger than their initial size while the S-S cross-linked samples swelled ~73%, as summarized in **Table 1**. Previous investigations have demonstrated that ethylene glycol hydrogels reach swelling equilibrium after 24 hours and this was verified in this study for hydrogels cross-linked with both species. The results demonstrated no significant additional swelling occurred in either cross-linked system following the initial 24 hours (data not shown).

Experiment	DEG	S-S
Swelling (%)	70.86 ± 3.70	73.46 ± 4.11
Percent Hydration (%)	96.71 ± 0.19	97.09 ± 0.51
Shore 00 Hardness	22.43 ± 2.88	18.85 ± 4.91

Table 1: Physical characteristics of TMA: CAA hydrogels formed with DEG or S-S cross-linkers.

Water content is an important criterion for evaluating the biocompatibility of hydrogels, therefore, the percent hydration was determined for both sets of hydrogels. To evaluate the water content, full hydration (48 hours in DI water) and dehydration in a desiccator, hydrogels formed with both the DEG and the S-S cross-linkers exhibited percent hydration values of ~97% (**Table 1**). Mechanical property is also another important criterion

for implanted biomaterials therefore, the surface hardness for both hydrogel systems were measured using a Shore 00 hardness durometer after the samples had reached their equilibrium swollen state (24 hours of soaking in pH 7.4 PBS). As before, both hydrogels demonstrated similar properties, with the DEG and S-S cross-linked hydrogels measuring ~22 and ~19 Shore 00, respectively (**Table 1**). All three physical property assessment study for both DEG and S-S cross-linked hydrogels demonstrated no quantifiable differences in the results, indicating that the differences in the subsequent protein adsorption and cellular adhesion work are directly corelated to differences in the underlying chemistry.

The incentive of this work was to exhibit whether S-S zwitterionic cross-linker species can enhance the non-fouling performance of polyampholyte hydrogels compared to DEG based cross-linker. FITC BSA was chosen as an initial assessment guide as it has been previously used to show non-fouling properties of polyampholyte systems [22]. Following exposure to FITC BSA, hydrogel samples formed with both cross-linkers were evaluated using fluorescent microscopy and representative images are shown in **Figure 2.4**. The left-hand side of each image has been used as a corresponding control hydrogel to account for any background fluorescence that has not been exposed to FITC BSA, and this side of the image was used for background subtraction. The right-hand side is a hydrogel exposed to FITC BSA (the hydrogel intersection is marked with a white line for clarity) and any nonspecifically adsorbed protein is visualized with a green FITC emission. It has been shown in **Figure 2.4** that there is no measurable difference in the non-fouling performance of hydrogels formed with these two cross-linker species.

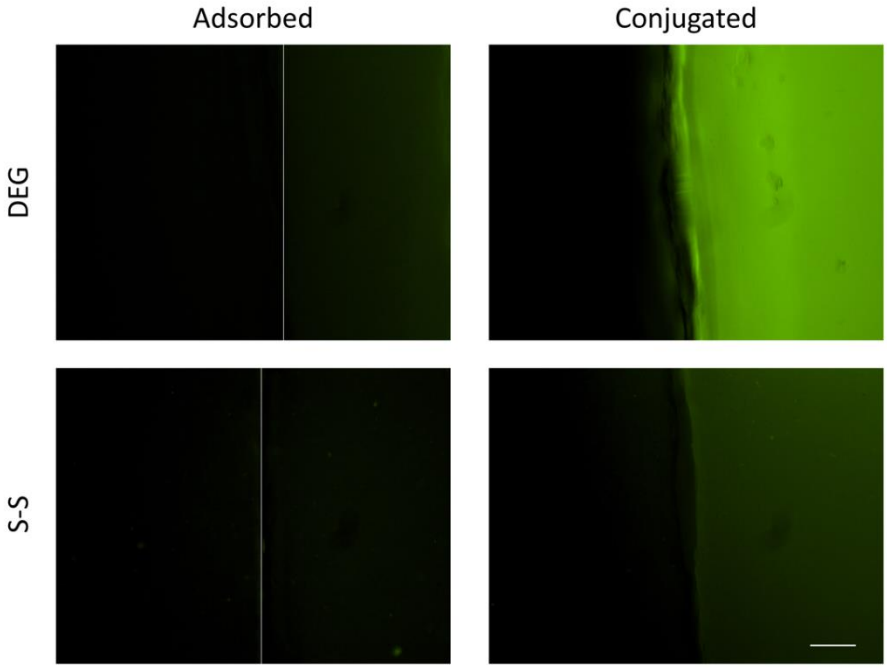

Figure 2. 4: Representative images of DEG and S-S hydrogels when FITC BSA is adsorbed or conjugated to the surface. A blank control hydrogel is present on the left-hand side in every image, and it was used for background subtraction. The scale bar represents 200 µm and is representative for all images.

In addition to non-fouling effect, the ability of a hydrogel to deliver biomolecules without impacting the underlying non-fouling properties is also important for directed cellular interactions[23]. However, subtle differences in hydrogel synthesis have been shown to influence the conjugation levels [22]. In order to verify the property of S-S cross-linker, FITC BSA was conjugated to the surface of hydrogels cross-linked with both DEG and S-S cross-linker using EDC/NHS conjugation chemistry, as reported previously.[76] Representative fluorescent microscopy images following conjugation are shown in **Figure 2.4** Similar to the earlier study, a blank hydrogel was again used as a control for background subtraction as shown on the left-

hand side of each image. The results in **Figure 2.4** demonstrate that both DEG and S-S hydrogels show a noticeable increase in fluorescence, indicating the successful conjugation of FITC BSA. However, S-S cross-linked hydrogels showed significantly less fluorescence than DEG cross-linked hydrogels indicating lower levels of conjugated protein. Although the protein conjugation conditions were not optimized, therefore it could be possible that alternative study might lead to greater levels of protein conjugation in the S-S cross-linked system.

While the previously studied hydrogels demonstrated resistance to nonspecific protein adsorption from single proteins in buffer failed to show similar activity in more complex environments [5,10]. The qualitative assessment of the non-fouling performance (**Figure 2.4**) indicated very similar behavior of the hydrogels cross-linked with either the DEG or S-S species. Hydrogels cross-linked by both cross-linkers were evaluated for their ability to prevent MC3T3-E1 cell adhesion even when in the presence of 10% FBS. The reason for the incorporation of 10% FBS complex protein solution is to mimic the conditions used for standard cell culture, which facilitates cell attachment and growth to TCPS. Following hydrogel exposure to cells in supplemented α-MEM for 2 hours, the cells were stained with a live-dead viability kit. The alive cells stained green with calcein AM indicating intracellular esterase activity consequently the dead cells stained red with ethidium homodimer driven by compromised cellular membranes. The representative confocal microscopy images shown in **Figure 2.5** indicate the presence of significantly fewer number of cells on both the DEG and S-S cross-linked systems. These results further support the non-fouling behavior of both hydrogel formulations within more complex systems.

Quantitative evaluation of multiple images from replicate samples confirms the representative confocal microscopy images as summarized in **Figure 2.6**. MC3T3-E1 cell adhesion to the positive TCPS control surface was extremely high (~250 cells/mm^2). Alongside the cells also demonstrated excellent viability. In contrast, cell adhesion levels were ~8 cells/mm^2 and ~2 cells/mm^2 for DEG and S-S cross-linked hydrogels respectively which is almost negligible. While the viability of these cells was strong, the non-fouling properties of both hydrogels in this complex environment is less which was indicated by these extremely low adhesion numbers.

The qualitative assessment of protein conjugation above indicated shows that the level of conjugated protein is more on the DEG cross-linked hydrogels (**Figure 2.5**) compared to the S-S cross-linked hydrogels. FBG, a well-known cell adhesion promoting protein was conjugated with both hydrogels in order to evaluate the bioactivity of the biomolecule being delivered from each platform, followed by exposure to MC3T3-E1 cells in non-supplemented media. No FBS was found in this evaluation to specifically isolate the cell adhesion bioactivity of the conjugated FBG. Representative confocal microscopy images of cell attachment to both hydrogel systems are shown in **Figure 2.5**. Cells are present on both hydrogels with similar rounded morphologies which shows the S-S hydrogel has higher initial cell adhesion levels.

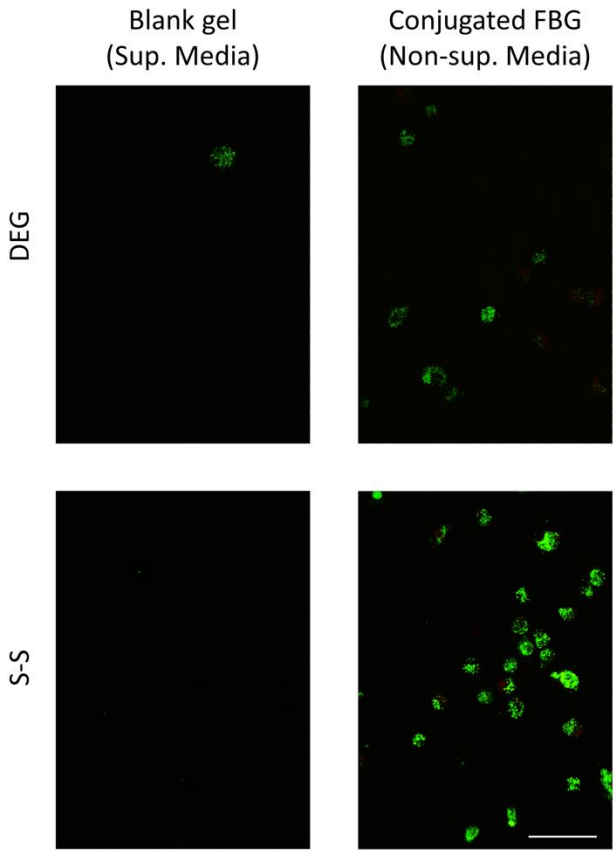

Figure 2. 5: Representative confocal microscopy images of MC3T3-E1 cell adhesion to polyampholyte hydrogels in the presence of supplemented media (left) and MC3T3-E1 cell adhesion to hydrogels with conjugated FBG (non-supplemented media, right). Cells are stained with a live-dead viability stain with live cells dyed green and dead cells dyed red. The scale bar represents 100 μm and is representative for all images.

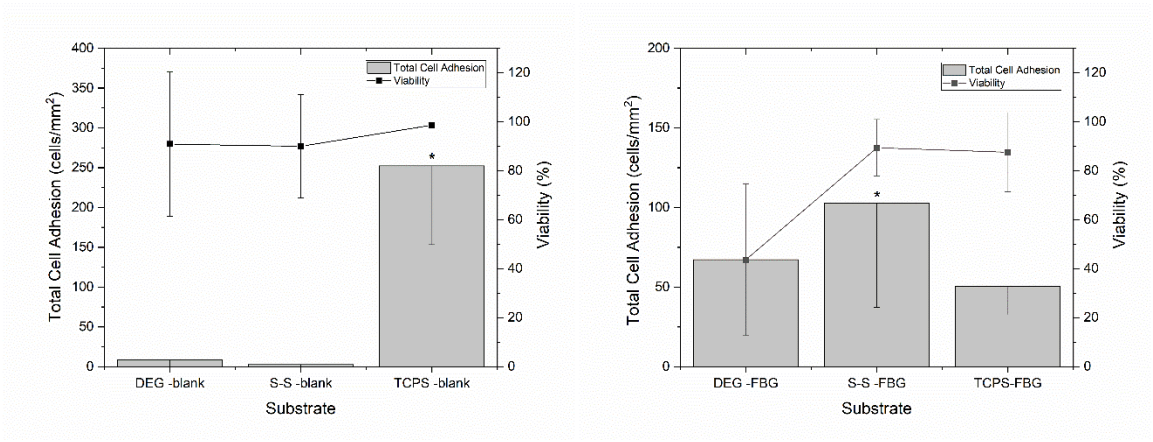

Figure 2. 6: Mean ± standard deviation of MC3T3-E1 cell adhesion to polyampholyte hydrogels with (a) supplemented media or (b) conjugated FBG (non-supplemented media). A * indicates a statistically significant difference from all other groups at a 95% confidence level ($p<0.05$).

Finally, the cell adhesion levels to polyampholyte hydrogels with conjugated FBG was quantified over multiple samples and images and the results are summarized in **Figure 2.6.** A positive control surface of FBG adsorbed to TCPS was included as a baseline for cell adhesion. Both DEG and S-S cross-linked polyampholyte hydrogels exhibit higher cell adhesion levels than that seen on the TCPS-FBG control surface. Further, the level of cell adhesion to the S-S cross-linked hydrogels (~103 cells/mm^2) is statistically greater than that seen for the other two groups. Additionally, the viability of cells attached to the S-S cross-linked hydrogels is ~90%, compared to the DEG cross-linked system which is significantly lower around ~44%. The combination of viability results and cell attachment levels, it can be easily seen that S-S cross-linked polyampholyte hydrogel demonstrates significantly better biocompatibility. Further, despite having lower protein conjugation levels (**Figure 2.4**), the S-S cross-linked polyampholyte hydrogel also promotes the most bioactive presentation of FBG. This may be

due to a more favorable conformation being imparted to FBG when bound to the S-S cross-linked hydrogel.

2.4. Conclusions:

The lack of availability of zwitterionic cross-linker species for in-vivo applications has been directly addressed in this work with the synthesis of a novel serine-serine dimethacrylate cross-linker species. Following synthesis and verification, the S-S cross-linker was incorporated into polyampholyte hydrogels and its impact on the overall hydrogel performance was compared with DEG based cross-linker. Both hydrogel systems demonstrated identical physical properties and non-fouling performance. Although the DEG cross-linked hydrogels demonstrated higher level of protein conjugation relative to S-S cross-linked hydrogels, the S-S cross-linked hydrogels demonstrated not only greater levels of cell adhesion to conjugated FBG, but also greater overall cell viability. Overall, these results suggest that there is tremendous potential of the S-S cross-linker as a polyampholyte hydrogels for tissue engineering applications.

Chapter 3: Outside-in strategy for the synthesis of peptide-based methacrylate and methacrylamide zwitterionic cross-linkers

Chakraborty, M.; Waynant, K. V.; Outside-in strategy for peptide-based methacrylate and methacrylamide Zwitterionic cross-linkers. *Synlett* **2022**, 33. 669-673.

Chapter 3 is a more detailed adaptation of a published manuscript

3.1 Introduction:

Serine based zwitterionic polyampholyte hydrogels have shown promise as functional biomaterial platforms with resistance to nonspecific protein adsorption (non-biofouling) which has been illustrated in the previous chapter.[77] However, very few zwitterionic cross-linkers exists that has controlled spacing between the charged group to provide an extended charge density throughout the 3D network.[78] The use of functionalizable amino acids allows the synthesis of a series of peptide-based zwitterionic methacrylate and methacrylamide cross-linkers. In this work the preparation of such dipeptide combinations as Ser-Lys, Lys-Ser, and Lys-Lys in zwitterionic bis(methacrylate/methacrylamide) cross-linkers has been described. Additionally, syntheses of the tripeptide Lys-Gly-Lys dimethacrylamide and Ser-Gly-Ser dimethacrylate has been described in order to highlight the utility of this method and its potential to increase the distance between zwitterionic components. The objective of this work is to yield a novel library of zwitterionic cross-linker species that will subsequently be evaluated for their impact on the biochemical and mechanical properties of polyampholyte hydrogels. Polyampholyte hydrogels have increasingly become a popular choice for regenerative therapies due to their non-fouling and low protein-adhesive properties.[79] Whereas most polymer matrices are defined by the monomer type and concentration, the 3D networks of hydrogels also rely upon the type and density of cross-linkers to provide the desired

chemical and physical properties.[78] The physical and chemical properties of the 3D networks of hydrogels shown to be highly dependent on the type and density of cross-linkers alongside monomer type and concentration. To date, only one group has demonstrated polymeric hydrogels that resist the foreign body response *in vivo*.[80,81] These polymers utilized zwitterionic monomers and the resulting hydrogels were formed with a carboxybetaine-based cross-linker resulting in fully zwitterionic systems.[82] However, the limited availability of zwitterionic cross-linker species restricts the ability to tune mechanical properties and adjustable degradation.[83,84] Moreover, minor structural changes of the zwitterionic species may have major huge impacts on its chemical structure and the resulting polymer performance.[85] The recently reported synthesis of the first peptide-based N-Ser-Ser-C zwitterionic cross-linker shows very promising data when it was incorporated into a polyampholyte hydrogel with improved non-fouling and protein-specific cell-adhesion properties compared with a DEG-based cross-linker of similar size (diethylene glycol dimethacrylate).[66] In this chapter those positive results were expanded on the first new knowledge generated from the previous project (**Figure 3.1**). This library of cross-linkers based on serine and lysine are investigated for their applicability in the polymeric biomaterial's community beyond the polyampholyte chemistries utilizing molecular-level control over the cross-linker type, length and charge spacing which will essentially lead to fully tunable polymer hydrogels for improving pre-existing biomaterials.

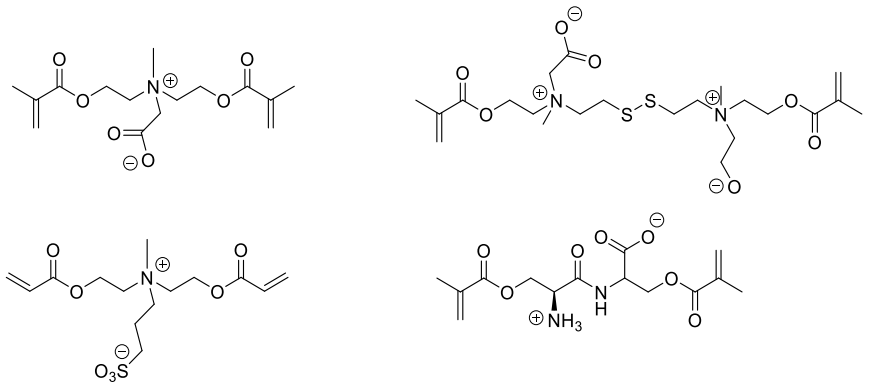

Figure 3. 1: Methacrylate and acrylate zwitterionic cross-linker incorporated into polyampholyte hydrogels

A novel class in zwitterionic cross-linker has emerged through peptide-based zwitterionic cross-linker development as shown in the previous chapter. In this series of cross-linkers the polymer type was varied (methacrylate/methacrylamide), which will be critical in regulating degradation rates through hydrolysis since methacrylamide has significantly lower rate of degradation compared to methacrylate. This series of cross-linkers offers tunable properties, such as the length of the cross-linker, and will permit variation of the distance between zwitterionic components through the incorporation of additional peptide units.[86] Peptide synthesis, with the aid of coupling agents is a well-established route for the formation of amide bond between a carboxylic acid and amine for both natural and non-natural amino acids. Moreover, a wide range of protecting-group manipulations are available for both the N- and C-termini of amino acids, which allows rapid access to both orthogonal and global protection/deprotection strategies. The increase in the abundance of polyampholytes has led to multiple reports on the addition of methacryloyl groups to functionalize amino acids (i.e., serine or lysine).[87,88] For the dipeptide N-Ser-Ser-C reported in the previous chapter, the cationic and anionic zwitterionic components are four bonds away from each other, with a rigid

peptide bond in between. The cationic ammonium component in these cross-linkers differs from other carboxy or sulfobetaine based cross-linkers because it is not quaternary and is therefore regulated by pH. Moreover, investigations of ethylene glycol (EG)-based cross-linker lengths have shown that minor changes in the overall type, length, and fixed charge spacing can have major effects on the physical properties of the resultant hydrogels.[37] It has been suggested that further alterations to polyampholyte chemistries based on monomer length, shape, functional groups, and skeletal attachment could diversify physical properties in bulk polyampholytes and have the potential to improve non-fouling behavior and to increase specific protein adhesion.[86,89] In the case of peptide-based zwitterionic cross-linkers, changes might include the relative polymer type (methacrylate or methacrylamide), the position of the carboxylate and ammonium functionalities, and the length of the cross-linker.

In this chapter, the outside-in strategy mentioned in the previous chapter has been extended to create a series of L-lysine and L-serine amino acid-based dimethacrylamide and mixed methacrylate/methacrylamide zwitterionic dipeptide cross-linkers **3-11** to **3-15** (**Figure 3.2**).

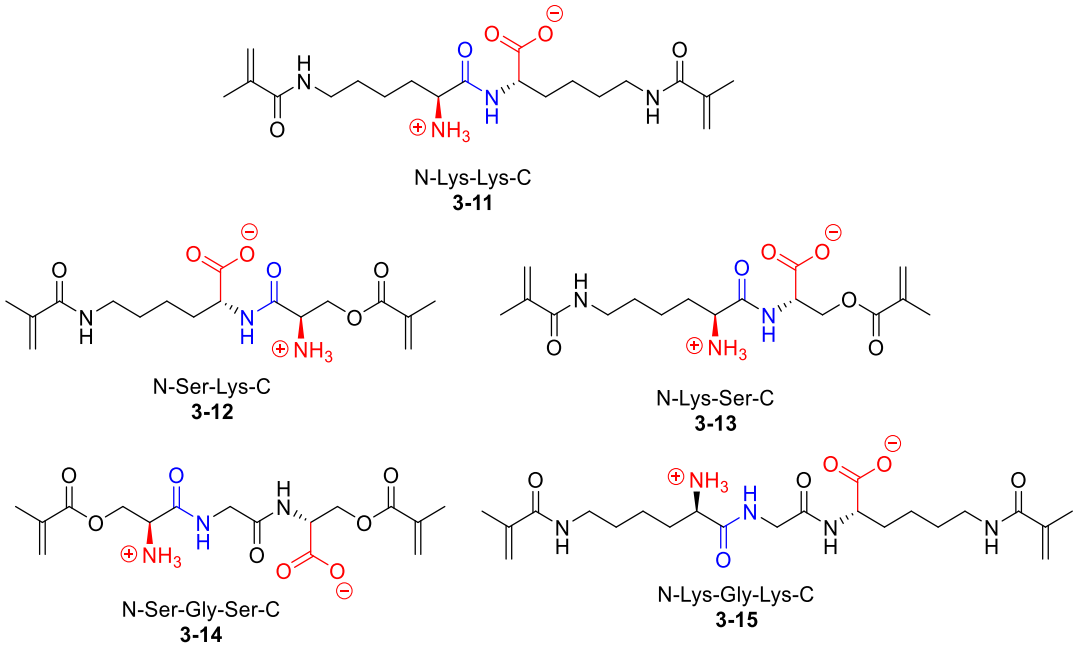

Figure 3. 2: A series of serine and lysine based zwitterionic cross-linker

Research shows that in polymer hydrogel systems, the distance between charges facilitates changes in the bulk material properties based on the strength of electrostatic interactions between charged regions of the cross-linker and the charged monomer functional group.[37] Most importantly, charge spacing will also influence the ionic solvation interactions throughout the 3D structure. These ionic solvation interactions lead to the formation of a tightly bound hydration layer that is critical for maintaining the non-fouling performance in complex environments. To extend the distance between the zwitterionic components the previous outside-in strategy has been employed to build tripeptide zwitterionic cross-linkers **3-14** and **3-15**, another key feature not available in carboxy- or sulfobetaine based cross-linkers.

Outside in strategy consists of three different synthetic strategies. Peptide coupling, methacrylation and chemo-selective protection and deprotection respectively. Whereas both methacrylation and peptide coupling are key to the development of these compounds, the choice of protecting groups was crucial due to the higher reactivity of the

methacrylate/methacrylamide group. For the selected outside-in strategy, N and C protected mono methacrylated products were coupled by a peptide coupling agent followed by a selective and global deprotection. The initially plan was to implement an orthogonal protection and deprotection strategy using acid labile group for the N-termini and base labile group for C termini. Even though protection of C and N termini were well tolerated through many different reaction schemes, attempted deprotections also cleaved the methacrylate group. For example, many known carboxylate ester-protection strategies including Bn, PMB, Me gave good yields followed by easy methacrylation step. However, conventional deprotection conditions such as hydrogenation using Pd-C/H_2, DDQ; LiOH/MeOH for Bn, PMB and Me deprotection respectively could not provide monomethacrylated carboxylate coupling partners. Non-conventional deprotection protocols such as NaSEt or Me_3SnOH/DCE failed to give the desired product as well.[90] However, *tert*-butyl esters (*t*-Bu), and Boc both of which could be deprotected under acidic conditions, where the rate of *tert*-butyl ester deprotection is more sluggish than Boc deprotection, allows Boc to be selectively deprotected under acidic environment. This strategy has proved valuable as chemo-selective protecting groups for the C-termini and N-termini respectively and has been utilized throughout all the outside-in cross-linker syntheses like the previous chapter, as shown below in **Scheme 3.1**.

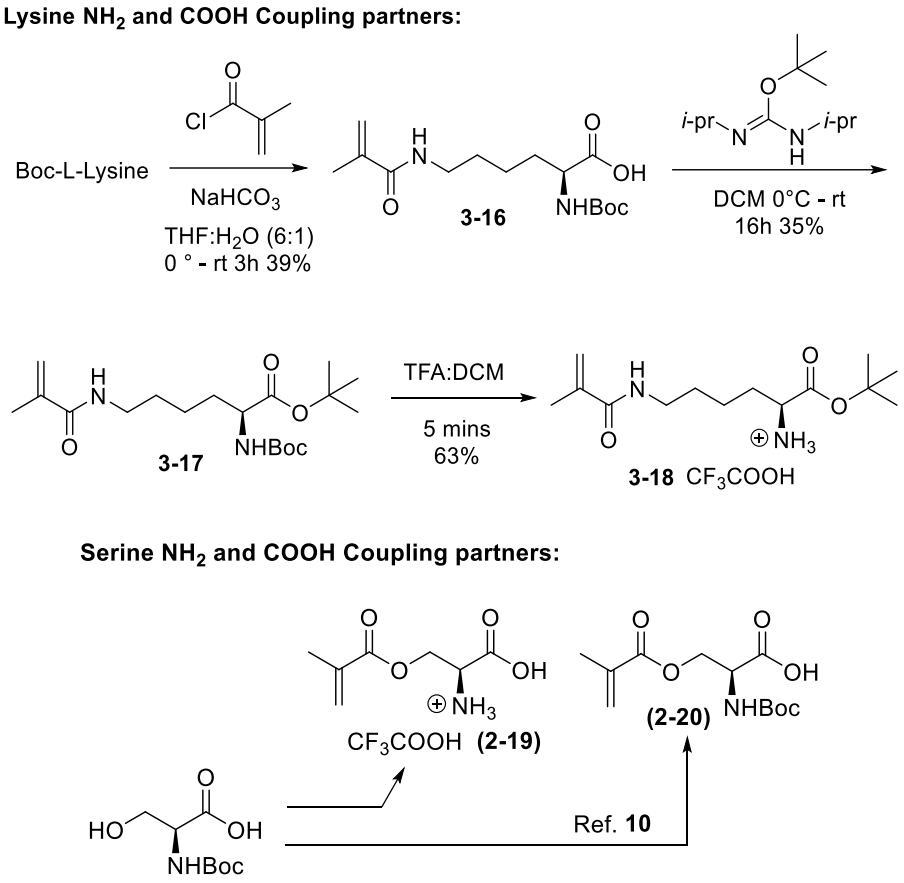

Scheme 3. 1: Synthesis of monomethacrylated serine and lysine coupling partners

3.2 Results and Discussion:

In order to synthesize dipeptide combinations N-Ser-Lys-C, N-Lys-Ser-C, and N-Lys-Lys-C in zwitterionic bis(methacrylate/methacrylamide) cross-linkers, first the synthesis of N and C coupling partner of serine and lysine was performed.[57] Synthesis of serine derivatives has been described in the previous chapter. The lysine C-terminus coupling partner **3-16** was obtained in 39% yield from commercially available *N*-Boc-L-lysine by treatment with $NaHCO_3$ and methacryloyl chloride in a 6:1 THF–H_2O solution.[91] Acid **3-16** was then protected at the C termini with *tert*-butyl group by treatment with *tert*-butyl *N*,*N*′-diisopropylcarbamimidate in DCM to afford **3-17**. Boc group was then selectively deprotected in presence of acid labile *tert*-butyl group through treatment with TFA in DCM to provide N

coupling partner **3-18** as its TFA salt in 63% yield by carefully monitoring the reaction with NMR. With all four required serine and lysine coupling partners in hand, three different mixed dimethacrylates for example *N*-Lys-Lys-C, *N*-Lys-Ser-C and *N*-Ser-Lys-C were obtained. The reactions are completed with the peptide bond formation reactions by using HBTU in DMF with DIPEA as a base at room temperature, obtaining the products in variable yields ranging from 47% to 55%. The final zwitterionic cross-linker dipeptide products **3-11**–**3-13** were prepared by global deprotection of dimethacrylated precursors **3-21**–**3-23**, respectively, through treatment with TFA in chloroform and were isolated as their TFA salts (**Scheme 3.2**).

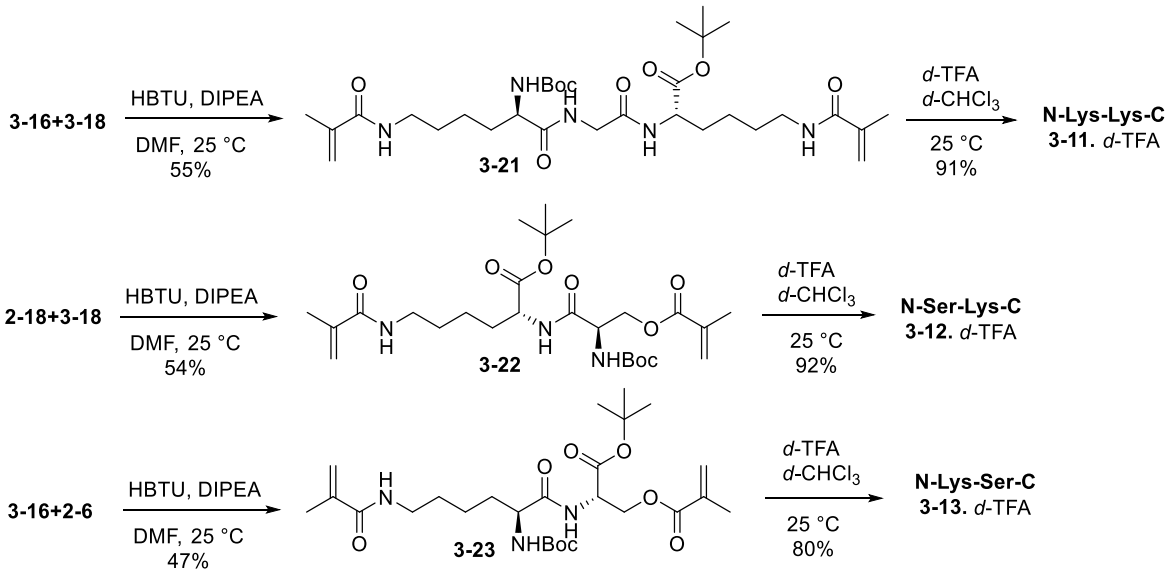

Scheme 3. 2: Peptide coupling of N and C coupling partners of Serine and Lysine to provide dimethacrylated precursors followed by global deprotection to provide a series of methacrylate and methacrylamide cross-linkers

The final deprotection step was monitored by NMR using TFA-*d*1 and $CDCl_3$ as solvents. Since Boc and *tert*-butyl both can be cleaved by TFA: DCM environment, it was necessary to monitor the reaction with the help of NMR. The peaks corresponding to Boc and *tert*-butyl rapidly falls off in TFA: DCM reaction environment with Boc group cleaves off first

compared to *tert*-butyl making it easy to monitor the reaction with the help of NMR. In **Scheme 3.2** Cross-linker **3-11** contains a dimethacrylamide species that might be more resistant to hydrolysis compared with dimethacrylates, while providing a longer length (14 atoms spacer meaning that there are 14 atoms between the polymerizable units) than that of N-Ser-Ser-C dimethacrylate cross-linker **10** reported in the previous chapter.[66] Compounds **3-12** and **3-13** provide an equal length (11 atoms) between polymerizable units but place the zwitterionic components on either the serine or lysine side, respectively which opens opportunities to see if these subtle differences affect the hydration layer and/or degradation rate.

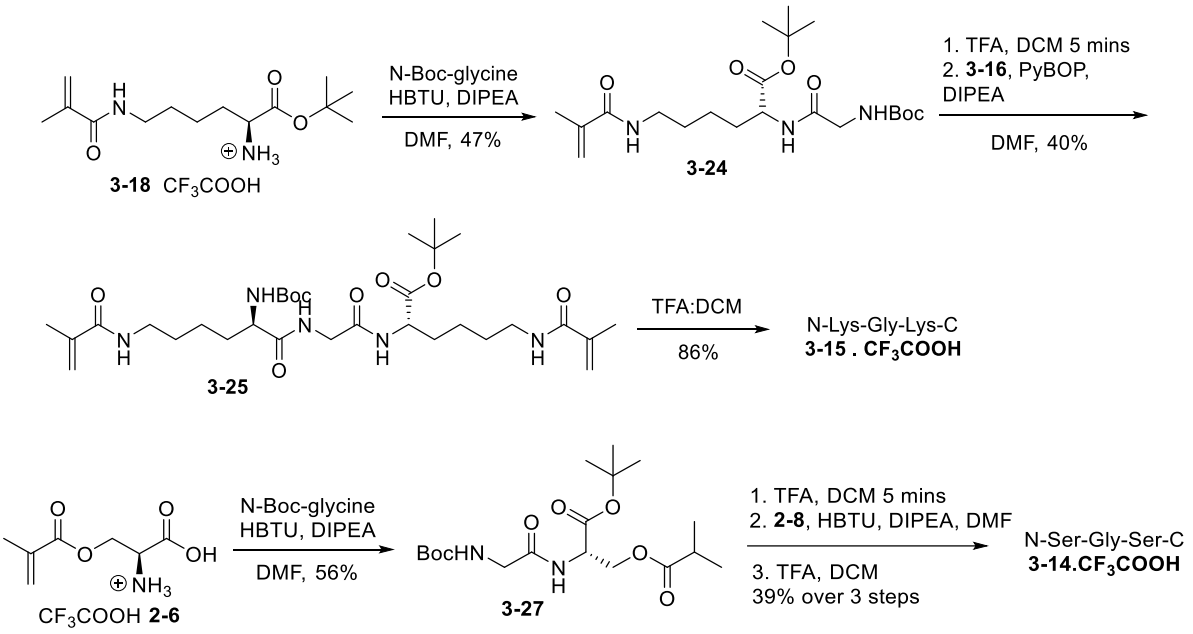

Scheme 3. 3: Synthetic Schemes to provide tripeptide cross-linkers

To complement the outside-in strategy and to highlight its utility, a glycine spacer was added between two lysine methacrylamide coupling partners, creating the N-Lys-Gly-Lys-C dimethacrylamide cross-linker **3-15**, and between two serine coupling partners to create the N-Ser-Gly-Ser-C dimethacrylate **3-14** (**Scheme 3.3**). The addition of glycine units increases the length between two zwitterionic charges, which will potentially affect the hydration layering.

With this family of zwitterionic cross-linkers, the aim is to determine how critical the atom spacing between charges in the zwitterionic cross-linker is on the properties of polyampholyte hydrogels during the completion of the Hydrogel Characterization Objectives. In these pair of compounds, the zwitterionic units are separated by seven atoms while the distance between charges, the length and type of the cross-linker are different. These are all very important variables that can contribute to understanding the physical and chemical properties of the polyampholyte synthesized from these monomeric units. N coupling partner of lysine **3-18** was coupled with commercially available *N* Boc-glycine in presence of HBTU to afford the Boc and *tert*-butyl protected dipeptide **3-24** in 47% yield. Rapid TFA deprotection removes the Boc group selectively and subsequent (1*H*-1,2,3-benzotriazol-1-yloxy) (tripyrrolidin-1-yl)phosphoniumhexafluorophosphate (PyBOP) coupling with **3-16** gave the fully protected dimethacrylated tripeptide **3-25**. In this case, the reason for using phosphonium coupling as opposed to HBTU as before is that PyBOP gave a slightly higher yield than HBTU. Finally, a final global deprotection using TFA and DCM produced cross-linker **3-15** as its TFA salt in 86% yield. The Ser-Gly-Ser dimethacrylate cross-linker was synthesized in a similar fashion starting from C protected serine **2-6** with coupling to *N*-Boc-glycine by using HBTU to give **3-27**. Followed by Boc deprotection, coupling of **2-8**, and global deprotection gave the tripeptide dimethacrylate **3-14** in 90% yield.

3.3 Experimental:

3.3.1 Characterization of molecules **3-11** to **3-27a**:

Procedures for compounds **2-6** and **2-8** can be found in a previous chapter.

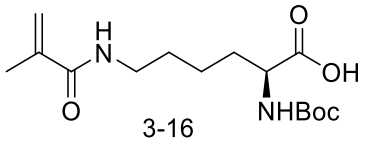

3-16

*ε-Methacryloyl-Boc L-Lysine (Bos-LysMA) (**3-16**)*: Boc-Lys-OH (5.0 g, 0.0203 mol) and sodium bicarbonate (3.44 g, 0.041 mol) were dissolved in 50 mL solution of THF and deionized water (6:1 v/v). Methacryloyl chloride (4 mL, 0.041 mol) in 10 mL THF was added dropwise to the solution over 30 min at 0 °C, and the reaction mixture was then warmed to room temperature and allowed to stir for 2 hrs. The solution was then concentrated under vacuum and the pH was adjusted to ∼2 using 0.1 M HCl aqueous solution. The mixture was extracted with ethyl acetate and the organic phase was collected and washed with 50 mL of deionized water. The organic phase was evaporated, and the resulting crude oil was purified using column chromatography (ethyl acetate) to obtain (2.51 g) of product **3-16** as a colorless oil in 39% yield and matched known characterization data.[2] ^{1}H NMR (500 MHz, Chloroform-d) δ 6.06 (d, *J* = 1.1 Hz, 1H), 5.70 (d, *J* = 1.1 Hz, 1H), 4.28 (s, 1H), 3.39 – 3.25 (m, *J* = 6.9 Hz, 2H), 1.95 (t, *J* = 1.1 Hz, 3H), 1.74 (ddt, *J* = 12.0, 9.6, 5.9 Hz, 2H), 1.63 – 1.53 (m, 2H), 1.50 – 1.45 (m, 2H), 1.44 (s, 9H). ^{13}C NMR (126 MHz, $CDCl_3$) δ 175.3, 169.2, 156.1, 139.9, 120.1, 80.3, 53.3, 39.4, 31.9, 29.1, 28.4, 22.5, 18.8. $[M+H]^+$ calcd for $C_{15}H_{26}N_2O_5$, 313.1763, found, 313.1754.

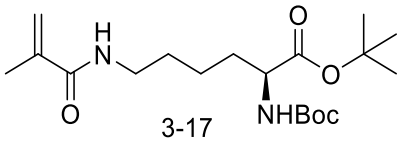

3-17

ε-Methacryloyl-t-butyl Boc L-Lysine (t-butyl-Boc-LysMA) (**3-17**): A solution of ε-methacryloyl-Boc L-lysine (**3-16**) (2.0 g, 6.3 mmol) in DCM (10 mL) was added to *tert*-butyl N, N'-diisopropylcarbamimidate (2.55 g, 0.0165 mol). The reaction was stirred in an ice bath for 30 min, and then allowed to warm up to RT and stirred for 12 hours. Hexanes (10 mL) was added to the reaction, and it was stirred for an additional 15 mins. The suspension was filtered through a pad of celite to remove the diisopropyl urea by-product, and the filtrate was concentrated under vacuo. The resulting residue was purified by column chromatography, (7:3 EtOAc/hexanes). Product containing fractions were concentrated in vacuo and *t*-butyl Boc-LysMA (**3-17**) was obtained as a clear oil (823 mg, Yield 35%). FTIR (cm^{-1}) 3336, 2977, 2931, 1702, 1657, 1524, 1366. 1H NMR (500 MHz, Chloroform-d) δ 5.86 (s, 1H), 5.65 (dt, *J* = 1.5 Hz, 1H), 5.29 (dt, *J* = 1.5 Hz, 1H), 5.05 (d, *J* = 8.2 Hz, 1H), 4.18 – 4.13 (m, 1H), 3.30 (td, *J* = 7.0, 5.7 Hz, 2H), 1.95 (dd, *J* = 1.6, 1.0 Hz, 3H), 1.83 – 1.74 (m, 2H), 1.67 – 1.55 (m, 3H), 1.45 (s, 9H), 1.43 (s, 9H), ^{13}C NMR (126 MHz, $CDCl_3$) δ 172.0, 168.6, 155.6, 140.4, 119.2, 82.0, 79.7, 53.9, 39.5, 32.8, 29.2, 28.5, 28.1, 22.7, 18.8. $[M+H]^+$ calcd for $C_{19}H_{34}N_2O_5$, 371.2546; found 371.2542.

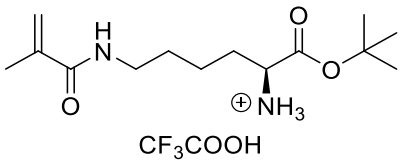

3-18

ε-Methacryloyl-t-butyl L-Lysine (t-butyl-LysMA•CF_3COOH) **(3-18)**: *t*-butyl-N-Boc-Lysine methacrylate (**3-17**) (100 mg, 0.270 mmol) was dissolved in 3.0 mL of DCM and 200 µL of TFA (giving 6% TFA) was added at room temperature and stirred for 3 hours. The solvent was removed in vacuo and product (**3-18**) was isolated as a light-yellow oil (65.70 mg, 63% yield) which was carried for the without any further purification. FTIR (cm^{-1}) 2943, 1739, 1155, 1676, 1537. ^{1}H NMR (500 MHz, Chloroform-*d*) δ 8.38 (s, 2H), 6.64 (d, *J* = 5.9 Hz, 1H), 5.71 – 5.63 (d, *J* = 5.9 Hz2H), 5.31 (tt, *J* = 2.7, 1.3 Hz, 2H), 3.89 (t, *J* = 6.2 Hz, 1H), 3.27 (q, *J* = 7.4, 6.3 Hz, 2H), 1.94 (dd, *J* = 1.6, 0.9 Hz, 2H), 1.90 (dd, *J* = 1.5, 0.9 Hz, 3H), 1.59 – 1.51 (m, 4H), 1.46 – 1.43 (m, 9H). ^{13}C NMR (126 MHz, $CDCl_3$) δ 169.6, 168.6, 161.3 (q, J_{C-F} = 43.19 Hz, C=O), 139.5, 120.5, 119.8 (q, J_{C-F} = 323.93 Hz, -CF_3), 84.5, 53.5, 39.2, 29.9, 28.7, 27.8, 21.9, 18.5. $[M+H]^+$ calcd for $C_{14}H_{26}N_2O_3$, 271.2022; found, 271.2016.

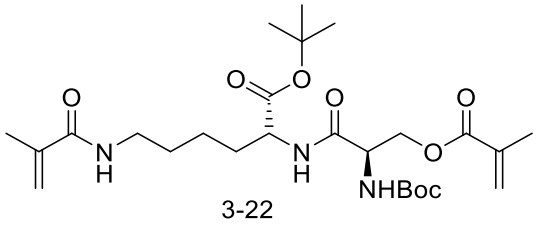

3-22

tert-butyl (tert-butoxycarbonyl) N-Ser-Lys-C dimethacrylate (**3-22**): Methacrylated N-Boc Serine (**2-8**) (67.4 mg, 0.246 mmol) was dissolved in DMF to which HBTU (93.53 mg, 0.246 mmol) was added in one portion. The reaction mixture was stirred for an hour before adding (**3-18**) (67.26 mg, 0.205 mmol) and DIPEA (82.1 mg, 0.635 mmol). The reaction was then

stirred for an additional 3 hours. The reaction mixture was then dissolved in water and extracted with ethyl acetate (5 x 10 mL). The crude reaction was then subjected to column chromatography (7:3 hexane: ethyl acetate) and collected 64.61 mg of (**3-22**) as a light-yellow oil (54% yield, telescoping over 2 steps). FTIR (cm^{-1}) 2979, 1720, 1658, 1533, 1168. ^{1}H NMR (500 MHz, Chloroform-*d*) δ 6.96 (d, *J* = 7.6 Hz, 1H), 6.09 (s, 1H), 5.67 (s, 1H), 5.57 (t, *J* = 1.7 Hz, 1H), 5.54 – 5.43 (m, 1H), 5.30 (s, 1H), 4.49 (s, 1H), 4.40 (ddt, *J* = 15.8, 11.4, 5.7 Hz, 3H), 3.27 (q, *J* = 6.0 Hz, 2H), 1.92 (d, *J* = 15.2 Hz, 6H), 1.83 (ddt, *J* = 14.4, 10.0, 5.6 Hz, 1H), 1.68 (ddt, *J* = 12.8, 8.6, 4.2 Hz, 1H), 1.61 – 1.49 (m, 2H), 1.43 (s, 18H), 1.39 – 1.29 (m, 2H). ^{13}C NMR (126 MHz, $CDCl_3$) δ 171.0, 169.07, 168.9, 167.1, 155.5, 140.1, 135.8, 126.5, 119.7, 82.4, 80.6, 64.7, 53.9, 52.8, 39.2, 32.2, 29.0, 28.4, 28.1, 22.4, 18.8, 18.3. $[M+Na]^+$ calcd for $C_{26}H_{43}N_3O_8Na$, 548.2948; found, 548.2961.

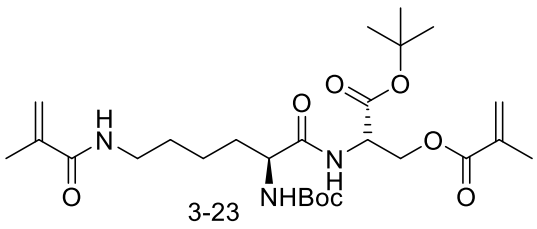

3-23

tert-butyl (tert-butoxycarbonyl) N-Lys-Ser-C dimethacrylate (**3-23**): ε-methacryloyl-Boc L-lysine (**3-16**) (914 mg, 2.91 mmol) was dissolved in DMF to which HBTU (1.1 g, 2.91 mmol) was added in one portion. The reaction mixture was stirred for an hour before adding (**2-6**) (832 mg, 2.42 mmol) and DIPEA (969.6 mg, 7.5 mmol). The reaction was then stirred for an additional 3 hours. The reaction mixture was dissolved in water and extracted with ethyl acetate (5 x 10 mL). The crude reaction mixture was then subjected to column chromatography (7:3 Hexanes: EtOAc) and the product (**3-23**) was collected as a yellow oil (598 mg, 47% yield, telescoping over 2 steps). FTIR (cm^{-1}) 2979, 1720, 1658, 1618, 1533, 1168. ^{1}H NMR (500

MHz, Chloroform-*d*) δ 6.98 (d, *J* = 7.9 Hz, 1H), 6.13 (d, *J* = 7.2 Hz, 1H), 6.05 (s, 1H), 5.64 (s, 1H), 5.54 (t, *J* = 1.8 Hz, 1H), 5.26 (d, *J* = 2.7 Hz, 2H), 4.68 (dt, *J* = 7.3, 3.5 Hz, 1H), 4.41 (d, *J* = 3.5 Hz, 2H), 4.07 (s, 1H), 3.27 (dtd, *J* = 22.6, 13.3, 6.6 Hz, 2H), 1.91 (s, 3H), 1.88 (s, 3H), 1.81 (p, *J* = 6.6 Hz, 1H), 1.62 (dt, *J* = 14.7, 7.9 Hz, 1H), 1.56 – 1.47 (m, 4H). 1.41 (s, 9H), 1.38 (s, 9H). ^{13}C NMR (126 MHz, $CDCl_3$) δ 172.1, 168.8, 168.1, 166.8, 155.8, 140.2, 135.6, 126.5, 119.4, 83.0, 80.06, 64.4, 54.4, 52.5, 38.9, 31.8, 29.1, 28.3, 27.9, 22.7, 18.7, 18.2. $[M+H]^+$ calcd for $C_{26}H_{43}N_3O_8$, 526.3128; found, 526.3154.

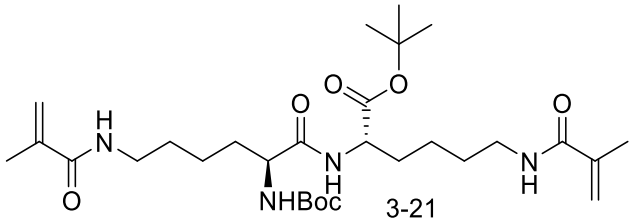

3-21

tert-butyl (tert-butoxycarbonyl) N-Lys-Lys-C dimethacrylate (**3-21**): ε-methacryloyl-Boc L-lysine (**3-16**) (116.3 mg, 0.37 mmol) was dissolved in DMF to which HBTU (167.30 mg, 0.44 mmol) was added in one portion. The reaction mixture was stirred for an hour before adding (**3-18**) (118 mg, 0.31 mmol) and DIPEA (148.25 mg, 1.147 mmol). The reaction was stirred for an additional 3 hours. The reaction mixture was dissolved in water and extracted with ethyl acetate (5 x 10 mL). The crude reaction was then subjected to column chromatography (8:2 ethyl acetate: hexane) to provide 60 mg of compound (**3-21**) as a white solid (Yield 55%, telescoping over 2 steps). FTIR (cm^{-1}) 2929, 2859, 1726, 1707, 1648, 1611, 1509, 1391, 1366. ^{1}H NMR (500 MHz, Chloroform-*d*) δ 6.78 (d, *J* = 7.7 Hz, 1H), 6.09 – 6.00 (d, *J* = 5.5 Hz, 2H), 5.68 (d, *J* = 5.5 Hz, 2H), 5.31 (dq, *J* = 6.5, 1.5 Hz, 2H), 4.41 (td, *J* = 7.8, 4.4 Hz, 1H), 4.15 – 4.03 (m, 1H), 3.30 (tt, *J* = 19.7, 6.8 Hz, 4H), 1.96 (t, *J* = 1.4 Hz, 6H), 1.90 – 1.78 (m, 3H), 1.69 (tt, *J* = 14.0, 8.0 Hz, 4H), 1.61 – 1.52 (m, 5H), 1.44 (dd, *J* = 8.5, 1.2 Hz, 18H). ^{13}C

NMR (126 MHz, $CDCl_3$) δ 172.1, 171.3, 168.9, 168.8, 155.9, 140.3, 140.2, 119.5, 119.5, 82.2, 54.5, 52.6, 39.2, 39.1, 31.9, 29.2, 28.4, 28.1, 22.7, 22.4, 18.9. $[M+Na]^+$ calcd for $C_{29}H_{50}N_4O_7Na$, 589.3577; found, 589.3605. mp 150 °C.

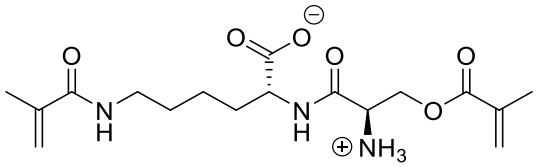

3-12 CF_3COOH

N-Ser-Lys-C •*CF_3COOH* (**3-12**): Compound **(3-22**) (10 mg, 0.019 mmol) was dissolved in 1 mL of 1:1 *d_1*-TFA: *d*-$CHCl_3$ and was stirred for an hour at room temperature while monitoring by NMR. The solvent was then removed in vacuo and the product (8.42 mg) was collected as a colorless oil. Yield 92%. FTIR (cm^{-1}) 2934, 2866, 1663, 1606, 1537, 1177, 1134. ^1H NMR (500 MHz, Methanol-d_4) δ 6.21 (s, 1H), 5.68 (d, *J* = 9.2 Hz, 2H), 5.36 (d, *J* = 9.2 Hz, 2H), 4.55 (qd, *J* = 12.4, 4.8 Hz, 2H), 4.43 (dd, *J* = 8.9, 4.8 Hz, 1H), 4.30 (ddd, *J* = 5.7, 3.8, 1.8 Hz, 1H), 3.24 (t, *J* = 7.1 Hz, 2H), δ 1.94 (dd, *J* = 5.3, 1.3 Hz, 6H), 1.81 – 1.70 (m, 2H), 1.57 (qd, *J* = 7.2, 3.2 Hz, 2H), 1.49 – 1.36 (m, 2H). ^{13}C NMR (126 MHz, Methanol-d_4) δ 174.5, 171.4, 167.8, 167.1, 162.2 (q, J_{C-F} = 36.55 Hz, C=O), 141.4, 136.7, 127.7, 121.1, 120.3, 118.8, 116.5 (q, J_{C-F} = 291.61 Hz, -CF_3), 63.8, 53.9, 53.5, 40.2, 31.9, 29.9, 24.1, 18.8, 18.3. $[M+H]^+$ calcd for $C_{17}H_{27}N_3O_6$, 370.1978; found, 370.1978.

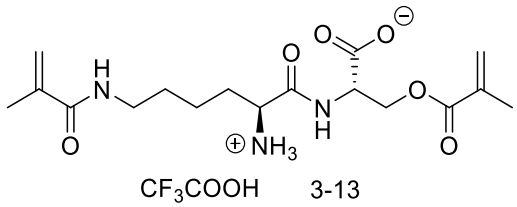

N-Lys-Ser-C •*CF_3COOH* (**3-13**): Compound **3-23** (10 mg, 0.019 mmol) was dissolved in 1 mL of 1:1 d_1-TFA: *d*-$CHCl_3$ and was stirred for an hour at room temperature while monitoring by NMR. The solvent was then removed in vacuo and the product (8.24 mg) was collected as a colorless oil. Yield 80%. FTIR (cm^{-1}) 2926, 1665, 1538, 1178, 1135. ^{1}H NMR (500 MHz, Methanol-d_4) δ 6.13 (d, *J* = 1.3 Hz, 2H), 5.69 (d, *J* = 1.3 Hz, 2H), 5.66 (t, *J* = 1.6 Hz, 1H), 5.41 – 5.35 (m, 1H), 4.82 (d, *J* = 4.3 Hz, 1H), 4.50 (dd, *J* = 4.4, 1.1 Hz, 2H), 3.93 (t, *J* = 6.4 Hz, 1H), 3.26 (td, *J* = 6.9, 4.7 Hz, 2H), 1.93 (q, *J* = 1.4 Hz, 6H), 1.87 (dtd, *J* = 15.4, 8.2, 7.5, 2.5 Hz, 2H), 1.60 (dd, *J* = 7.8, 6.4 Hz, 2H), 1.52 – 1.47 (m, 2H).^{13}C NMR (126 MHz, Methanol-d_4) δ 171.5, 171.3, 170.3, 168.2, 163.0 (q, $J_{C\text{-}F}$ = 36.23 Hz, C=O),162.6, 162.3, 161.8, 141.3, 137.2, 126.9, 122.3, 120.4, 119.1, 116.3 (q, $J_{C\text{-}F}$ = 281.52 Hz, -CF_3), 114.1, 64.9, 54.2, 53.3, 40.0, 32.3, 30.1, 22.9, 18.8, 18.3. $[M-H]^-$ calcd for $C_{17}H_{27}N_3O_6$, 368.1822; found, 368.1823.

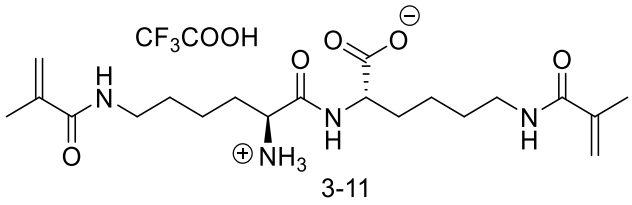

N-Lys-Lys-C •*CF_3COOH* **(3-11**): Compound (**3-21**) (10 mg, 0.017 mmol) was dissolved in 1 mL of 1:1 d_1-TFA: *d*-$CHCl_3$ and was stirred for an hour at room temperature while monitoring by NMR. The solvent was then removed in vacuo and the product (**3-11**) (8.1 mg) was collected as a colorless oil. Yield 91% FTIR (cm^{-1}) 2932, 2870, 1724, 1654, 1604, 1534, 1179, 1134.^{1}H

NMR (500 MHz, Methanol-d_4) δ 5.68 (d, J = 7.4 Hz, 2H), 5.36 (d, J = 7.4 Hz, 2H), 4.42 (dd, J = 9.0, 4.8 Hz, 1H), 3.89 (t, J = 6.4 Hz, 1H), 3.25 (q, J = 7.4 Hz, 4H), 1.93 (d, J = 1.3 Hz, 6H), 1.92 – 1.72 (m, 4H), 1.63 – 1.56 (m, 3H), 1.53 – 1.40 (m, 5H). ^{13}C NMR (126 MHz, Methanol-d_4) δ 174.7, 171.4, 170.2, 161.6 (q, $J_{C\text{-}F}$ = 37.93 Hz, C=O), 141.4, 141.3, 120.7, 120.4, 120.3 (q, $J_{C\text{-}F}$ = 287.47 Hz, -CF_3), 54.3, 53.7, 40.2, 40.0, 32.3, 31.9, 30.0, 29.9, 24.2, 22.9, 18.8. [M-H]$^-$ calcd for $C_{20}H_{34}N_4O_5$, 409.2451; found, 409.2461.

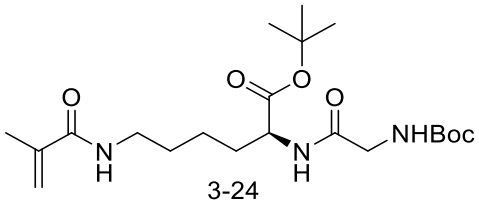

3-24

ε-methacryloyl-tert-butyl-Lysine (tert-butoxycarbonyl) glycine (t-butyl-Lys-N-Boc-Gly) (**3-24**): N-Boc-Glycine (100 mg, 0.57 mmol) was dissolved in DMF to which HBTU (178.24 mg, 0.47 mmol) was added in one portion. The reaction mixture was stirred for an hour before adding **3-18** (80.9 mg, 0.47 mmol) and DIPEA (188.31 mg, 1.45 mmol). The reaction was stirred for an additional 3 hours. At that time, the reaction mixture was diluted with water and extracted with ethyl acetate (5 x 10 mL). The crude reaction was then subjected to column chromatography (2:1 ethyl acetate: hexane) providing the coupled product (**3-24**) as a colorless oil (94.3 mg, 47% yield, telescopic over 2 steps). FTIR (cm^{-1}) 2977, 2932, 1718, 1655, 1615, 1522, 1366, 1155. ^{1}H NMR (500 MHz, Chloroform-d) δ 6.67 (d, J = 7.9 Hz, 2H), 6.02 (d, J = 7.9 Hz, 2H) 5.30 (dd, J = 1.6, 1.2 Hz, 1H), 5.24 (s, 1H), 4.47 (td, J = 7.9, 4.7 Hz, 1H), 3.80 (dd, J = 6.0, 1.7 Hz, 2H), 3.31 – 3.24 (m, 2H), 1.95 (dd, J = 1.6, 0.9 Hz, 3H), 1.89 – 1.79 (m, 1H), 1.71 – 1.51 (m, 4H), 1.43 – 1.34 (m, 1H). ^{13}C NMR (126 MHz, $CDCl_3$) δ 171.4, 169.3,

168.8, 156.1, 140.3, 119.4, 82.42, 80.34, 52.5, 44.4, 39.2, 32.2, 29.1, 28.4, 28.1, 22.4, 18.8. $[M+H]^+$ calcd for $C_{21}H_{37}N_3O_6$, 428.2772; found, 428.2761.

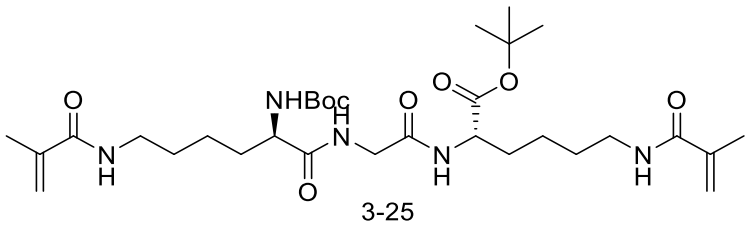

3-25

ε-methacryloyl-N-Boc-Lys-Gly tert-butyl N-Lys-Glycine (**3-25**): Compound (**3-24)** (100 mg, 0.23 mmol) was dissolved in 0.4 mL TFA in 2 mL DCM and stirred for an hour at room temperature. The solvent was then removed in vacuo and the product was collected as a light-yellow oil and was used as is for the next step without any further purification. Yield: 82.2 mg (81%). $[M+H]^+$ calcd for $C_{16}H_{29}N_3O_4$, 328.2236; found, 328.2247.

Compound (**3-16**) (48 mg, 0.152 mmol) was dissolved in DMF to which PyBOP (93.7 mg, 0.18 mmol) was added in one portion. The reaction mixture was stirred for an hour before adding the deprotected salt (55.8 mg, 0.13 mmol) and DIPEA (52.08 mg, 0.40 mmol). The reaction was stirred for an additional 3 hours, diluted with water, and extracted with ethyl acetate (5 x 10 mL). The crude reaction was then subjected to column chromatography (9:1 ethyl acetate: methanol) to yield 49%, telescopic over 2 steps (40 mg). FTIR (cm^{-1}) 2977, 2932, 1719, 1665, 1622, 1155. ^{1}H NMR (500 MHz, Chloroform-*d*) δ 7.10 (s, 1H), 6.88 (d, *J* = 7.9 Hz, 1H), 6.19 (d, *J* = 7.9 Hz, 2H), 5.69 (dt, *J* = 2.3, 1.2 Hz, 2H), 5.31 (q, *J* = 1.5 Hz, 2H), 4.42 (td, *J* = 7.9, 4.7 Hz, 1H), 4.08 – 3.87 (m, 2H), 3.29 (dp, *J* = 13.4, 6.8 Hz, 5H), 1.95 (dq, *J* = 2.0, 1.0 Hz, 6H), 1.92 – 1.79 (m, 3H), 1.76 – 1.62 (m, 3H), 1.62 – 1.48 (m, 6H), 1.43 (d, *J* = 9.2 Hz, 18H). ^{13}C NMR (126 MHz, $CDCl_3$) δ 172.9, 171.2, 169.1, 168.7, 156.1, 140.1, 119.9,

82.4, 80.38, 54.8, 52.8, 43.3, 39.3, 39.0, 31.8, 29.2, 29.2, 28.513, 28.2, 22.7, 22.5, 18.9. $[M+Na]^+$ calcd for $C_{31}H_{53}N_5O_8Na$, 646.3792; found, 646.3813.

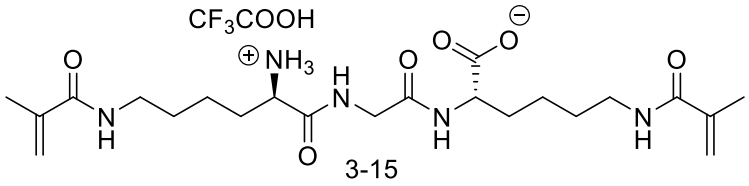

N-Lys-Gly-Lys dimethacrylate •CF_3COOH (**3-15**): The purified globally protected compound (**3-25**) (10 mg, 0.16 mmol) was dissolved in 1:2 d_1-TFA: d-$CHCl_3$ and was stirred at room temperature while monitoring by NMR. The solvent was then removed in vacuo and the product (**3-15**) was collected as a colorless oil. (8 mg, 86% yield). FTIR (cm^{-1}) 2935, 1736, 1655, 1609, 1534, 1176, 1132. ^{1}H NMR (500 MHz, Methanol-d_4) δ 5.70 – 5.65 (m, 2H), 5.36 (dq, J = 6.3, 1.5 Hz, 2H), 4.39 (dd, J = 8.7, 4.9 Hz, 1H), 3.98 (d, J = 6.8 Hz, 1H), 3.90 – 3.85 (m, 2H), 3.29 – 3.20 (m, 5H), 1.93 (d, J = 1.3 Hz, 6H), 1.91 – 1.84 (m, 4H), 1.76 – 1.70 (m, 2H), 1.58 (ddd, J = 15.2, 7.6, 3.3 Hz, 4H), 1.49 – 1.39 (m, 2H). ^{13}C NMR (126 MHz, Methanol-d_4) δ 175.2, 171.4, 171.3, 170.8, 170.6, 162.2 (q, $J_{C\text{-}F}$ = 35.11 Hz, C=O), 141.4, 141.3, 130.5 (q, $J_{C\text{-}F}$ = 292.75 Hz, -CF_3) 120.4, 120.2, 54.5, 53.6, 43.0, 40.3, 39.9, 32.3, 32.1, 30.0, 29.9, 24.2, 23.1, 18.8. 18.8 $[M-H]^-$ calcd for $C_{22}H_{37}N_5O_6$, 466.2666; found, 466.2673.

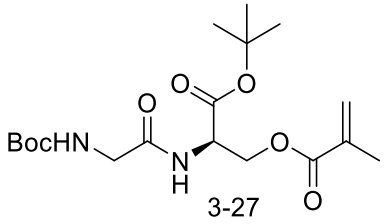

ε-methacryloyl-Ser-Gly tert-butyl (tert-butoxycarbonyl) N-Ser-Gly-C (**3-27**): N-Boc Glycine (292 mg, 1.66 mmol) was dissolved in DMF to which HBTU (640 mg, 1.66

mmol) was added in one portion. The reaction mixture was stirred for an hour before adding (**2-6**) (400 mg, 1.4 mmol) and DIPEA (560 mg, 4.4 mmol). The reaction was then stirred for an additional 3 hours. The reaction mixture was dissolved in water and extracted with ethyl acetate (5 x 10 mL). The crude reaction was then subjected to column chromatography (7:3 hexane: ethyl acetate) and (**3-27**) was collected as a yellow oil (100 mg, 56% yield, telescopic over 2 steps). FTIR (cm^{-1}) 3313, 2978, 1720, 1509, 1144. 1H NMR (500 MHz, Chloroform-*d*) δ 6.83 (d, *J* = 7.6 Hz, 1H), 6.09 (dq, *J* = 1.9, 1.0 Hz, 1H), 5.58 (p, *J* = 1.6 Hz, 1H), 4.76 (dt, *J* = 7.4, 3.4 Hz, 1H), 4.50 – 4.39 (m, 2H), 3.83 (dd, *J* = 15.3, 10.3 Hz, 2H), 1.92 (dd, *J* = 1.6, 1.0 Hz, 3H), 1.45 (s, 9H), 1.45 (s, 9H). ^{13}C NMR (126 MHz, $CDCl_3$) δ 169.4, 168.2, 166.9, 156.1, 135.7, 126.5, 83.3, 80.51, 64.6, 52.5, 46.0, 44.4, 28.4, 28.0, 18.3. $[M+H]^+$ calcd for $C_{18}H_{30}N_2O_7$, 387.2131; found, 387.2133.

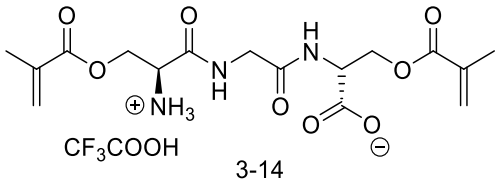

3-14

N-Ser-Gly-Ser dimethacrylate •*CF_3COOH* (**3-14**): Compound (**3-27**) (100 mg, 0.258 mmol) was dissolved in 2:1 DCM: TFA at RT and stirred for 3 hours. The solvent was removed in vacuo and the product was isolated as a light-yellow oil was used as is for the next step without any further purification. Yield 80% (82 mg). Methacrylated Boc-Serine (**2-8**) (100 mg, 0.366 mmol) was dissolved in DMF to which HBTU (139.2 mg, 0.366 mmol) was added in one portion. The reaction mixture was stirred for an hour before adding the product from the last step (122 mg, 0.305 mmol) and DIPEA (122.1 mg, 0.945 mmol). The reaction was then stirred for an additional 3 hours. The reaction mixture was dissolved in water and

extracted with ethyl acetate (5 x 10 mL). The crude reaction was then subjected to column chromatography (2:1 hexane: ethyl acetate) and collected as a white solid (90 mg, 54% yield). ^{1}H NMR (500 MHz, Chloroform-*d*) δ 7.01 (t, *J* = 5.3 Hz, 1H), 6.86 (d, *J* = 7.6 Hz, 1H), 6.10 (d, *J* = 8.7 Hz, 2H), 5.63 – 5.54 (m, 2H), 5.39 (d, *J* = 7.4 Hz, 1H), 4.73 (dt, *J* = 7.3, 3.6 Hz, 1H), 4.46 (d, *J* = 3.0 Hz, 3H), 4.40 (dd, *J* = 11.3, 4.9 Hz, 1H), 4.09 (dd, *J* = 16.7, 5.6 Hz, 1H), 3.93 (dd, *J* = 16.8, 5.0 Hz, 1H), 1.93 – 1.91 (m, 6H), 1.45 (s, 9H), 1.44 (s, 9H). ^{13}C NMR (126 MHz, $CDCl_3$) δ 169.8, 168.2, 168.0, 167.1, 155.6, 135.8, 135.6, 126.8, 126.7, 83.4, 80.9, 64.5, 64.4, 54.0, 52.8, 43.7, 28.4, 28.0, 18.4, 18.3. $[M+Na]^+$ calcd for $C_{25}H_{39}N_{30}O_{10}Na$, 564.2544; found, 564.2533. mp 91°C. Finally, the dimethacrylated precursor (10 mg, 0.018 mmol) was dissolved in 1 mL of 1:1 d_1-TFA: *d*-$CHCl_3$ and was stirred for an hour at room temperature while monitoring by NMR. The solvent was then removed in vacuo and the product (**3-14**) was collected as a light-yellow oil. (8.1 mg, 90% yield, telescopic over 2 steps). FTIR (cm^{-1}) 3204, 2926, 1698, 1539, 1149. ^{1}H NMR (500 MHz, Methanol-d_4) δ 6.21 (t, *J* = 1.3 Hz, 1H), 6.11 (dt, *J* = 6.3, 1.3 Hz, 1H), 5.71 (t, *J* = 1.5 Hz, 1H), 5.65 (dq, *J* = 3.1, 1.6 Hz, 1H), 4.83 – 4.78 (m, 1H), 4.60 – 4.40 (m, 6H), 4.33 (dd, *J* = 5.7, 3.9 Hz, 1H), 4.10 – 3.94 (m, 2H), 1.95 (t, *J* = 1.3 Hz, 3H), 1.93 – 1.91 (m, 3H). ^{13}C NMR (126 MHz, Methanol-d_4) δ 171.9, 170.8, 168.3, 167.8, 167.6, 161.6, (q, $J_{C\text{-}F}$ = 37.78 Hz, C=O), 137.3, 136.7, 127.7, 126.9, 118.5 (q, $J_{C\text{-}F}$ = 292.76 Hz, -CF_3), 65.0, 63.6, 53.7, 53.1, 43.1, 18.3. $[M+H]^+$ calcd for $C_{16}H_{23}N_3O_8$, 386.1563; found, 386.1555.

^{1}H and ^{13}C NMRs for these compounds can be found in **Appendix A**.

3.4 Conclusion:

A series of dipeptide dimethacrylamide and mixed dimethacrylate zwitterionic cross-linkers have been created through an outside-in strategy. Dipeptide based zwitterionic cross-linkers for example N-Ser-Ser-C, N-Ser-Lys-C, N-Lys-Ser-C, and N-Lys-Lys-C are charge separated by four atoms (the peptide bond and alpha-carbons). It is synthesized from peptide coupling of mono methacryloyl components of each amino acid followed by careful deprotection of the C and N termini, chemo-selective protection and deprotection being the most crucial step. While zwitterionic properties have proven necessary for maintaining non-fouling behavior, the impact of charge spacing have never been tested for cross-linkers.[82] Studies have shown that charge spacing within monomer subunits has a direct influence on the non-fouling behavior in polymer brush and thin film hydrogel investigations. In polymer hydrogel systems, the distance between charges could also facilitate changes in the bulk material properties based on the strength of electrostatic interactions between charged regions of the cross-linker and the charged monomer functional group.[86] Most importantly, charge spacing will also influence the ionic solvation interactions throughout the 3D structure and these ionic solvation interactions lead to the formation of a tightly bound hydration layer that is critical for maintaining the non-fouling performance in complex environments. The next set of cross-linkers i.e., Ser-Gly-Ser and Lys-Gly-Lys will be used to correlate the structural variations in the cross-linker to the resulting polyampholyte hydrogel characteristics of non-fouling, protein conjugation, mechanical properties, and degradation behavior. The results from this study will in turn guide the biomaterials community towards molecular-level design strategies for polymeric biomaterials to improve tissue regeneration.

Chapter 4: Outside-in Strategy for the introduction of glycol unit spacers and functionalizable groups to the cross-linker

4.1. Introduction:

Spacing between the polymerizable entities in the monomeric units can impact the hydrogel properties. For example, Zhang *et al.* and Chiu *et al.* demonstrated that changing the number of carbon spacers between the charged groups in their zwitterionic structures resulted in significant impacts on the non-fouling properties.[36,61] In order to investigate this aspect with the technology mentioned in the previous chapters, two strategies were devised: 1) adding glycol unit spacers between the zwitterionic component; 2) adding functionalizable groups (as peptide units) to the cross-linker. The glycol units offer properties similar to PEG groups to potentially make the cross-linkers more PEG like (biocompatible) and the addition of functional groups to the cross-linker show the many possibilities of addition different reactive site to these materials. An example of adding cell-cell signaling peptides to the cross-linkers is provided along with the solid-phase peptide synthesis of the small tripeptide DGR.

To retain the Ser-Ser zwitterionic component as mentioned in previous chapters yet extending the length of the cross-linker, the incorporation of a glycol spacer was proposed. A previous project in our group looked at the synthesis of a 3-bromopropyl methacrylate (3-BPM) appendage unit which was also applicable to this project. The 3-BPM appendage can be synthesized readily through the DCC coupling of 3-bromopropan-1-ol and methacrylic acid. With this compound in hand the propylene glycol extended cross-linker could then be quickly synthesized.

Secondly, the outside-in strategy discussed in the previous chapters present the possibility to further incorporate functionalizable amino acids and specific cell-cell and cell-

matrix signaling cues as pendant side chains into the zwitterionic cross-linkers, as shown in **scheme 4.2, 4.3** and **4.4** respectively. For example, incorporation of amino acids with anionic side chains in between two serine moieties act as a spacer for use in coupling other amino acid/peptide sequences as well as acts a control for zwitterionic cross-linker evaluation due to their charge imbalance. They could also demonstrate zwitterionic property at much lower pH which could be beneficial for in-vivo applications.

4.2. Results and Discussion:

To produce the glycol lengthened cross-linker, both amine and carboxylic acid coupling partners needed to be synthesized. Following a similar strategy as discussed in previous chapters Boc-protected serine was first appended with the methacrylated unit using 3-BPM in the presence of a base where the oxygen of the primary alcohol nucleophilically attacks the carbonyl carbon of the 3-BPM. Different bases were screened for example inorganic bases such as NaH, CS_2CO_3 as well as common organic bases such as triethylamine and DIPEA, out of which potassium carbonate produced significantly higher yield and therefore has been used for this reaction. Bromo propyl methacrylate was synthesized following a procedure previously reported using DCC/DMAP.

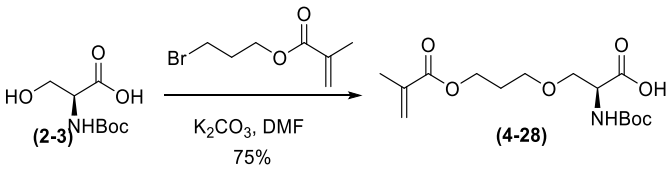

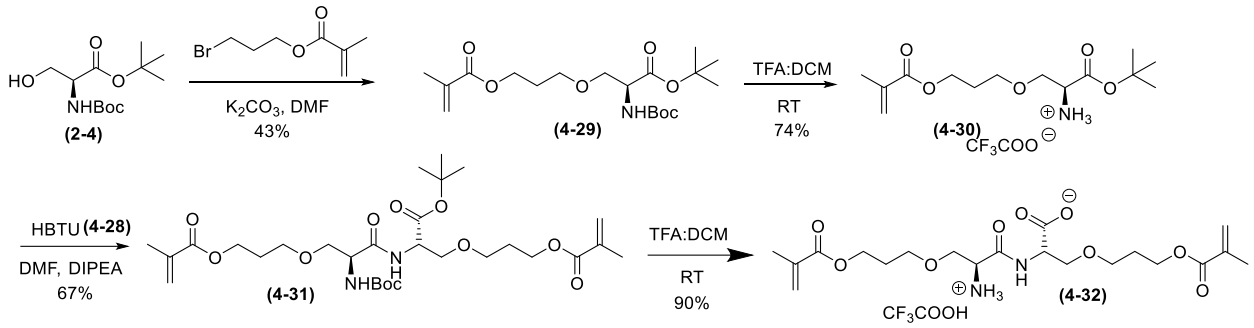

Scheme 4. 1: Outside-in approach for the synthesis of propylene glycol serine dipeptide

For the N-coupling partner, Boc and *t*-butyl protected serine was methacrylated using potassium carbonate as described before which provides the C-protected termini for peptide coupling. The C and N coupling partners **(4-28** and **4-30)** were then coupled using HBTU in presence of Hünigs base with the formation of dimethacrylated precursor which then underwent extensive TFA deprotection to provide the cross-linker **(4-32)** as a TFA salt.

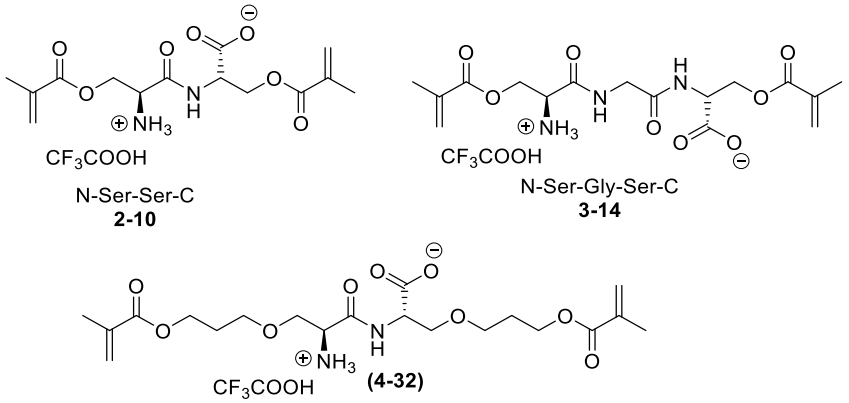

Figure 4. 1: Structure of N-Ser-Ser-C, N-Ser-Gly-Ser-C and N-PM-Ser-Ser-PM-C

"Outside-In" strategy has been used to incorporate an aspartic acid spacer for later use in COOH coupling reactions as shown in (**Scheme 4.3**). Additionally, lengthier tethers such as glutamic acid and 2-aminohexanedioic acid can be inserted as a spacer in a similar fashion to evaluate the impact of tether length on the bioactivity of the appended compounds. For

example, the cell-cell signaling hormone NH_2-arginine-glycine-aspartic acid-COOH (RGD), if properly protected, can be attached to the cross-linker. Synthesis of DGR peptide using SPPS has been described in **Scheme 4.4.** These spacers with an anionic side chain all differ by one methylene group which can act as a control zwitterion cross-linker evaluation due to their lowered IEP.

Similarly, additional cross-linker variables discussed in previous chapters (length, charge spacing, charge density), can be examined, as additional charged groups can be added with aspartic acids and orthogonally protected cationic arginine groups. This family of synthesized cross-linkers will allow for evaluation of type, length, charge separation, and charge density on the delivery of cell signaling peptide sequences. For example, the synthesis of SDS lowers the IEP of the cross-linker below pH of 4, about 100x more acidic than simple dipeptide S-S cross-linker.

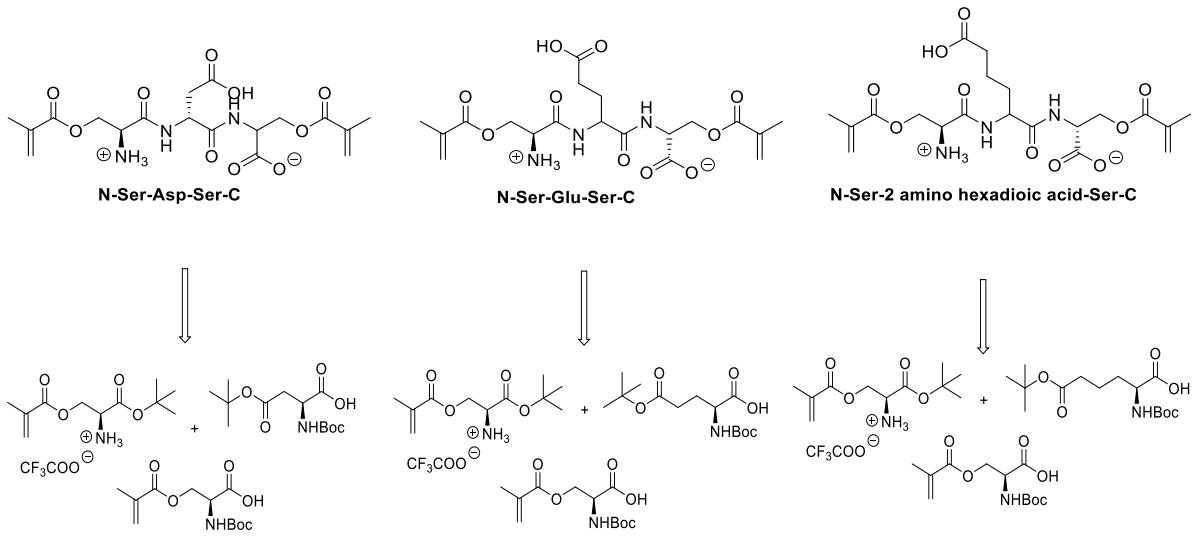

Scheme 4. 2: Retrosynthesis for incorporation of anionic side chains as a spacer

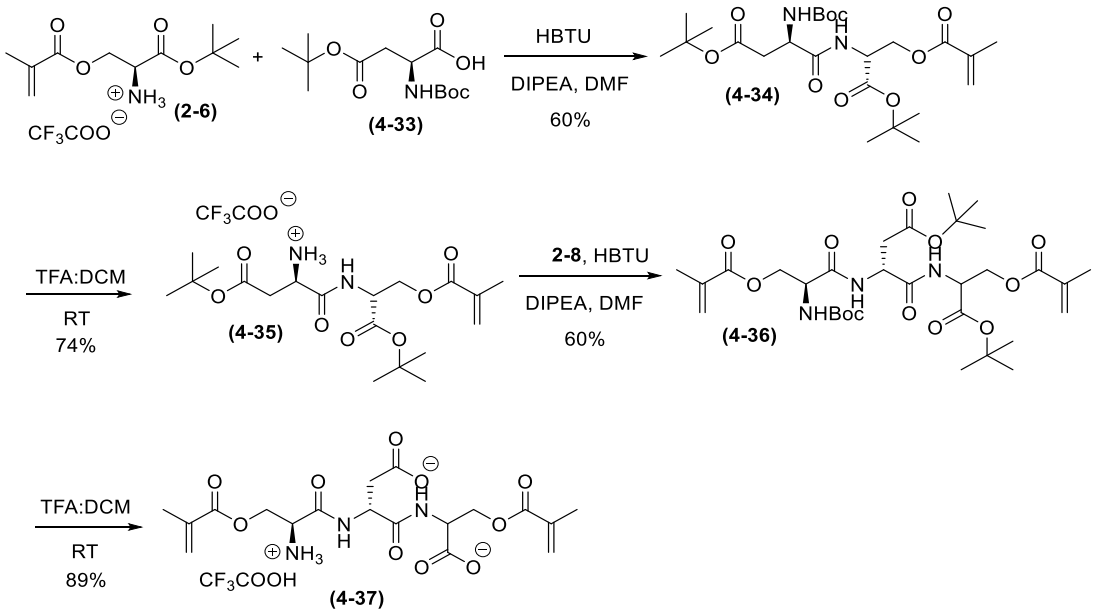

Scheme 4. 3: Incorporation of aspartic acid as a spacer

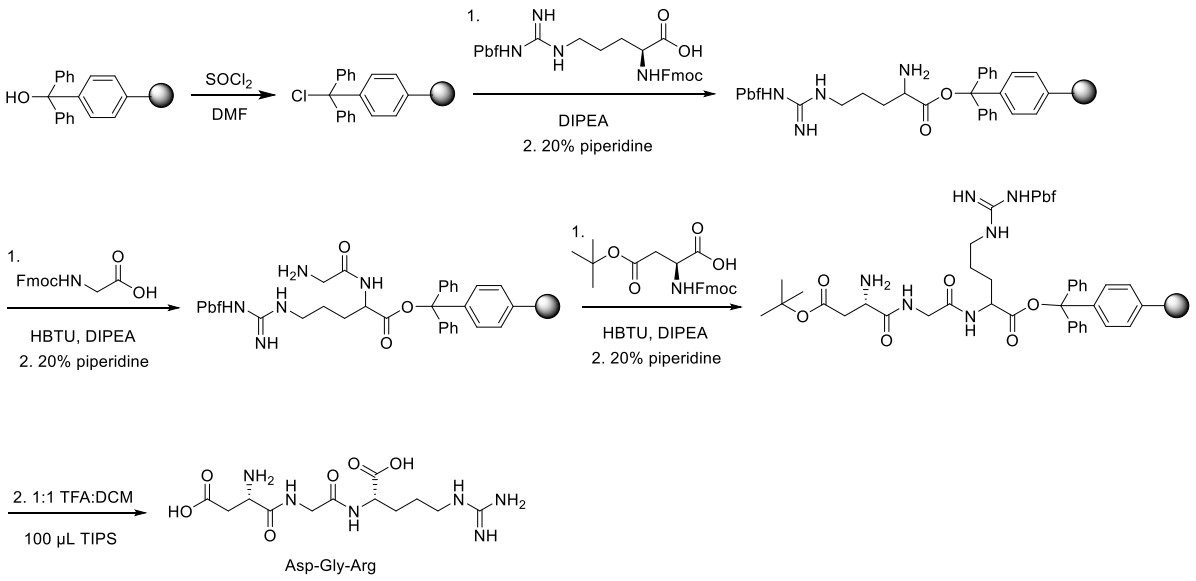

Scheme 4. 4: Synthesis of DGR using SPPS

4.3. Experimental:

4.3.1. Characterization of molecules **4-28** to **4-37**

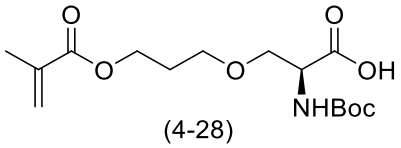

(4-28)

N-(tert-butoxycarbonyl)-O-(3-(methacryloyloxy)propyl)-L-serine (**4-28**): N-Boc Serine (125 mg, 0.609 mmol) and 3 Bromo propyl methacrylate (151.03 mg, 0.732 mmol) was dissolved in DMF to which potassium carbonate (126.25 mg, 0.913 mmol) was added and the reaction mixture was stirred at RT for 30 hours. The reaction mixture was dissolved in water and extracted with ethyl acetate (5 x 10 mL). The crude reaction was then subjected to column chromatography (7:3 hexane: ethyl acetate) and collected 150 mg of **4-28** as a colorless oil. (75% yield). FTIR (cm^{-1}) 3375.87, 2976.69, 1714.36, 1506.37, 1156.48. 1H NMR (500 MHz, Chloroform-*d*) δ 6.10 (dd, *J* = 1.6, 0.9 Hz, 1H), 5.58 (dd, *J* = 1.6 Hz, 0.9 Hz, 1H), 5.44 (s, 1H), 4.39 – 4.27 (m, 3H), 4.22 (ddt, *J* = 11.5, 9.3, 6.0 Hz, 2H), 4.02 (dd, *J* = 11.2, 3.5 Hz, 1H), 3.89 (dd, *J* = 11.2, 3.5 Hz, 1H), 2.05 (dt, *J* = 6.2, 3.0 Hz 2H), 1.93 (dd, *J* = 1.6, 1.0 Hz, 3H), 1.45 (s, 9H). 13C NMR (500 MHz, CDCl3) δ 170.9, 167.6, 155.8, 136.2, 126.0, 80.4, 63.7, 62.0, 60.8, 56.0, 28.4, 28.2, 18.4. $[M+H]^+$ calcd for $C_{15}H_{25}NO_7$, 332.1709, found, 332.1702.

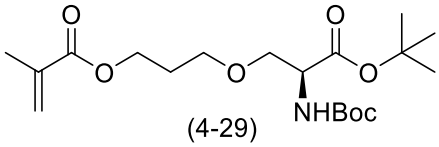

(4-29)

(S)-3-(3-(tert-butoxy)-2-((tert-butoxycarbonyl)amino)-3-oxopropoxy)propyl methacrylate (**4-29**): N-Boc *t*-butyl-Serine (125 mg, 0.478 mmol) and 3-bromopropyl methacrylate (118.23 mg, 0.574 mmol) was dissolved in DMF to which potassium carbonate (99 mg, 0.717 mmol)

was added and the reaction mixture was stirred at RT for 30 hours. The reaction mixture was dissolved in water and extracted with ethyl acetate (5 x 10 mL). The crude reaction was then subjected to column chromatography (8:2 hexane: ethyl acetate) and collected 80 mg of **(4-29)** as a white solid. (43% yield). FTIR (cm^{-1}) 3323.13, 2929.39, 1649.59, 1175.54, 1568.88. 1H NMR (500 MHz, Chloroform-*d*) δ 6.10 (dt, *J* = 1.8, 1.0 Hz, 1H), 5.56 (dt, *J* = 1.8, 1.0 Hz, 1H), 5.34 (dt, *J* = 9.0 Hz, , 3.0 Hz, 1H), 4.37 (dt, *J* = 9.0, 3.0 Hz, 1H), 4.32 – 4.19 (m, 4H), 3.80 (dd, *J* = 8.9, 3.0 Hz, 1H), 3.56 (dd, *J* = 8.9, 3.0 Hz, 1H), 2.03 (p, *J* = 6.3 Hz, 2H), 1.94 (t, *J* = 1.3 Hz, 3H), 1.45 (s, 9H), 1.13 (s, 9H). 13C NMR (500 MHz, CDCl3) δ 171.0, 167.3, 155.8, 136.3, 125.7, 79.9, 73.5, 62.3, 61.9, 61.2, 54.4, 28.5, 28.2, 27.4, 18.4. $[M+H]^+$ calcd for $C_{19}H_{33}NO_7$, 388.2335, found, 388.2346.

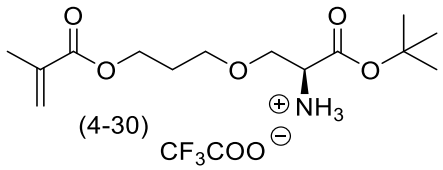

(4-30)

(S)-3-(2-amino-3-(tert-butoxy)-3-oxopropoxy)propyl methacrylate. TFA (**4-29**): (40 mg, 0.103 mmol) was dissolved in 3:1 DCM: TFA at RT and stirred for 3 hours. The solvent was removed in vacuo and the (**4-30**) isolated as a light-yellow oil was used as is for the next step without any further purification.

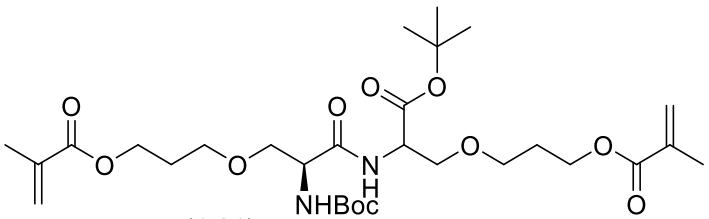

(4-31)

(6S,9S)-9-(tert-butoxycarbonyl)-6-((tert-butoxycarbonyl)amino)-17-methyl-7,16-dioxo-4,11,15-trioxa-8-azaoctadec-17-en-1-yl methacrylate (**4-31**): **4-28** (50 mg, 0.150 mmol) was dissolved in DMF to which HBTU (57 mg, 0.150 mmol) was added in one portion. The reaction mixture was stirred for an hour before adding **4-30** (51 mg, 0.125 mmol) and DIPEA (81 mg, 0465 mmol). The reaction was then stirred for an additional 3 hours. The reaction mixture was dissolved in water and extracted with ethyl acetate (5 x 10 mL). The crude reaction was then subjected to column chromatography (2:1 hexane: ethyl acetate) and collected 60 mg of **(4-31)** as a colorless oil (67% yield, telescopic over 2 steps). FTIR (cm^{-1}) 3453.80, 2974.76, 1715.48, 1155.7, 1391.72, 1496.70 ^{1}H NMR (600 MHz, Chloroform-*d*) δ 6.10 (d, *J* = 1.6 Hz, 2H), 5.58 (d, *J* = 1.6 Hz, 2H), 5.46 (s, 1H), 4.34 – 4.27 (m, 6H), 4.21 (ddt, *J* = 11.5, 9.5, 6.0 Hz, 5H), 4.05 – 4.00 (m, 2H), 3.91 – 3.86 (m, 2H), 2.05 (p, *J* = 6.2 Hz, 4H), 1.93 (dd, *J* = 1.6, 1.0 Hz, 6H), 1.45 (s, 18H). ^{13}C NMR (126 MHz, $CDCl_3$) δ 170.9, 167.6, 155.8, 136.1, 126.1, 80.3, 63.6, 62.0, 60.8, 55.9, 28.4, 28.2, 18.4.

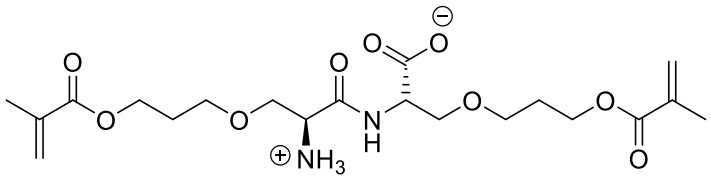

(4-32)

O-(3-(methacryloyloxy)propyl)-N-(O-(3-(methacryloyloxy)propyl)-L-seryl)-L-serine · TFA **(4-32)**: **4-31** (50 mg, 0.07 mmol) was dissolved in 4 mL of a 1:1 DCM: TFA solution and stirred at RT until all the starting material was consumed. The solvent was removed in vacuo and the TFA-salt was isolated as a sticky oil. Yield: 35 mg (90%). FTIR (cm^{-1}) 3453.08, 2974.73, 1715.48, 1155.71, 1496.70, 1391.72, 1319.87. ^{1}H NMR (500 MHz, Methanol-d_4) δ 6.12 – 6.08 (d, *J* = 1.6 Hz, 2H), 5.63 (d, *J* = 1.6 Hz, 2H), 4.37 (td, *J* = 6.3, 1.0 Hz, 4H), 4.26 (t, *J* = 6.3 Hz,

4H), 4.14 (dd, *J* = 4.5, 3.4 Hz, 2H), 4.02 (dd, *J* = 11.8, 4.5 Hz, 2H), 3.94 (dd, *J* = 11.8, 3.5 Hz, 2H), 2.10 (p, *J* = 6.3 Hz, 4H), 1.93 (t, *J* = 1.3 Hz, 6H). ^{13}C NMR (126 MHz, MeOD) δ 168.9, 168.7, 162.4, 137.6, 126.3, 126.2, 63.3, 64.1, 62.1, 60.7, 56.7, 56.0, 28.9, 18.3.

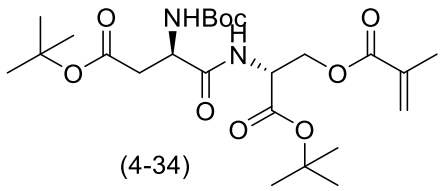

(4-34)

*tert-butyl (R)-4-(((S)-1-(tert-butoxy)-3-(methacryloyloxy)-1-oxopropan-2-yl)amino)-3-((tert-butoxycarbonyl)amino)-4-oxobutanoate (**4-34**)*: *t*-butyl Boc Asp (**4-33**) (202 mg, 0.69 mmol) was dissolved in DMF to which HBTU (265.55 mg, 0.69 mmol) was added in one portion. The reaction mixture was stirred for an hour before adding (**2-6**) **(**200 mg, 0.58 mmol) and DIPEA (233.2 mg, 1.8 mmol). The reaction was then stirred for an additional 3 hours. The reaction mixture was dissolved in water and extracted with ethyl acetate (5 x 10 mL). The crude reaction was then subjected to column chromatography (7:3 hexane: ethyl acetate) and collected 200 mg of **(4-34)** as a colorless oil (60% yield, telescopic over 2 steps). FTIR (cm^{-1}) 3308.19, 2984.05, 1724.20, 1532.58, 1367.37, 1148.11. ^{1}H NMR (500 MHz, Chloroform-*d*) δ 6.39 (d, *J* = 7.5 Hz, 1H), 6.08 (t, *J* = 1.2 Hz, 1H), 5.63 (d, *J* = 7.5 Hz, 1H), 5.58 (t, *J* = 1.6 Hz, 1H), 4.72 (dt, *J* = 7.1, 3.4 Hz, 1H), 4.46 (dd, *J* = 11.3, 3.6 Hz, 1H), 4.39 (dd, *J* = 11.3, 3.2 Hz, 2H), 2.87 (dd, *J* = 15.8, 4.8 Hz, 1H), 2.72 (dd, *J* = 15.7, 4.5 Hz, 1H), 1.91 (t, *J* = 1.2 Hz, 3H), 1.48 – 1.38 (m, 27H). ^{13}C NMR (126 MHz, $CDCl_3$) δ 170.3, 169.9, 168.3, 166.8, 155.8, 135.7, 126.5, 83.2, 82.2, 79.8, 64.7, 52.5, 50.9, 38.2, 28.4, 27.9, 18.3. $[M+H]^+$ calcd for $C_{24}H_{40}N_2O_9$, 501.2821, found, 501.2821.

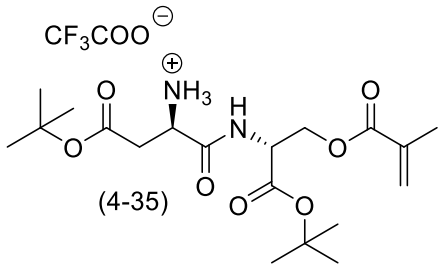

(4-35)

tert-butyl (S)-3-amino-4-(((R)-1-(tert-butoxy)-3-(methacryloyloxy)-1-oxopropan-2-yl)amino)-4-oxobutanoate · TFA **(4-35): 4-34** (20 mg, 0.037 mmol) was dissolved in 3:1 DCM: TFA at RT and stirred for 3 hours. The solvent was removed in vacuo and the (**4-35**) isolated as a light-yellow oil was used as is for the next step without any further purification. Yield 87% (18 mg).

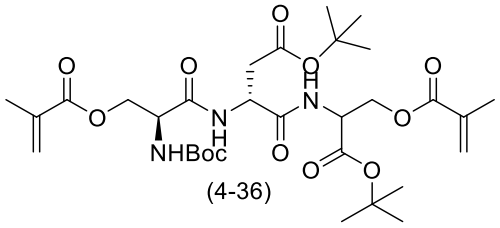

(4-36)

(*3R)-4-((1-(tert-butoxy)-3-(methacryloyloxy)-1-oxopropan-2-yl)amino)-3-((S)-2-((tert-butoxycarbonyl)amino)-3-(methacryloyloxy)propanamido)-4-oxobutanoic acid* (**4-36**): Mono methacrylated Boc serine (155.6 mg, 0.57 mmol) was dissolved in DMF to which HBTU (216.73 mg, 0.57 mmol) was added in one portion. The reaction mixture was stirred for an hour before adding **4-35** (200 mg, 0.38 mmol) and DIPEA (152.26 mg, 1.18 mmol). The reaction was then stirred for an additional 3 hours. The reaction mixture was dissolved in water and extracted with ethyl acetate (5 x 10 mL). The crude reaction was then subjected to column chromatography (7:3 hexane: ethyl acetate) and collected 70 mg of **(4-36)** as a light-yellow oil (60% yield, telescopic over 2 steps). FTIR (cm^{-1}) 3314.71, 2979.37, 1719.75, 1367.46, 1151.01. ^{1}H NMR (500 MHz, Chloroform-*d*) δ 7.37 (d, *J* = 7.6 Hz, 2H), 6.07 (d, *J* = 7.6 Hz, 2H), 5.58 (t, *J* = 1.6 Hz, 1H), 5.55 (t, *J* = 1.6 Hz, 1H), 4.73 (dd, *J* = 7.5, 4.4 Hz, 1H), 4.65 (dd,

J = 8.0, 4.4 Hz, 1H), 4.54 (t, *J* = 7.0 Hz, 1H), 4.46 (dt, *J* = 11.2, 4.3 Hz, 2H), 4.42 – 4.32 (m, 2H), 2.86 (dd, *J* = 15.1, 4.0 Hz, 1H), 2.78 (dd, *J* = 15.1, 4.9 Hz, 1H), 1.91 (dd, *J* = 3.2, 1.5 Hz, 6H), 1.48 – 1.36 (m, 27H). ^{13}C NMR (500 MHz, $CDCl_3$) δ 169.7, 169.2, 169.07, 168.8, 167.0, 166.8, 155.6, 135.8, 135.6, 126.6, 126.4, 83.5, 82.7, 80.5, 73.9, 64.5, 64.4, 53.87, 52.6, 50.0, 37.9, 28.4, 27.4, 18.3, 18.3. $[M+H]^+$ calcd for $C_{24}H_{40}N_2O_9$, 501.2821, found, 501.2812.

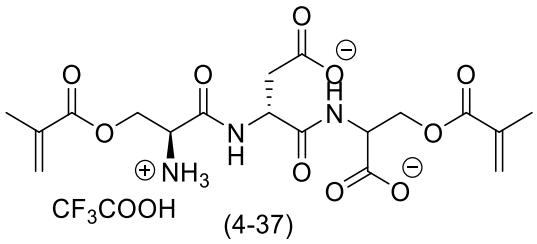

(4-37)

(3R)-3-((S)-2-amino-3-(methacryloyloxy)propanamido)-4-((1-carboxylato-2-(methacryloyloxy)ethyl)amino)-4-oxobutanoate **(4-37): 4-36** (50 mg, 0.07 mmol) was dissolved in 4 mL of a 1:1 DCM: TFA solution and stirred at RT until all the starting material was consumed (6 h). The solvent was removed in vacuo and the TFA-salt (**4-37**) was isolated as a sticky oil. Yield: 35 mg (89%). FTIR (cm^{-1}) 2976.46, 1660.03, 1425.19, 1350.00 ^{1}H NMR (500 MHz, Methanol-d_4) δ 6.17 (dt, *J* = 6.2 Hz, 2H), 5.67 (dt, *J* = 6.2, 1.7 Hz, 2H), 4.78 (dd, *J* = 5.3, 3.8 Hz, 1H), 4.60 – 4.39 (m, 4H), 4.30 (dd, *J* = 5.9, 3.8 Hz, 1H), 3.25 – 3.15 (m, 1H), 2.93 – 2.82 (m, 2H), 1.94 (d, *J* = 11.0 Hz, 6H). ^{13}C NMR (126 MHz, MeOD) δ 173.5, 172.3, 172.1, 168.5, 167.9, 167.1, 137.4, 136.9, 127.9, 127.1, 65.2, 63.8, 53.7, 53.3, 50.8, 37.6, 18.4. $[M+H]^+$ calcd for $C_{18}H_{24}N_3O_{10}$, 444.1618, found, 444.1615.

4.2.1. General Procedure for SPPS**:**

General procedure for SPPS of peptides following the Fmoc strategy. Solid-phase peptide synthesis was carried out in syringes, equipped with Teflon filters. Trityl chloride resin was initially washed (2x DCM, 2x DMF). For pre-activation of the first amino acid a solution of

0.8 eq. Fmoc protected amino acid in DMF was added to the resin along with 139 µl DIPEA. After 5 mins the resin was washed (2x DMF, 2x DCM, 2x DMF), capped with methanol/DMF (2:8) (2x 5 min) and washed (2x DMF, 2x DCM, 2x DMF) again.

Iterative peptide assembly:

Deprotection: The resin was treated with 20% piperidine/DMF (2x 5 min) and subsequently washed (2x DMF, 2x DCM, 2x DMF).

Amino acid coupling: A solution of 0.8 mmol protected amino acid in 2 mL DMF using 2 mL 0.4(M) HBTU and 139 µL DIPEA was added to the resin. After 5 min, the resin was washed with DMF (2x), DCM (2x) and DMF (2x).

Capping: Methanol/DMF (2:8) was added to the resin. After 5 min the resin was washed with DMF (2x), DCM (2x) and DMF (2x). Coupling of the different peptide sequences was carried out by adding a solution of 4 eq. of the respective amino acids using 0.4 (M) HBTU and 139 µL DIPEA. After each coupling step the resin was washed with DMF (5x), DCM (5x) and DMF (5x).

Acidic side chain deprotection and cleavage: The resin was washed with DMF (2x) and DCM (2x) before treating with 1:1 v/v DCM/TFA and 100 TIPS (triisopropyl silane) for 2h to remove the acidic side chain on the peptide along with cleavage of the fully formed peptide sequence from the resin. Work-up: The combined solutions were concentrated in vacuo and cold ether was added to the liquid residue. A white solid was precipitated out as a product which was then analyzed using HPLC and HRMS.

Synthesis of DGR:

The peptide sequence was assembled via manual solid-phase Fmoc-synthesis in 0.2mmol scale and DGR was synthesized following the general procedure. First the trityl chloride resin (0.2 mmol, 0.105 gm) was swelled with DFM for 30 mins and then drained and rinsed with 5 mL DCM followed by addition of $SOCl_2$ (100 µl, 1.38 mmol) and 4 mL DCM for one hour. The solvent was then drained, and the resin was washed twice with DMF (2 mL). The first amino acid, Fmoc-L-(Arg) PBF-OH (0.8 mmol, 519.01 mg) was added to the resin dissolved in 2 mL DMF along with 139 µl DIPEA and stirred for 5 mins. The resin bed was then washed with DMF (2 mLx2) followed by 20 mL of 10% MeOH solution for 10 mins for capping. The Fmoc group was then deprotected with 20% piperidine (1 mLx2) and washed again with DMF. The next amino acid, Fmoc-Gly (0.8 mmol, 237.85 mg) was then added to the resin dissolved in 2 mL DMF along with 2 mL 0.4(M) HBTU solution and 139 µl DIPEA. It was stirred for an hour, followed by DMF wash (2 mLx2) and cleavage of Fmoc group by 20% piperidine (1 mLx2). The last amino acid Fmoc-Asp (O-*t*Bu) OH (0.8 mmol, 328.36 mg) was added to the resin bed dissolved in 2 mL DMF along with 2 mL 0.4(M) HBTU solution and 139 µl DIPEA. Finally, the resin was washed with DCM (2 mLx3) and the newly synthesized peptide chain was cleaved from the resin bed and the acidic side chains were deprotected with 5 mL 1:1 DCM: TFA and 100 µl TIPS for an hour. After an hour, the solvent was removed using rotavap and cold ether was added where the product crashed out as a form of a white solid. The crude (40 mg, 50%) was then subjected to HRMS. The mass for $[M+H]^+$ calcd for C12H22N6O6, 347.1679, found, 347.1671.

4.4. Conclusion:

This family of synthesized cross-linkers will allow for evaluation of type, length, charge separation, and charge density on the delivery of cell signaling peptide sequences. Following the same SPPS approach as other key cell-cell adhesion peptide sequences like His-Ala-Val-Asp-Ile (HAVDI) and Gln-Ala-Val (QAV), and cell-matrix adhesion peptide sequences like Gly-Arg-Pyl-Gly-Glu-Arg (GROGER) can be easily synthesized using SPPS and can be incorporated into the cross-linkers.

Future Directions

Building upon our preliminary data on Ser-Ser dimethacrylate hydrogels discussed in the chapter 2, the first obvious future direction is the synthesis of new hydrogels utilizing the many untested cross-linkers produced in chapters 3 and 4 from N-Ser-Lys-C dimethacrylate (**3-12)**; zwitterionic spaced compounds N-Ser-Gly-Ser-C, **3-14** and N-Lys-Gly-Lys **3-15**. Additionally, hydrogels from the propylene glycol spaced dimethacrylate compound **4-32** and aspartic acid spaced cross-linker **4-37** would also offer a glimpse into how methacrylate spacings units would behave as well as an adjusted IEP. Initial tests should follow the synthesis outlined in Chapter 2, where the polyampholyte being prepared from an equimolar mixture of [2-acryloyloxy ethyl] trimethyl ammonium chloride (TMA) and 2-carboxyethyl acrylate (CAA) as to compare these compounds with Ser-Ser dimethacrylate **(2-10).** However – a variety of hydrogels can be synthesized using these cross-linkers with other zwitterionic monomer species and in varied amounts of cross-linker to monomer ratios. Despite the many new hydrogels that can be prepared, further expansions of new cross-linker species are also possible and will be discussed below.

5.1. Enhancing zwitterionic cross-linkers with varied type and controlled spacing between polymerizable entities:

Studies shows that subtle changes in structure impact the non-fouling performance of the resulting polymers.[36,61,89] For example, a recent report evaluated the performance of zwitterionic hydrogels incorporating a long chain cross-linker containing a sulfobetaine functional group.[82] Hydrogels formed with this cross-linker did not completely inhibit the inflammatory response *in vivo*, but it is unclear if this is a result of the length of the cross-

linker or if it's the overall structure and charge distribution. The library of zwitterionic cross-linkers will help conduct a systematic study by directly addressing this need. It is also possible to controllably vary the structure through a series of amino acids utilizing peptide-based strategy. The first modifications to build different sets of cross-linkers will be an extension in the overall type and length of the cross-linker. It has recently been demonstrated that the cross-linker length impacts the mechanical properties and the degradation behavior of polyampholyte hydrogels through a complex interplay of steric hindrance, packing density, and electrostatic interactions.[37] Therefore, it is possible to tune the mechanical and degradation characteristics of hydrogels by controlling the peptide-based cross-linker length. Specific cross-linkers proposed to determine how the overall length effects the physical properties of the hydrogels are shown in **Figure 5.1**. Using the previously mentioned "outside-in" strategy, a series of methacrylate, methacrylamide, and thiomethacrylate dipeptides containing heteroatom oxygen, nitrogen, and sulfur atoms respectively of various length will be synthesized and tested by varying the heteroatom. Spacing of the cross-linking components can vary from 8 to 16 atoms (spacing is counted from sp^3 heteroatom O, N, S between polymerizable units) and will simultaneously investigate the specific cross-linker types in addition to the lengths. The methacrylate unit could also be varied from 3-bromopropyl methacrylate (discussed in Chapter 3 and can be added to the Y components below) instead of methacrylic acid to provide a propylene glycol spacer as shown before.

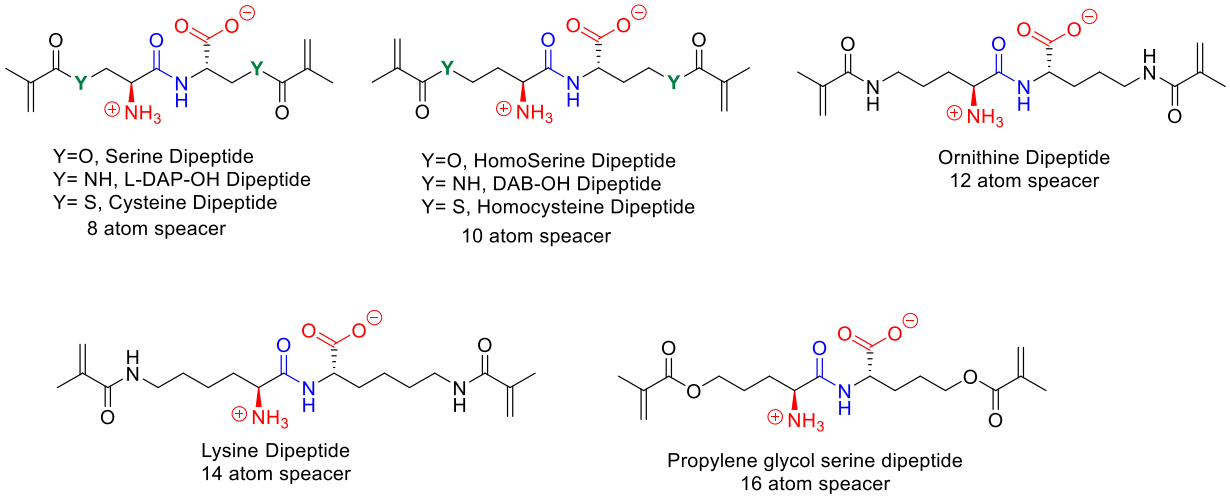

Figure 5. 1: Cross-linkers with varied type and spacing

5.2. Expanding upon the spacing units between charges:

Dipeptide based zwitterionic cross-linkers N-Ser-Ser-C, N-Ser-Lys-C, N-Lys-Ser-C and N-Lys-Lys-C synthesized in the previous chapter are charge separated by four atoms (the peptide bond and alpha-carbons). Although the zwitterionic properties have proven necessary for maintaining non-fouling behavior, the impact of charge spacing, and charge density have never been explored on cross-linkers. Research shows that charge spacing within monomer subunits has a direct effect on the non-fouling behavior in polymer brush and thin film hydrogels.[36,61,89] The distance between charges could also facilitate changes in the bulk material properties in polymer hydrogel systems, based on the strength of electrostatic interactions between charged regions of the cross-linker and the charged monomer functional groups. Above all, charge spacing effects the ionic solvation interactions which essentially leads to the formation of a tightly bound hydration layer that is responsible for maintaining the non-fouling performance in complex environments.[64,92,93] With the help of peptide based zwitterionic cross-linkers it is possible to probe both the spacing between charges and the number of charges. Tripeptides Ser-Gly-Ser and Lys-Gly-Lys (from chapter 3) dimethacrylates

synthesized along with addition cross-linkers from various non-natural amino acids for example, DAP, DAB, Homoserine etc. (**Figure 5.2**) using SPPS, and outside-in strategy will be evaluated for this purpose by utilizing variation in monomer type and length alongside additions of glycine. The addition of one or more glycine units increases the length between charges, which can potentially affect the hydration layering.

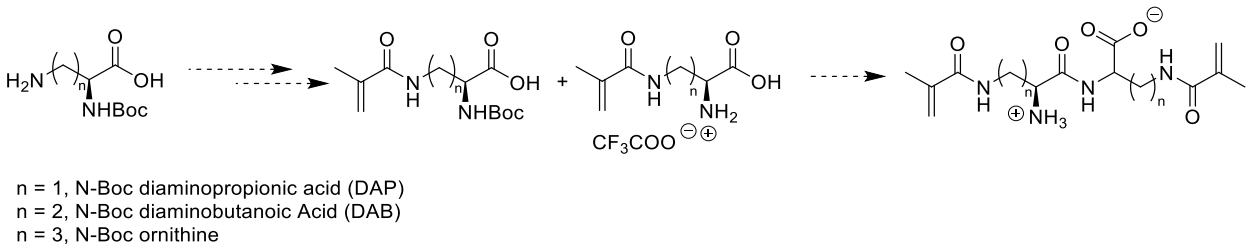

Figure 5. 2: Cross-linkers from various non-natural amino acids

5.3. Varying the charge density of the cross-linkers:

In addition to variations in charge separation, many charged amino acid spacers could be added to investigate how added charges affect the material properties. A series of cross-linkers based on additional charged amino acid residues will be synthesized to provide larger charge density in the cross-linkers which will essentially increase the hydration layer strength.[35] For example, adding an internal Pbf-protected arginine group which has a cationic side chain and *t*-Bu protected aspartic acid which has an anionic side chain as shown in the Ser-Asp-Arg-Ser compound **5-5** in **Figure 5.3** can lead to cross-linker **5-6** which has an additional set of charges at biological pH. The sequence of the charged functional groups could be of importance which could be interchanged by starting from the same precursors. An example is shown in cross-linker **5-4**, formed from protected peptide dimethacrylates synthesized before, which maintains the same charge density**,** yet it co-locates the positively and negatively charged groups. The charge differences between compounds **5-4** and **5-6** is

color-coded with blue being cationic and red being anionic and giving (+ + - -) vs. (+ - + -) charge locations in the cross-linker. Four (or more) amino acid containing peptide sequences can be accomplished using both solution phase and SPPS coupling strategies.

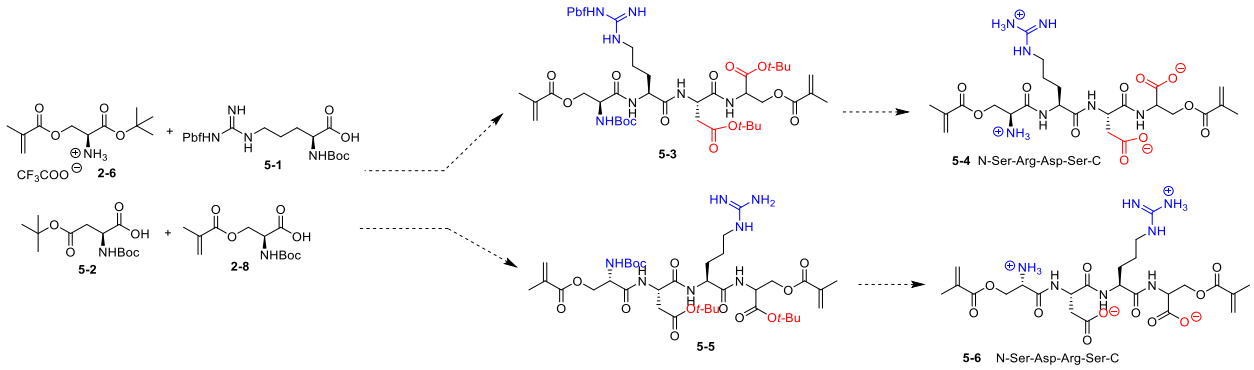

Figure 5. 3: Variation of charge density in cross-linkers

5.4. Addition of clickable entities:

In order to further demonstrate the impact of rigidity or length for peptide-cell interactions, alkyne-azide "click" coupling strategies will be investigated through different natural and non-natural azide functionalized amino acid derivatives.[82] An example of which is demonstrated below where a tripeptide sequence of three serine will be synthesized following "outside-in" strategy as described in the previous chapter where the amino acid in the middle has a terminal alkyne group. A triazole ring could be synthesized which is attached with a small molecular such as a fluorophore (color coded with green) by reacting the alkyne with an azide following click chemistry (**Figure 5.4**). Reaction of alkynes with azides generally involves the in-situ formation of copper(I) from a copper (II) source (e.g., $CuSO_4$) in the presence of reducing agent, sodium ascorbate. This type of biorthogonal fluorescent labeling experiment could be useful for incorporating into biomolecules by using the genetic code

expansion, or the cellular metabolic machinery. Small triazole adducts also impose a minimal perturbation of resulting conjugates.[94]

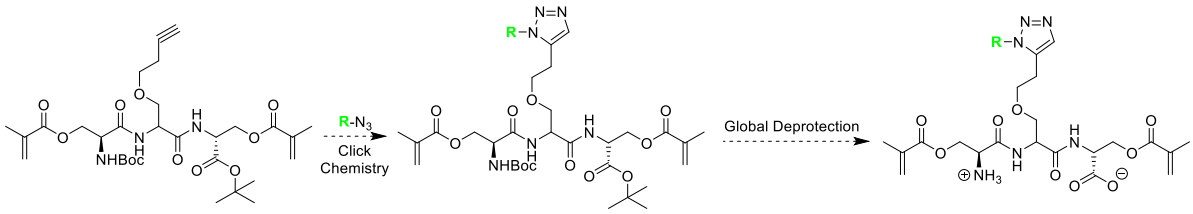

Figure 5. 4: Introduction of clickable entities

5.5. Introducing cell-cell and cell-matrix adhesion peptides as tailored side chains from zwitterionic cross-linkers as a proof-of-concept strategy for biochemical signal delivery:

Another direction would be to incorporate cell-signaling peptides into the cross-linker as an alternative approach for delivering biochemical signals. For example, RGD which is a cell adhesion peptide that binds to the protein integrin present in the ECM could be incorporated as a proof-of-concept peptide to demonstrate the delivery of bioactive peptide sequences from zwitterionic cross-linkers.[95] The synthesis of DGR has been described in the previous chapter. The accessibility and activity of this peptide sequence in this subset of zwitterionic cross-linkers will be evaluated in polyampholyte hydrogels using the same cell adhesion and viability approaches as those used to assess the bioactivity of conjugated proteins.[96] These results will provide a direct correlation between variations in the cross-linker structure and the resulting RGD bioactivity. While this approach is focused on the delivery of RGD, it is also applicable to other key cell-cell adhesion peptide sequences like His-Ala-Val-Asp-Ile (HAVDI) and Gln-Ala-Val (QAV), and cell-matrix adhesion peptide sequences like Gly-Arg-Pyl-Gly-Glu-Arg (GROGER).

The use of cell-signaling tripeptide sequence RGD represents the ability to further integrate specific cell-cell and cell-matrix signaling cues as pendant side chains from the zwitterionic cross-linkers, as shown in **Figure 5.5**. The cell signaling peptide unit can be added either before the hydrogel is formed or after the cross-linker has been incorporated into a hydrogel. RGD could be incorporated using SPPS using a synthetic strategy described below (**Scheme 5.1**).[97]

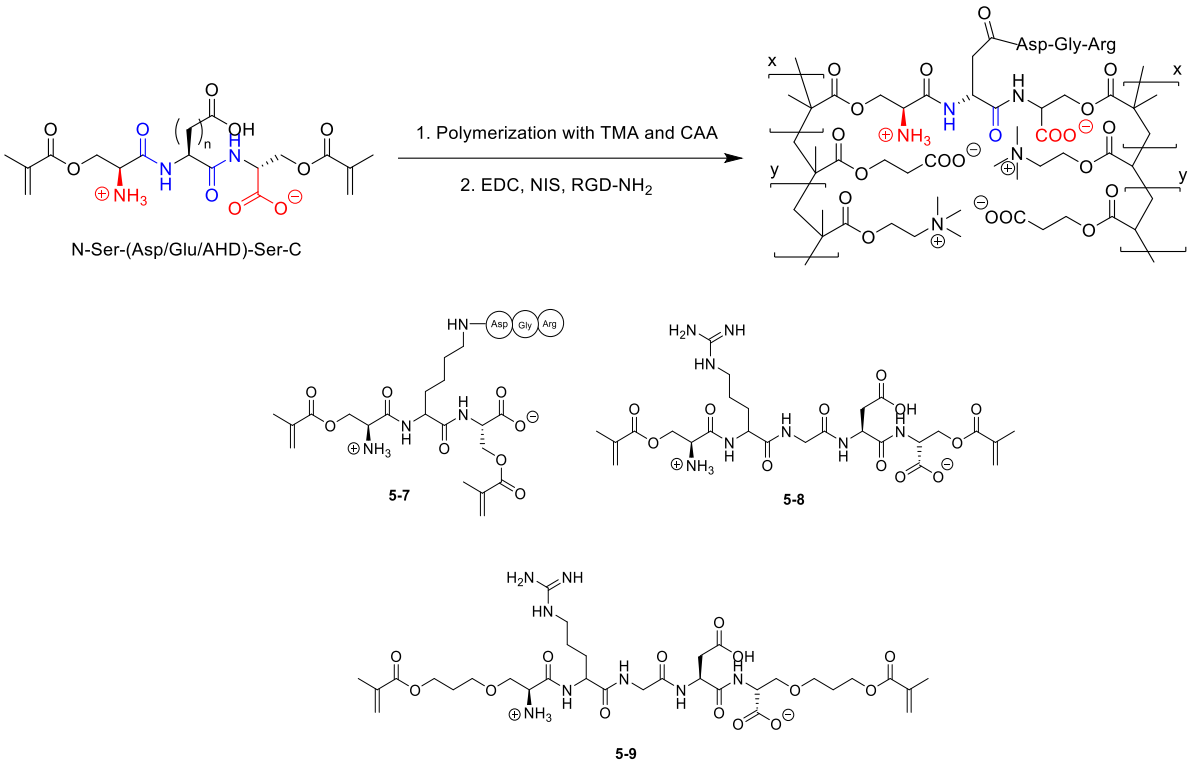

Figure 5. 5: Introduction of RGD as a cell-signaling motif

Proposed Synthesis of Ser-RGD-Ser using SPPS:

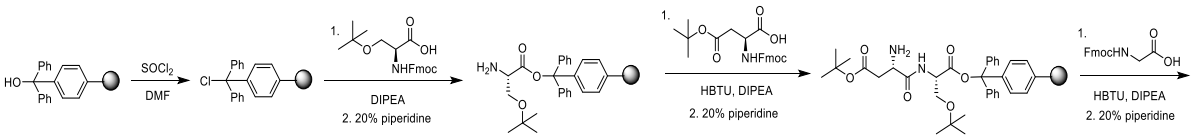

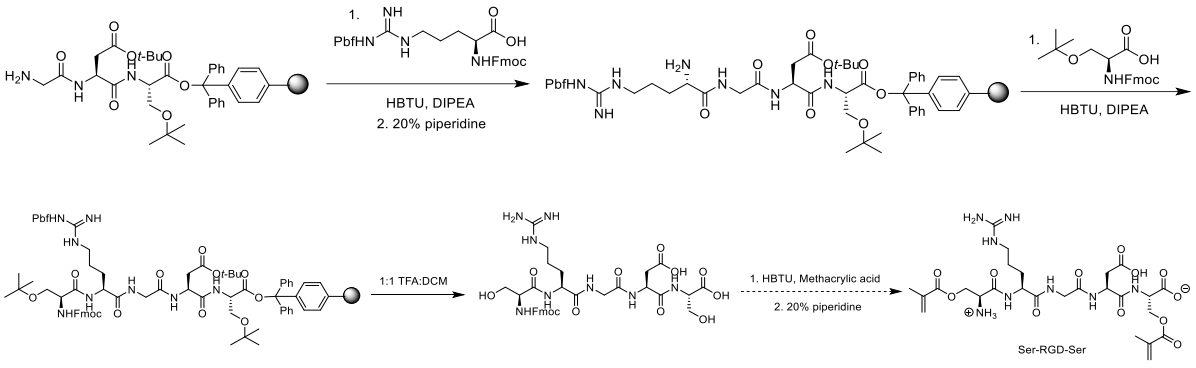

Scheme 5. 1: Synthesis of Ser-RGD-Ser

5.6 References:

(1) Ratner, B. D. Biomaterials: Been There, Done That, and Evolving into the Future. *Annu. Rev. Biomed. Eng.* **2019**, *21* (1), 171–191. https://doi.org/10.1146/annurev-bioeng-062117-120940.

(2) David F. Williams. *Biocompatibility of Tissue Analogs*; Boca Raton, Fla. : CRC Press, 1985.

(3) Francolini, I.; Vuotto, C.; Piozzi, A.; Donelli, G. Antifouling and Antimicrobial Biomaterials: An Overview. *APMIS* **2017**, *125* (4), 392–417. https://doi.org/10.1111/apm.12675.

(4) Shit, S. C.; Shah, P. A Review on Silicone Rubber. *Natl. Acad. Sci. Lett.* **2013**, *36* (4), 355–365. https://doi.org/10.1007/s40009-013-0150-2.

(5) Hunziker, E.; Spector, M.; Libera, J.; Gertzman, A.; Woo, S. L.-Y.; Ratcliffe, A.; Lysaght, M.; Coury, A.; Kaplan, D.; Vunjak-Novakovic, G. Translation from Research to Applications. *Tissue Eng.* **2006**, *12* (12), 3341–3364. https://doi.org/10.1089/ten.2006.12.3341.

(6) Hench, L. L.; Polak, J. M. Third-Generation Biomedical Materials. *Science* **2002**, *295* (5557), 1014–1017. https://doi.org/10.1126/science.1067404.

(7) Goldberg, M.; Langer, R.; Jia, X. Nanostructured Materials for Applications in Drug Delivery and Tissue Engineering. *J. Biomater. Sci. Polym. Ed.* **2007**, *18* (3), 241–268. https://doi.org/10.1163/156856207779996931.

(8) Johnson, P. C.; Mikos, A. G.; Fisher, J. P.; Jansen, J. A. Strategic Directions in Tissue Engineering. *Tissue Eng.* **2007**, *13* (12), 2827–2837. https://doi.org/10.1089/ten.2007.0335.

(9) Hacker, M. C.; Mikos, A. G. Trends in Tissue Engineering Research. *Tissue Eng.* **2006**, *12* (8), 2049–2057. https://doi.org/10.1089/ten.2006.12.2049.

(10) Langer, R. Biomaterials in Drug Delivery and Tissue Engineering: One Laboratory's Experience. *Acc. Chem. Res.* **2000**, *33* (2), 94–101. https://doi.org/10.1021/ar9800993.

(11) Fenton, O. S.; Olafson, K. N.; Pillai, P. S.; Mitchell, M. J.; Langer, R. Advances in Biomaterials for Drug Delivery. *Adv. Mater.* **2018**, *30* (29), 1705328. https://doi.org/10.1002/adma.201705328.

(12) Teo, A. J. T.; Mishra, A.; Park, I.; Kim, Y.-J.; Park, W.-T.; Yoon, Y.-J. Polymeric Biomaterials for Medical Implants and Devices. *ACS Biomater. Sci. Eng.* **2016**, *2* (4), 454–472. https://doi.org/10.1021/acsbiomaterials.5b00429.

(13) Pignatello, R. *Advances in Biomaterials Science and Biomedical Applications*; 2013.

(14) Tanaka, M.; Sato, K.; Kitakami, E.; Kobayashi, S.; Hoshiba, T.; Fukushima, K. Design of Biocompatible and Biodegradable Polymers Based on Intermediate Water Concept. *Polym. J.* **2015**, *47* (2), 114–121. https://doi.org/10.1038/pj.2014.129.

(15) Asadi, N.; Del Bakhshayesh, A. R.; Davaran, S.; Akbarzadeh, A. Common Biocompatible Polymeric Materials for Tissue Engineering and Regenerative Medicine. *Mater. Chem. Phys.* **2020**, *242*, 122528. https://doi.org/10.1016/j.matchemphys.2019.122528.

(16) Wang, X. Overview on Biocompatibilities of Implantable Biomaterials. In *Advances in Biomaterials Science and Biomedical Applications*; Pignatello, R., Ed.; InTech, 2013. https://doi.org/10.5772/53461.

(17) Opdahl, A.; Kim, S. H.; Koffas, T. S.; Marmo, C.; Somorjai, G. A. Surface Mechanical Properties of PHEMA Contact Lenses: Viscoelastic and Adhesive Property Changes on Exposure to Controlled Humidity. *J. Biomed. Mater. Res.* **2003**, *67A* (1), 350–356. https://doi.org/10.1002/jbm.a.10054.

(18) Zare, M.; Bigham, A.; Zare, M.; Luo, H.; Rezvani Ghomi, E.; Ramakrishna, S. PHEMA: An Overview for Biomedical Applications. *Int. J. Mol. Sci.* **2021**, *22* (12), 6376. https://doi.org/10.3390/ijms22126376.

(19) Lehr, C.-M.; Bouwstra, J. A.; Kok, W.; De Boer, A. G.; Tukker, J. J.; Verhoef, J. C.; Breimer, D. D.; Junginger, H. E. Effects of the Mucoadhesive Polymer Polycarbophil on the Intestinal Absorption of a Peptide Drug in the Rat. *J. Pharm. Pharmacol.* **2011**, *44* (5), 402–407. https://doi.org/10.1111/j.2042-7158.1992.tb03633.x.

(20) Ratner, B. D.; Bryant, S. J. Biomaterials: Where We Have Been and Where We Are Going. *Annu. Rev. Biomed. Eng.* **2004**, *6* (1), 41–75. https://doi.org/10.1146/annurev.bioeng.6.040803.140027.

(21) Chang, Y.; Chang, W.-J.; Shih, Y.-J.; Wei, T.-C.; Hsiue, G.-H. Zwitterionic Sulfobetaine-Grafted Poly(Vinylidene Fluoride) Membrane with Highly Effective Blood Compatibility via Atmospheric Plasma-Induced Surface Copolymerization. *ACS Appl. Mater. Interfaces* **2011**, *3* (4), 1228–1237. https://doi.org/10.1021/am200055k.

(22) Kopeček, J. Hydrogel Biomaterials: A Smart Future? *Biomaterials* **2007**, *28* (34), 5185–5192. https://doi.org/10.1016/j.biomaterials.2007.07.044.

(23) Albers, P. T. M.; van der Ven, L. G. J.; van Benthem, R. A. T. M.; Esteves, A. C. C.; de With, G. Water Swelling Behavior of Poly(Ethylene Glycol)-Based Polyurethane Networks. *Macromolecules* **2020**, *53* (3), 862–874. https://doi.org/10.1021/acs.macromol.9b02275.

(24) Peppas, N. A. Hydrogels and Drug Delivery. *Curr. Opin. Colloid Interface Sci.* **1997**, *2* (5), 531–537. https://doi.org/10.1016/S1359-0294(97)80103-3.

(25) *Hydrogels for Medical and Related Applications*; Andrade, J. D., Ed.; ACS Symposium Series; AMERICAN CHEMICAL SOCIETY: WASHINGTON, D. C., 1976; Vol. 31. https://doi.org/10.1021/bk-1976-0031.

(26) Huglin, M. R. Hydrogels in Medicine and Pharmacy Edited by N. A. Peppas, CRC Press Inc., Boca Raton, Florida, 1986 (Vol. l), 1987 (Vols 2 and 3). Vol. 1 Fundamentals, Pp. Vii + 180, £72.00, ISBN 0-8493-5546-X; Vol. 2 Polymers, Pp. Vii + 171, £72.00, ISBN 0-8493-5547-8; Vol. 3 Properties and Applications, Pp. Vii + 195, £8000, ISBN 0-8493-5548-6. *Br. Polym. J.* **1989**, *21* (2), 184–184. https://doi.org/10.1002/pi.4980210223.

(27) Varaprasad, K.; Reddy, N. N.; Ravindra, S.; Vimala, K.; Raju, K. M. Synthesis and Characterizations of Macroporous Poly(Acrylamide-2-Acrylamido-2-Methyl-1-Propanesulfonic Acid) Hydrogels for In Vitro Drug Release of Ranitidine Hydrochloride. *Int. J. Polym. Mater.* **2011**, *60* (7), 490–503. https://doi.org/10.1080/00914037.2010.531816.

(28) Hoffman, A. S. Hydrogels for Biomedical Applications. *Adv. Drug Deliv. Rev.* **2002**, *54* (1), 3–12. https://doi.org/10.1016/S0169-409X(01)00239-3.

(29) Nikolaos A. Peppas and Richard W. Korsmeyer. *Hydrogels in Medicine and Pharmacy*; Vol. 3.

(30) Cao, S.; Barcellona, M. N.; Pfeiffer, F.; Bernards, M. T. Tunable Multifunctional Tissue Engineering Scaffolds Composed of Three-Component Polyampholyte Polymers: ARTICLE. *J. Appl. Polym. Sci.* **2016**, *133* (40). https://doi.org/10.1002/app.43985.

(31) S.L. Haag, M.T. Bernards, Enhanced Biocompatibility of Polyampholyte Hydrogels, Langmuir 36(13) (2020) 3292-3299.

(32) Bergstrand, A.; Rahmani-Monfared, G.; Östlund, Å.; Nydén, M.; Holmberg, K. Comparison of PEI-PEG and PLL-PEG Copolymer Coatings on the Prevention of Protein Fouling. *J. Biomed. Mater. Res. A* **2009**, *88A* (3), 608–615. https://doi.org/10.1002/jbm.a.31894.

(33) Sophia Alexandridou and Costas Kiparissides. *Nanotechnology in Medicine and Health*.

(34) Hoffman, A. S. Non-Fouling Surface Technologies. *J. Biomater. Sci. Polym. Ed.* **1999**, *10* (10), 1011–1014. https://doi.org/10.1163/156856299X00658.

(35) Leng, C.; Huang, H.; Zhang, K.; Hung, H.-C.; Xu, Y.; Li, Y.; Jiang, S.; Chen, Z. Effect of Surface Hydration on Antifouling Properties of Mixed Charged Polymers. *Langmuir* **2018**, *34* (22), 6538–6545. https://doi.org/10.1021/acs.langmuir.8b00768.

(36) Zhang, Z.; Vaisocherová, H.; Cheng, G.; Yang, W.; Xue, H.; Jiang, S. Non-fouling Behavior of Polycarboxybetaine-Grafted Surfaces: Structural and Environmental Effects. *Biomacromolecules* **2008**, *9* (10), 2686–2692. https://doi.org/10.1021/bm800407r.

(37) Mariner, E.; Haag, S. L.; Bernards, M. T. Impacts of Cross-Linker Chain Length on the Physical Properties of Polyampholyte Hydrogels. *Biointerphases* **2019**, *14* (3), 031002. https://doi.org/10.1116/1.5097412.

(38) Chang, Y.; Chen, S.; Yu, Q.; Zhang, Z.; Bernards, M.; Jiang, S. Development of Biocompatible Interpenetrating Polymer Networks Containing a Sulfobetaine-Based

Polymer and a Segmented Polyurethane for Protein Resistance. *Biomacromolecules* **2007**, *8* (1), 122–127. https://doi.org/10.1021/bm060739m.

(39) Chang, Y.; Chen, S.; Zhang, Z.; Jiang, S. Highly Protein-Resistant Coatings from Well-Defined Diblock Copolymers Containing Sulfobetaines. *Langmuir* **2006**, *22* (5), 2222–2226. https://doi.org/10.1021/la052962v.

(40) Feng, W.; Brash, J.; Zhu, S. Atom-Transfer Radical Grafting Polymerization of 2-Methacryloyloxyethyl Phosphorylcholine from Silicon Wafer Surfaces. *J. Polym. Sci. Part Polym. Chem.* **2004**, *42* (12), 2931–2942. https://doi.org/10.1002/pola.20095.

(41) Feng, W.; Zhu, S.; Ishihara, K.; Brash, J. L. Adsorption of Fibrinogen and Lysozyme on Silicon Grafted with Poly(2-Methacryloyloxyethyl Phosphorylcholine) via Surface-Initiated Atom Transfer Radical Polymerization. *Langmuir* **2005**, *21* (13), 5980–5987. https://doi.org/10.1021/la050277i.

(42) Hirota, K.; Murakami, K.; Nemoto, K.; Miyake, Y. Coating of a Surface with 2-Methacryloyloxyethyl Phosphorylcholine (MPC) Co-Polymer Significantly Reduces Retention of Human Pathogenic Microorganisms. *FEMS Microbiol. Lett.* **2005**, *248* (1), 37–45. https://doi.org/10.1016/j.femsle.2005.05.019.

(43) Guo, Q.; Sun, H.; Wu, X.; Yan, Z.; Tang, C.; Qin, Z.; Yao, M.; Che, P.; Yao, F.; Li, J. In Situ Clickable Purely Zwitterionic Hydrogel for Peritoneal Adhesion Prevention. *Chem. Mater.* **2020**, *32* (15), 6347–6357. https://doi.org/10.1021/acs.chemmater.0c00889.

(44) Yang, W.; Xue, H.; Li, W.; Zhang, J.; Jiang, S. Pursuing “Zero” Protein Adsorption of Poly(Carboxybetaine) from Undiluted Blood Serum and Plasma. *Langmuir* **2009**, *25* (19), 11911–11916. https://doi.org/10.1021/la9015788.

(45) Ishida, T.; Kiwada, H. Accelerated Blood Clearance (ABC) Phenomenon upon Repeated Injection of PEGylated Liposomes. *Int. J. Pharm.* **2008**, *354* (1–2), 56–62. https://doi.org/10.1016/j.ijpharm.2007.11.005.

(46) Tagami, T.; Uehara, Y.; Moriyoshi, N.; Ishida, T.; Kiwada, H. Anti-PEG IgM Production by SiRNA Encapsulated in a PEGylated Lipid Nanocarrier Is Dependent on the Sequence of the SiRNA. *J. Controlled Release* **2011**, *151* (2), 149–154. https://doi.org/10.1016/j.jconrel.2010.12.013.

(47) Walker, J. A.; Robinson, K. J.; Munro, C.; Gengenbach, T.; Muller, D. A.; Young, P. R.; Lua, L. H. L.; Corrie, S. R. Antibody-Binding, Antifouling Surface Coatings Based on Recombinant Expression of Zwitterionic EK Peptides. *Langmuir* **2019**, *35* (5), 1266–1272. https://doi.org/10.1021/acs.langmuir.8b00810.

(48) Anderson, J. M. Biological Responses to Materials. *Annu. Rev. Mater. Res.* **2001**, *31* (1), 81–110. https://doi.org/10.1146/annurev.matsci.31.1.81.

(49) Anderson, J. M.; Rodriguez, A.; Chang, D. T. Foreign Body Reaction to Biomaterials. *Semin. Immunol.* **2008**, *20* (2), 86–100. https://doi.org/10.1016/j.smim.2007.11.004.

(50) Zhang, L.; Cao, Z.; Bai, T.; Carr, L.; Ella-Menye, J.-R.; Irvin, C.; Ratner, B. D.; Jiang, S. Zwitterionic Hydrogels Implanted in Mice Resist the Foreign-Body Reaction. *Nat. Biotechnol.* **2013**, *31* (6), 553–556. https://doi.org/10.1038/nbt.2580.

(51) Jain, P.; Hung, H.-C.; Li, B.; Ma, J.; Dong, D.; Lin, X.; Sinclair, A.; Zhang, P.; O'Kelly, M. B.; Niu, L.; Jiang, S. Zwitterionic Hydrogels Based on a Degradable Disulfide Carboxybetaine Cross-Linker. *Langmuir* **2019**, *35* (5), 1864–1871. https://doi.org/10.1021/acs.langmuir.8b02100.

(52) Tian, L.; George, S. C. Biomaterials to Prevascularize Engineered Tissues. *J Cardiovasc. Transl. Res.* **2011**, *4* (5), 685–698. https://doi.org/10.1007/s12265-011-9301-3.

(53) Tirrell DA. Biomaterials: Important Areas for Future Investment. Arlington, VA: 2012.

(54) Dong, D.; Tsao, C.; Hung, H.-C.; Yao, F.; Tang, C.; Niu, L.; Ma, J.; MacArthur, J.; Sinclair, A.; Wu, K.; Jain, P.; Hansen, M. R.; Ly, D.; Tang, S. G.; Luu, T. M.; Jain, P.; Jiang, S. High-Strength and Fibrous Capsule–Resistant Zwitterionic Elastomers. *Sci. Adv.* **2021**, *7* (1), eabc5442. https://doi.org/10.1126/sciadv.abc5442.

(55) Hucknall, A.; Rangarajan, S.; Chilkoti, A. In Pursuit of Zero: Polymer Brushes That Resist the Adsorption of Proteins. *Adv. Mater.* **2009**, *21* (23), 2441–2446. https://doi.org/10.1002/adma.200900383.

(56) Ladd, J.; Zhang, Z.; Chen, S.; Hower, J. C.; Jiang, S. Zwitterionic Polymers Exhibiting High Resistance to Nonspecific Protein Adsorption from Human Serum and Plasma. *Biomacromolecules* **2008**, *9* (5), 1357–1361. https://doi.org/10.1021/bm701301s.

(57) Twibanire, J. K.; Grindley, T. B. Efficient and Controllably Selective Preparation of Esters Using Uronium-Based Coupling Agents. *Org. Lett.* **2011**, *13* (12), 2988–2991. https://doi.org/10.1021/ol201005s.

(58) Jiang, S.; Cao, Z. Ultralow-Fouling, Functionalizable, and Hydrolyzable Zwitterionic Materials and Their Derivatives for Biological Applications. *Adv. Mater.* **2010**, *22* (9), 920–932. https://doi.org/10.1002/adma.200901407.

(59) Schroeder, M. E.; Zurick, K. M.; McGrath, D. E.; Bernards, M. T. Multifunctional Polyampholyte Hydrogels with Fouling Resistance and Protein Conjugation Capacity. *Biomacromolecules* **2013**, *14* (9), 3112–3122. https://doi.org/10.1021/bm4007369.

(60) Carr, L. R.; Xue, H.; Jiang, S. Functionalizable and Non-fouling Zwitterionic Carboxybetaine Hydrogels with a Carboxybetaine Dimethacrylate Cross-linker. *Biomaterials* **2011**, *32* (4), 961–968. https://doi.org/10.1016/j.biomaterials.2010.09.067.

(61) Chiu, C.-Y.; Chang, Y.; Liu, T.-H.; Chou, Y.-N.; Yen, T.-J. Convergent Charge Interval Spacing of Zwitterionic 4-Vinylpyridine Carboxybetaine Structures for Superior Blood-Inert Regulation in Amphiphilic Phases. *J. Mater. Chem. B* **2021**, *9* (40), 8437–8450. https://doi.org/10.1039/D1TB01374B.

(62) Alswieleh, A. M.; Cheng, N.; Canton, I.; Ustbas, B.; Xue, X.; Ladmiral, V.; Xia, S.; Ducker, R. E.; El Zubir, O.; Cartron, M. L.; Hunter, C. N.; Leggett, G. J.; Armes, S. P. Zwitterionic Poly(Amino Acid Methacrylate) Brushes. *J. Am. Chem. Soc.* **2014**, *136* (26), 9404–9413. https://doi.org/10.1021/ja503400r.

(63) Cui, J.; Ju, Y.; Liang, K.; Ejima, H.; Lörcher, S.; Gause, K. T.; Richardson, J. J.; Caruso, F. Nanoscale Engineering of Low-Fouling Surfaces through Polydopamine Immobilisation of Zwitterionic Peptides. *Soft Matter* **2014**, *10* (15), 2656–2663. https://doi.org/10.1039/C3SM53056F.

(64) He, Y.; Hower, J.; Chen, S.; Bernards, M. T.; Chang, Y.; Jiang, S. Molecular Simulation Studies of Protein Interactions with Zwitterionic Phosphorylcholine Self-Assembled Monolayers in the Presence of Water. *Langmuir* **2008**, *24* (18), 10358–10364. https://doi.org/10.1021/la8013046.

(65) Ziemba, C.; Khavkin, M.; Priftis, D.; Acar, H.; Mao, J.; Benami, M.; Gottlieb, M.; Tirrell, M.; Kaufman, Y.; Herzberg, M. Antifouling Properties of a Self-Assembling Glutamic Acid-Lysine Zwitterionic Polymer Surface Coating. *Langmuir* **2019**, *35* (5), 1699–1713. https://doi.org/10.1021/acs.langmuir.8b00181.

(66) Chakraborty, M.; Waynant, K. V. Outside-In Strategy for Peptide-Based Methacrylate and Methacrylamide Zwitterionic Cross-Linkers. *Synlett* **2022**, *33* (07), 669–673. https://doi.org/10.1055/a-1754-2437.

(67) Chakraborty, M.; Haag, S. L.; Bernards, M. T.; Waynant, K. V. Synthesis of a Zwitterionic N-Ser–Ser-C Dimethacrylate Cross-Linker and Evaluation in Polyampholyte Hydrogels. *Biomater. Sci.* **2021**, *9* (16), 5508–5518. https://doi.org/10.1039/D1BM00603G.

(68) Chien, H.-C.; Colas, C.; Finke, K.; Springer, S.; Stoner, L.; Zur, A. A.; Venteicher, B.; Campbell, J.; Hall, C.; Flint, A.; Augustyn, E.; Hernandez, C.; Heeren, N.; Hansen, L.; Anthony, A.; Bauer, J.; Fotiadis, D.; Schlessinger, A.; Giacomini, K. M.; Thomas, A. A. Reevaluating the Substrate Specificity of the L-Type Amino Acid Transporter (LAT1). *J. Med. Chem.* **2018**, *61* (16), 7358–7373. https://doi.org/10.1021/acs.jmedchem.8b01007.

(69) Bush, S. M.; North, M.; Sellarajah, S. Synthesis and Chiro-Optical Properties of Copolymers from N-Boc-O-Methacryloyl-(S)-Serine Benzhydryl Ester and Methyl Methacrylate. *Polymer* **1998**, *39* (13), 2991–2993. https://doi.org/10.1016/S0032-3861(97)10004-0.

(70) Shendage, D. M.; Fröhlich, R.; Haufe, G. Highly Efficient Stereoconservative Amidation and Deamidation of α-Amino Acids. *Org. Lett.* **2004**, *6* (21), 3675–3678. https://doi.org/10.1021/ol048771l.

(71) Roskoski, R.; Lim, C. T.; Roskoski, L. M. Human Brain and Placental Choline Acetyltransferase: Purification and Properties. *Biochemistry* **1975**, *14* (23), 5105–5110. https://doi.org/10.1021/bi00694a013.

(72) Bland, R. D.; Clarke, T. L.; Harden, L. B. Rapid Infusion of Sodium Bicarbonate and Albumin into High-Risk Premature Infants Soon after Birth: A Controlled, Prospective Trial. *Am. J. Obstet. Gynecol.* **1976**, *124* (3), 263–267. https://doi.org/10.1016/0002-9378(76)90154-x.

(73) Haag, S. L.; Bernards, M. T. Enhanced Biocompatibility of Polyampholyte Hydrogels. *Langmuir* **2020**, *36* (13), 3292–3299. https://doi.org/10.1021/acs.langmuir.0c00114.

(74) Barcellona, M. N.; Johnson, N.; Bernards, M. T. Characterizing Drug Release from Non-fouling Polyampholyte Hydrogels. *Langmuir* **2015**, *31* (49), 13402–13409. https://doi.org/10.1021/acs.langmuir.5b03597.

(75) Kahn, T.; Bosch, J.; Levitt, M. F.; Goldstein, M. H. Effect of Sodium Nitrate Loading on Electrolyte Transport by the Renal Tubule. *Am. J. Physiol.* **1975**, *229* (3), 746–753. https://doi.org/10.1152/ajplegacy.1975.229.3.746.

(76) Powell, H. M.; Boyce, S. T. EDC Cross-Linking Improves Skin Substitute Strength and Stability. *Biomaterials* **2006**, *27* (34), 5821–5827. https://doi.org/10.1016/j.biomaterials.2006.07.030.

(77) Zurick, K. M.; Bernards, M. Recent Biomedical Advances with Polyampholyte Polymers. *J. Appl. Polym. Sci.* **2014**, *131* (6), n/a-n/a. https://doi.org/10.1002/app.40069.

(78) Hu, W.; Wang, Z.; Xiao, Y.; Zhang, S.; Wang, J. Advances in Crosslinking Strategies of Biomedical Hydrogels. *Biomater. Sci.* **2019**, *7* (3), 843–855. https://doi.org/10.1039/C8BM01246F.

(79) Bernards, M.; He, Y. Polyampholyte Polymers as a Versatile Zwitterionic Biomaterial Platform. *J. Biomater. Sci. Polym. Ed.* **2014**, *25* (14–15), 1479–1488. https://doi.org/10.1080/09205063.2014.938976.

(80) P. Jain, H.C. Hung, B.W. Li, J.R. Ma, D.Y. Dong, X.J. Lin, A. Sinclair, P. Zhang, M.B. O'Kelly, L.Q. Niu, S.Y. Jiang, Zwitterionic Hydrogels Based on a Degradable Disulfide Carboxybetaine Cross-Linker, Langmuir 35(5) (2019) 1864-1871.

(81) Carr, L. R.; Xue, H.; Jiang, S. Functionalizable and Non-fouling Zwitterionic Carboxybetaine Hydrogels with a Carboxybetaine Dimethacrylate Cross-linker. *Biomaterials* **2011**, *32* (4), 961–968. https://doi.org/10.1016/j.biomaterials.2010.09.067.

(82) Guo, Q.; Sun, H.; Wu, X.; Yan, Z.; Tang, C.; Qin, Z.; Yao, M.; Che, P.; Yao, F.; Li, J. In Situ Clickable Purely Zwitterionic Hydrogel for Peritoneal Adhesion Prevention. *Chem. Mater*. **2020**, *32* (15), 6347–6357. https://doi.org/10.1021/acs.chemmater.0c00889.

(83) Ferris, R.; Hucknall, A.; Kwon, B. S.; Chen, T.; Chilkoti, A.; Zauscher, S. Field-Induced Nanolithography for Patterning of Non-Fouling Polymer Brush Surfaces. *Small* **2011**, *7* (21), 3032–3037. https://doi.org/10.1002/smll.201100923.

(84) Fontes, C. M.; Achar, R. K.; Joh, D. Y.; Ozer, I.; Bhattacharjee, S.; Hucknall, A.; Chilkoti, A. Engineering the Surface Properties of a Zwitterionic Polymer Brush to Enable the Simple Fabrication of Inkjet-Printed Point-of-Care Immunoassays. *Langmuir* **2019**, *35* (5), 1379–1390. https://doi.org/10.1021/acs.langmuir.8b01597.

(85) Ma, H.; Hyun, J.; Stiller, P.; Chilkoti, A. "Non-Fouling" Oligo(Ethylene Glycol)-Functionalized Polymer Brushes Synthesized by Surface-Initiated Atom Transfer Radical Polymerization. *Adv. Mater.* **2004**, *16* (4), 338–341. https://doi.org/10.1002/adma.200305830.

(86) Koc, J.; Schönemann, E.; Wanka, R.; Aldred, N.; Clare, A. S.; Gardner, H.; Swain, G. W.; Hunsucker, K.; Laschewsky, A.; Rosenhahn, A. Effects of Crosslink Density in Zwitterionic Hydrogel Coatings on Their Antifouling Performance and Susceptibility to

Silt Uptake. *Biofouling* **2020**, *36* (6), 646–659. https://doi.org/10.1080/08927014.2020.1796983.

(87) Liu, Q.; Li, W.; Singh, A.; Cheng, G.; Liu, L. Two Amino Acid-Based Superlow Fouling Polymers: Poly(Lysine Methacrylamide) and Poly(Ornithine Methacrylamide). *Acta Biomater.* **2014**, *10* (7), 2956–2964. https://doi.org/10.1016/j.actbio.2014.02.046.

(88) Liu, Q.; Singh, A.; Liu, L. Amino Acid-Based Zwitterionic Poly(Serine Methacrylate) as an Antifouling Material. *Biomacromolecules* **2013**, *14* (1), 226–231. https://doi.org/10.1021/bm301646y.

(89) Laschewsky, A.; Rosenhahn, A. Molecular Design of Zwitterionic Polymer Interfaces: Searching for the Difference. *Langmuir* **2019**, *35* (5), 1056–1071. https://doi.org/10.1021/acs.langmuir.8b01789.

(90) Wuts, P. G. M.; Greene, T. W. *Greene's Protective Groups in Organic Synthesis, 4th Ed*.

(91) Xu, Q.; He, C.; Xiao, C.; Yu, S.; Chen, X. ε-Methacryloyl- L -Lysine Based Polypeptides and Their Thiol–Ene Click Functionalization. *Polym. Chem.* **2015**, *6* (10), 1758–1767. https://doi.org/10.1039/C4PY01523A.

(92) Zheng, J.; Li, L.; Tsao, H.-K.; Sheng, Y.-J.; Chen, S.; Jiang, S. Strong Repulsive Forces between Protein and Oligo (Ethylene Glycol) Self-Assembled Monolayers: A Molecular Simulation Study. *Biophys. J.* **2005**, *89* (1), 158–166. https://doi.org/10.1529/biophysj.105.059428.

(93) Han, X.; Leng, C.; Shao, Q.; Jiang, S.; Chen, Z. Absolute Orientations of Water Molecules at Zwitterionic Polymer Interfaces and Interfacial Dynamics after Salt Exposure. *Langmuir* **2019**, *35* (5), 1327–1334. https://doi.org/10.1021/acs.langmuir.8b01515.

(94) Flon, V.; Bénard, M.; Schapman, D.; Galas, L.; Renard, P.-Y.; Sabot, C. Fluorophore-Assisted Click Chemistry through Copper(I) Complexation. *Biomolecules* **2020**, *10* (4), 619. https://doi.org/10.3390/biom10040619.

(95) Ruoslahti, E. RGD AND OTHER RECOGNITION SEQUENCES FOR INTEGRINS. *Annu. Rev. Cell Dev. Biol.* **1996**, *12* (1), 697–715. https://doi.org/10.1146/annurev.cellbio.12.1.697.

(96) Yang, M.; Zhang, Z.-C.; Liu, Y.; Chen, Y.-R.; Deng, R.-H.; Zhang, Z.-N.; Yu, J.-K.; Yuan, F.-Z. Function and Mechanism of RGD in Bone and Cartilage Tissue Engineering. *Front. Bioeng. Biotechnol.* **2021**, *9*, 773636. https://doi.org/10.3389/fbioe.2021.773636.

(97) Coin, I.; Beyermann, M.; Bienert, M. Solid-Phase Peptide Synthesis: From Standard Procedures to the Synthesis of Difficult Sequences. *Nat. Protoc.* **2007**, *2* (12), 3247–3256. https://doi.org/10.1038/nprot.2007.454.

Appendix A

^{1}H and ^{13}C NMR Spectra of

Chapter 2,3 & 4

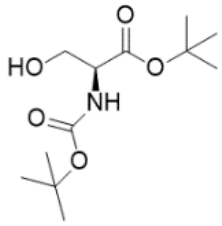

Compound **2-4**

^{1}H NMR spectrum (MeOD, 500 MHz)

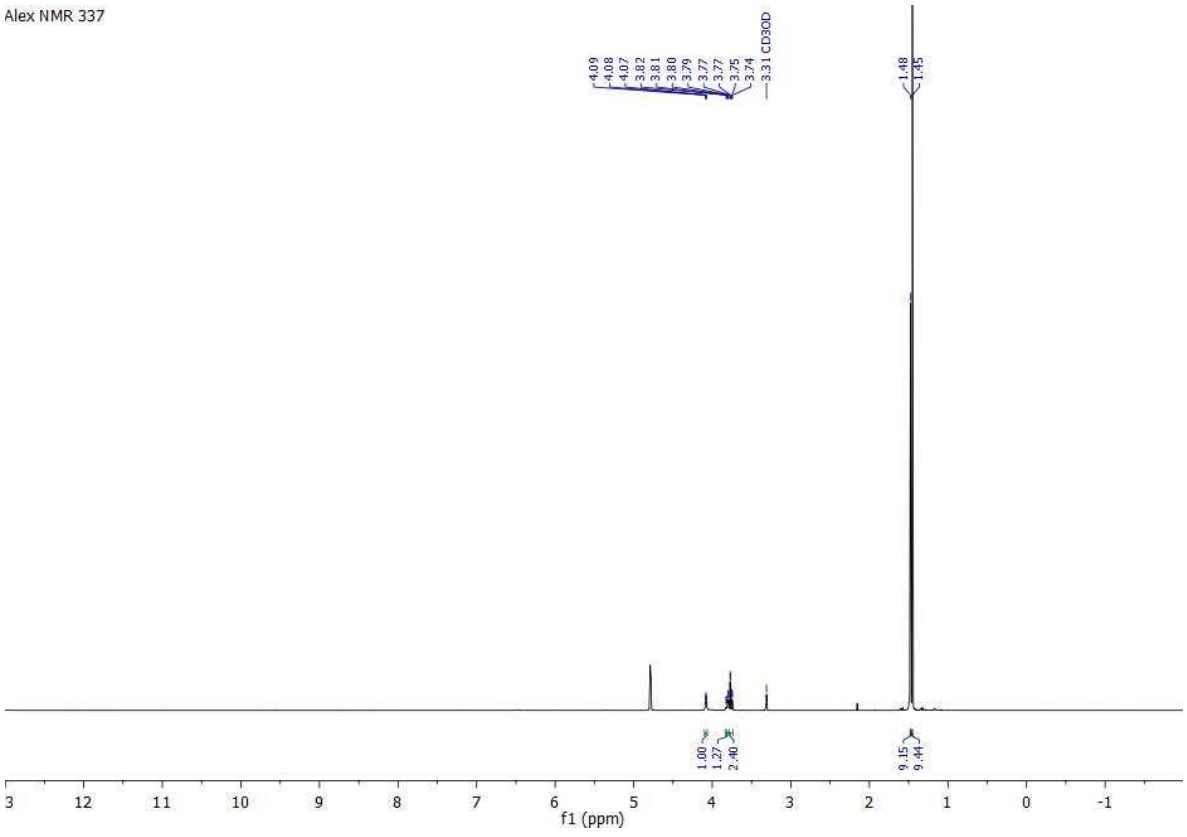

^{13}C NMR spectrum (MeOD, 126 MHz)

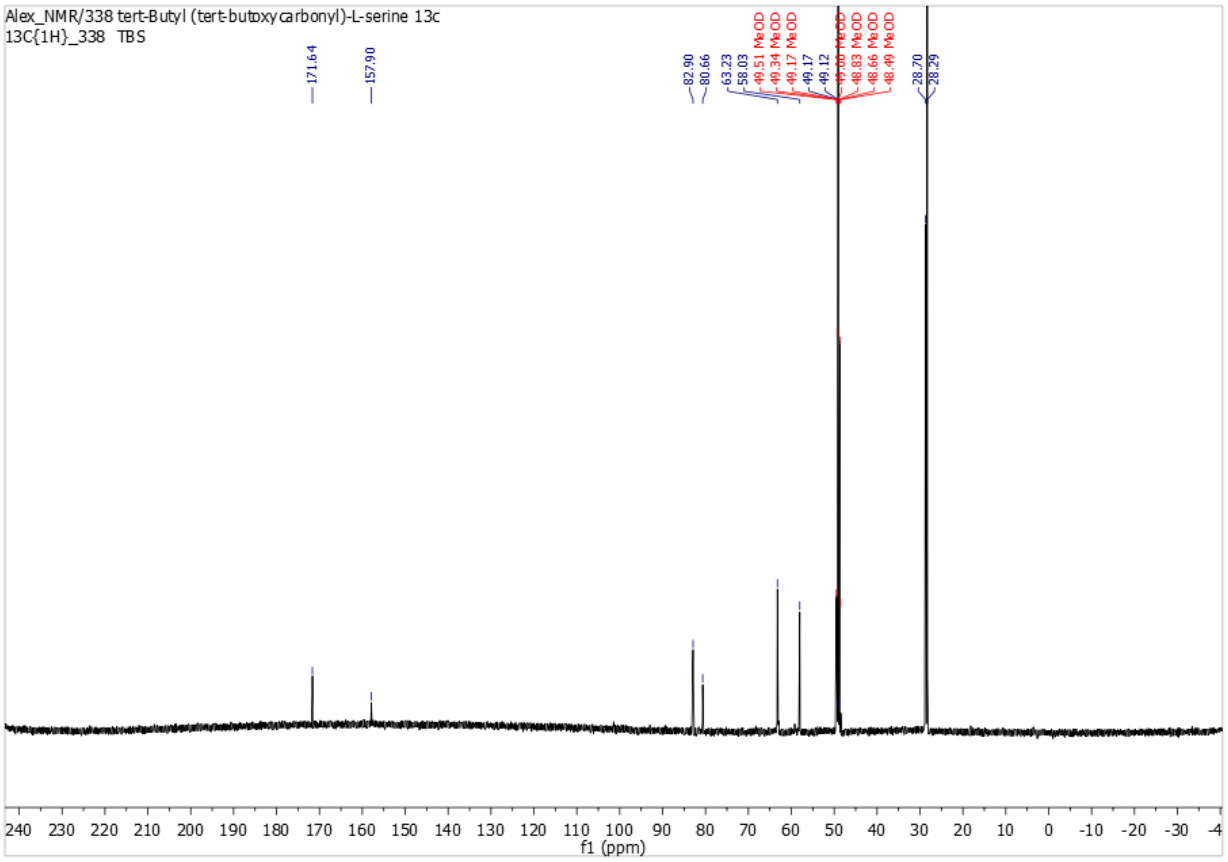

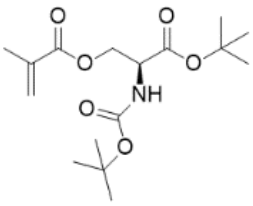

Compound **2-5**

^{1}H NMR spectrum (MeOD, 500 MHz)

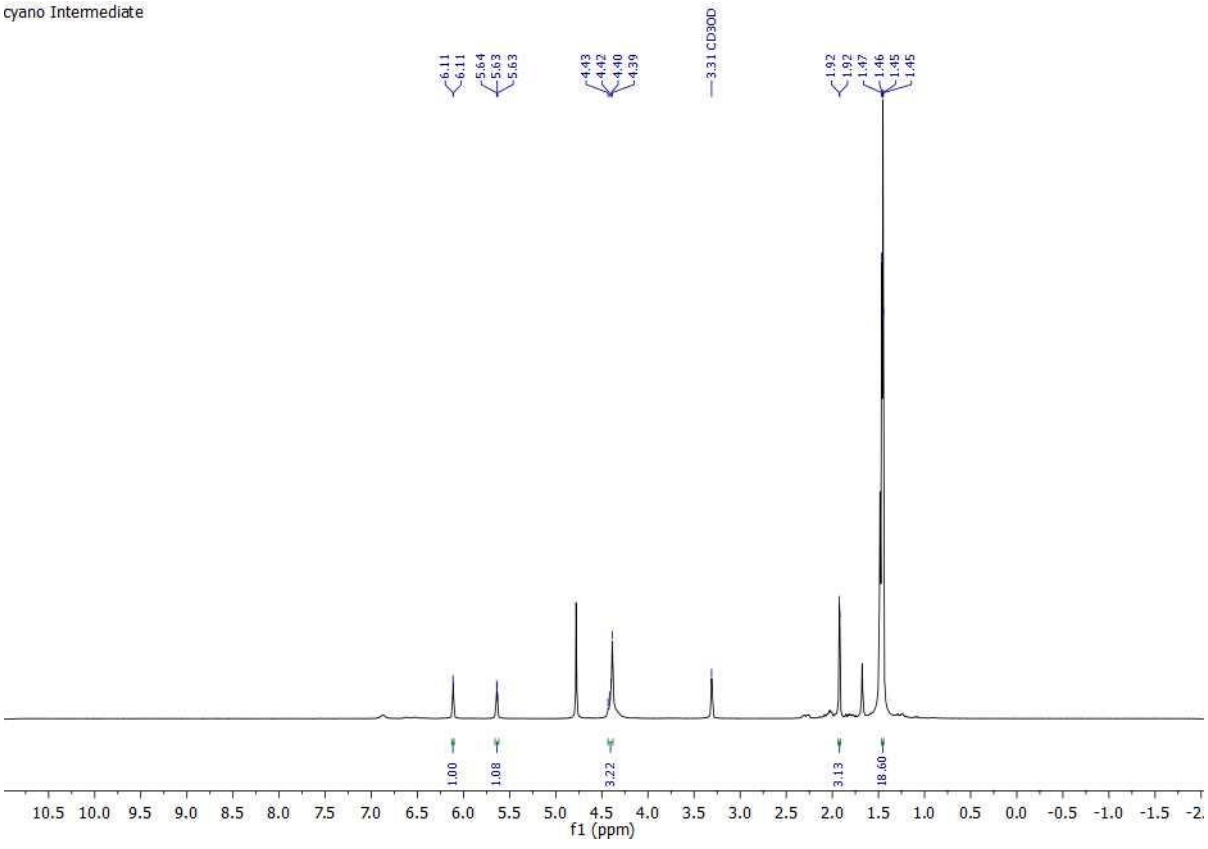

^{13}C NMR spectrum (MeOD, 126 MHz)

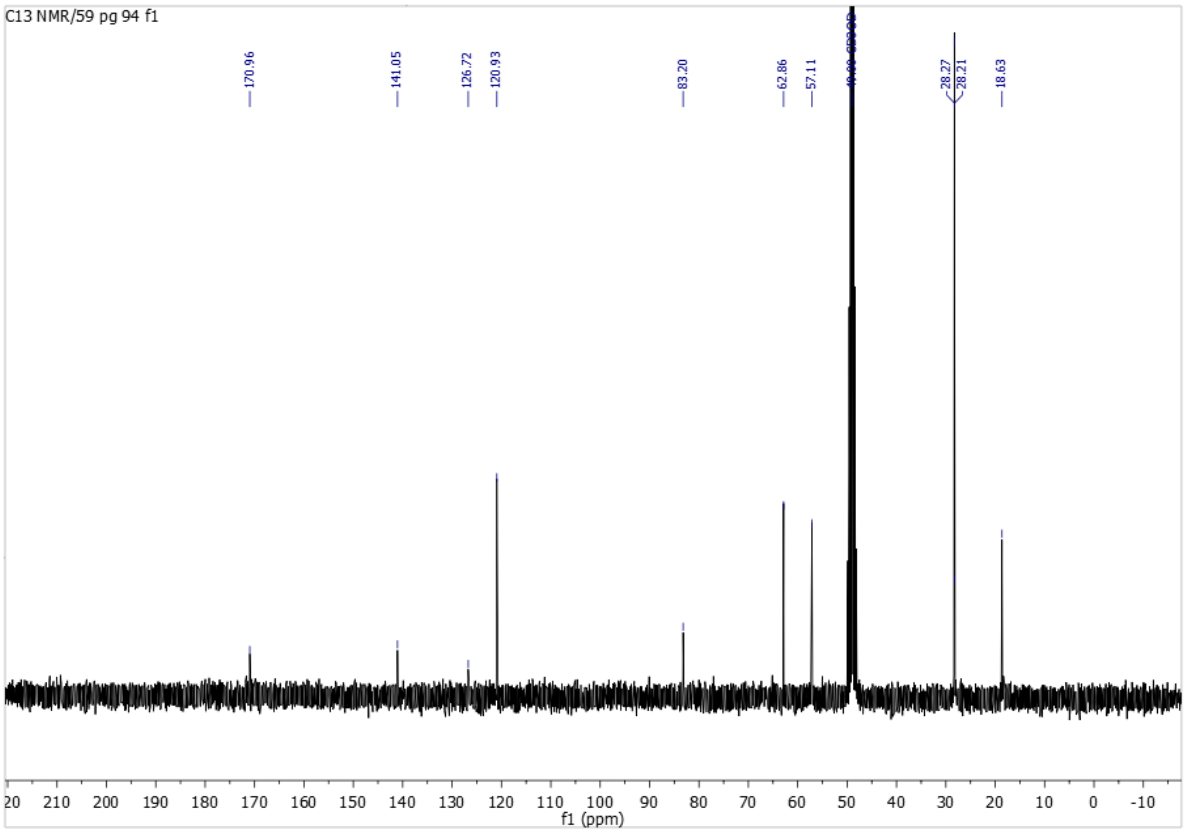

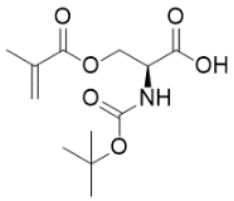

Compound **2-8**

^{1}H NMR spectrum (MeOD, 500 MHz)

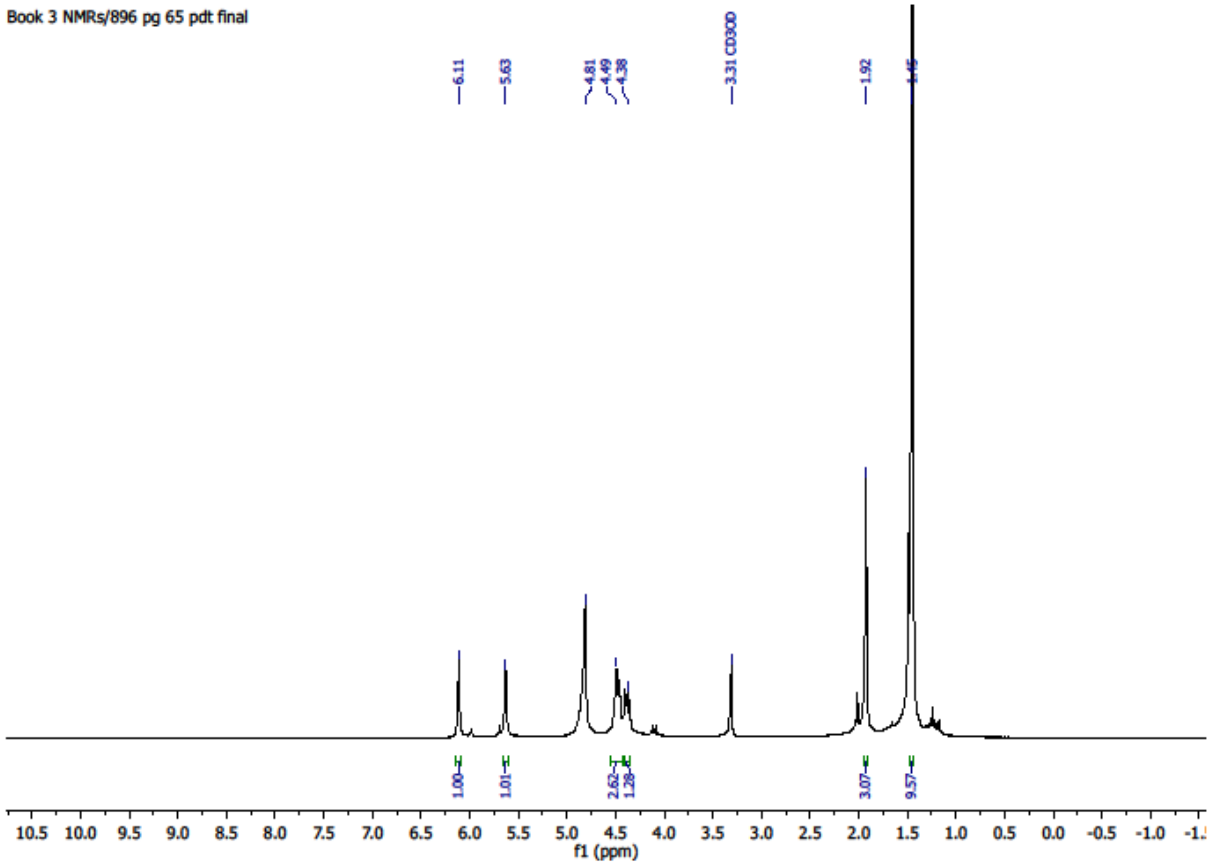

^{13}C NMR spectrum (MeOD, 126 MHz)

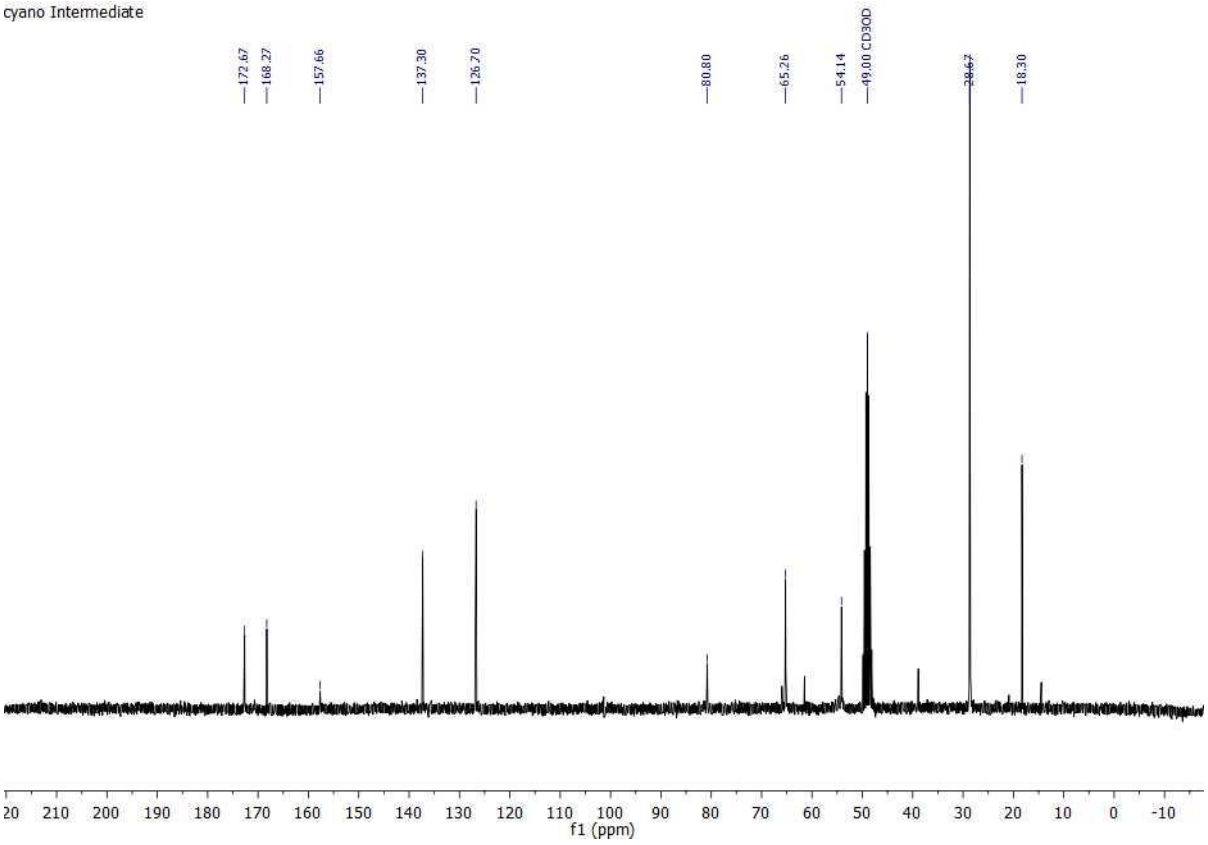

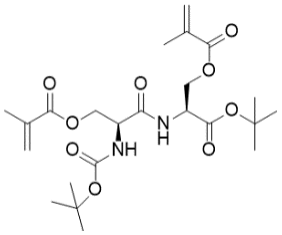

Compound **2-9**

^{1}H NMR spectrum (MeOD, 500 MHz)

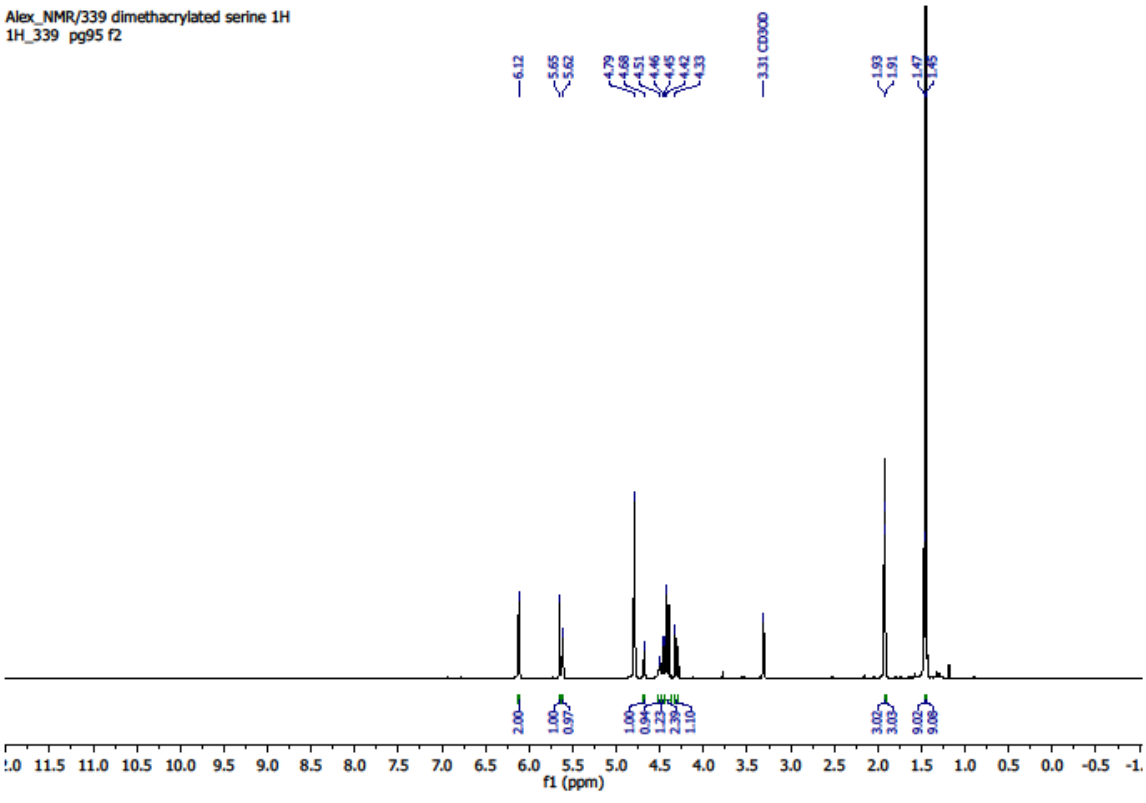

^{13}C NMR spectrum (MeOD, 126 MHz)

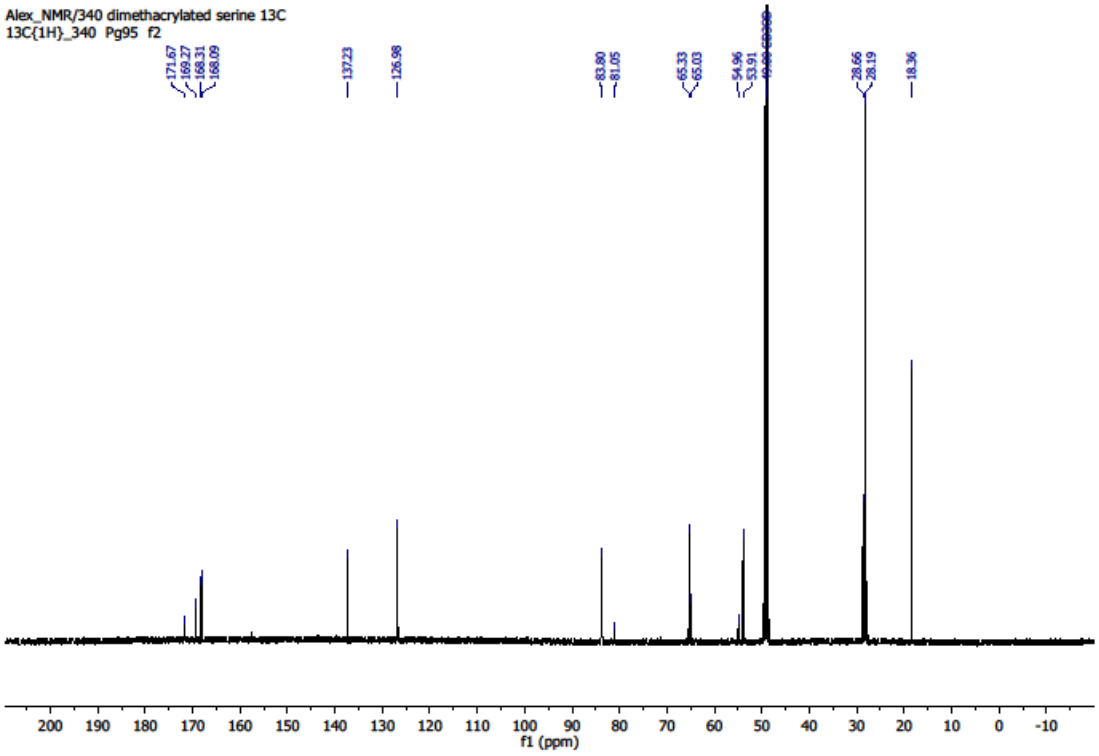

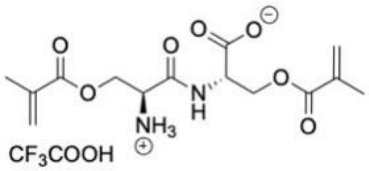

Compound **2-10**

^{1}H NMR spectrum (MeOD, 500 MHz)

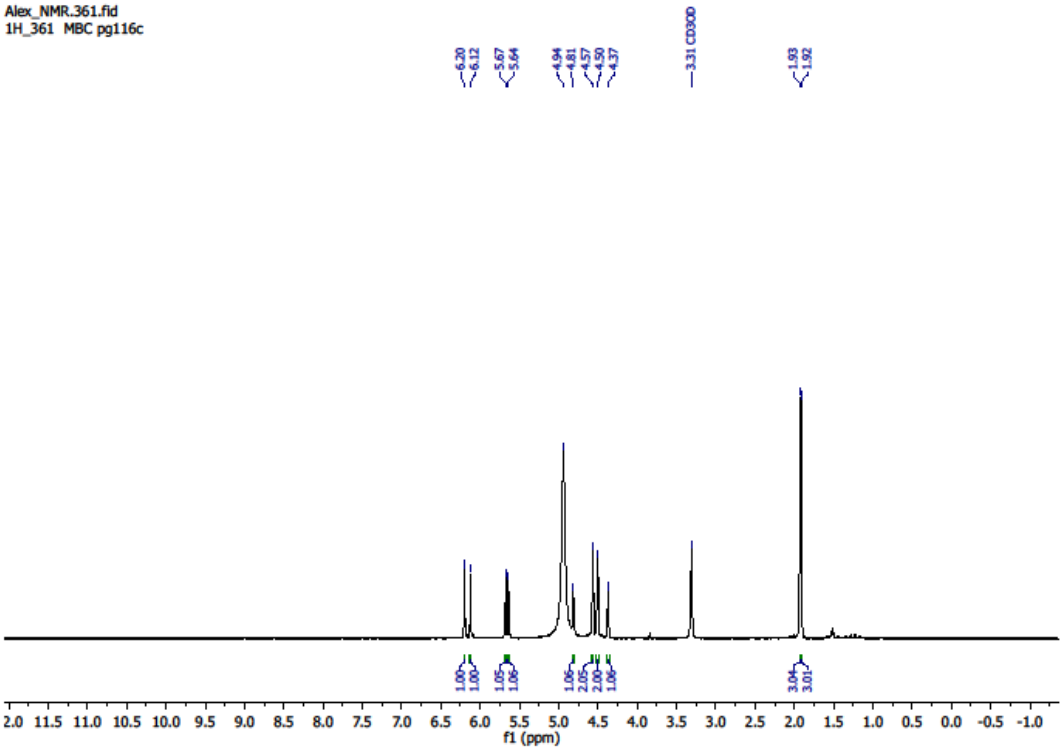

^{13}C NMR spectrum (MeOD, 126 MHz)

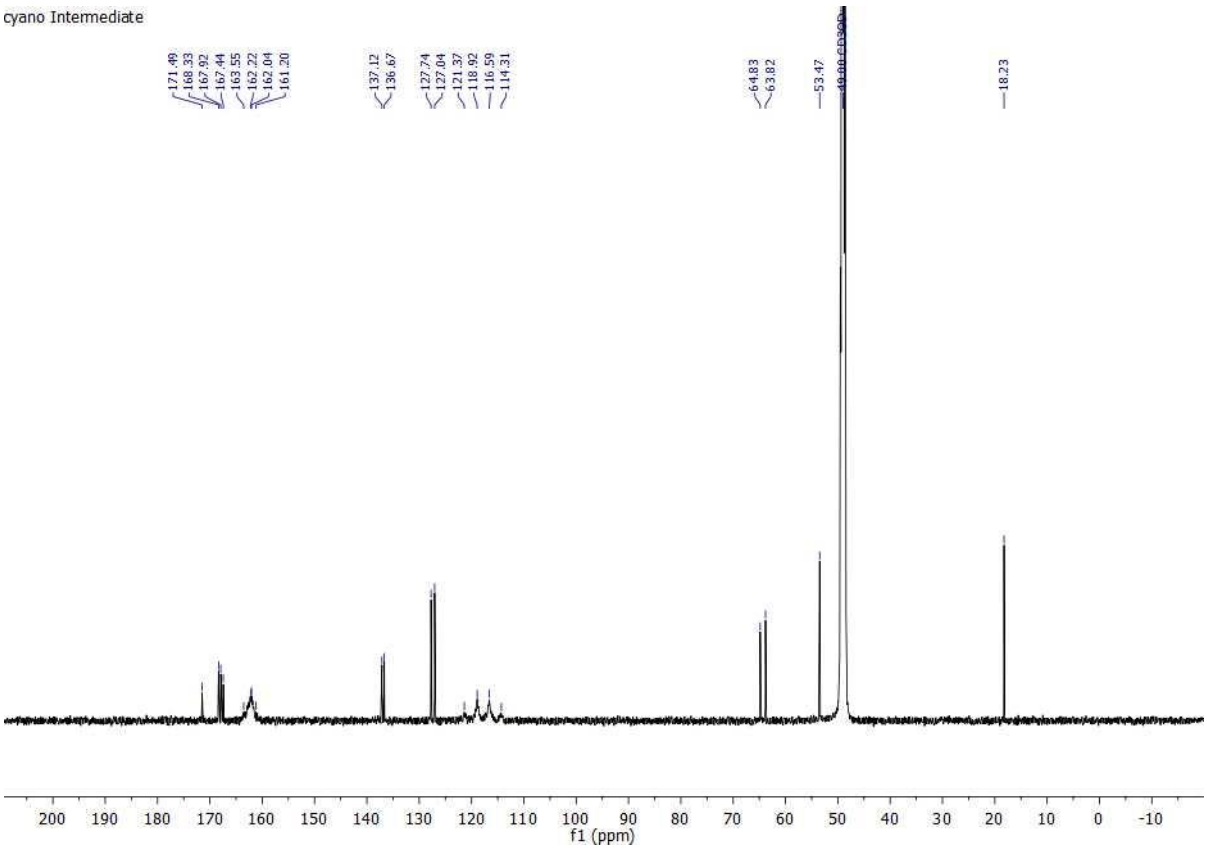

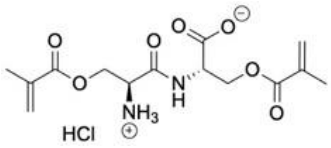

HCl Salt of Compound **2-10**

^{13}C NMR spectrum (MeOD, 126 MHz)

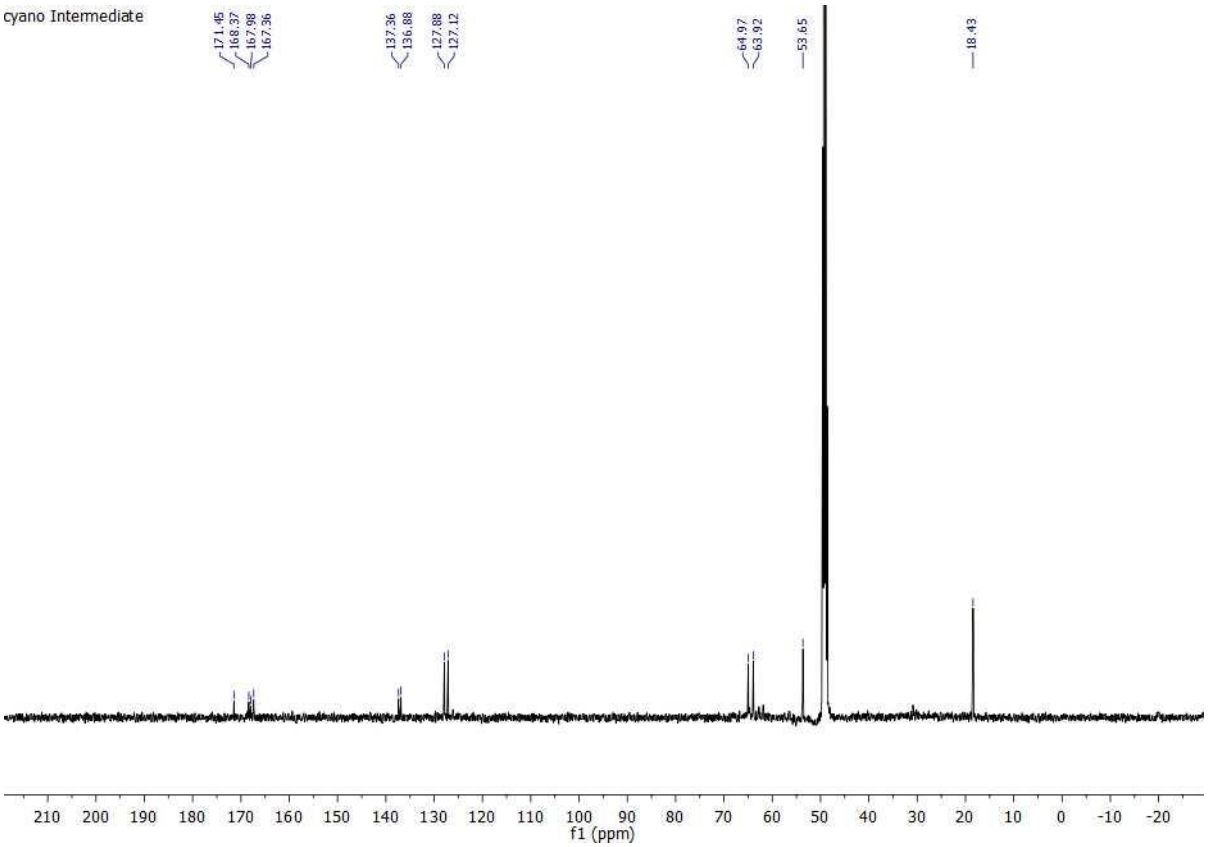

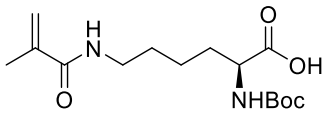

Compound **3-16**

^{1}H NMR spectrum ($CDCl_3$, 500 MHz)

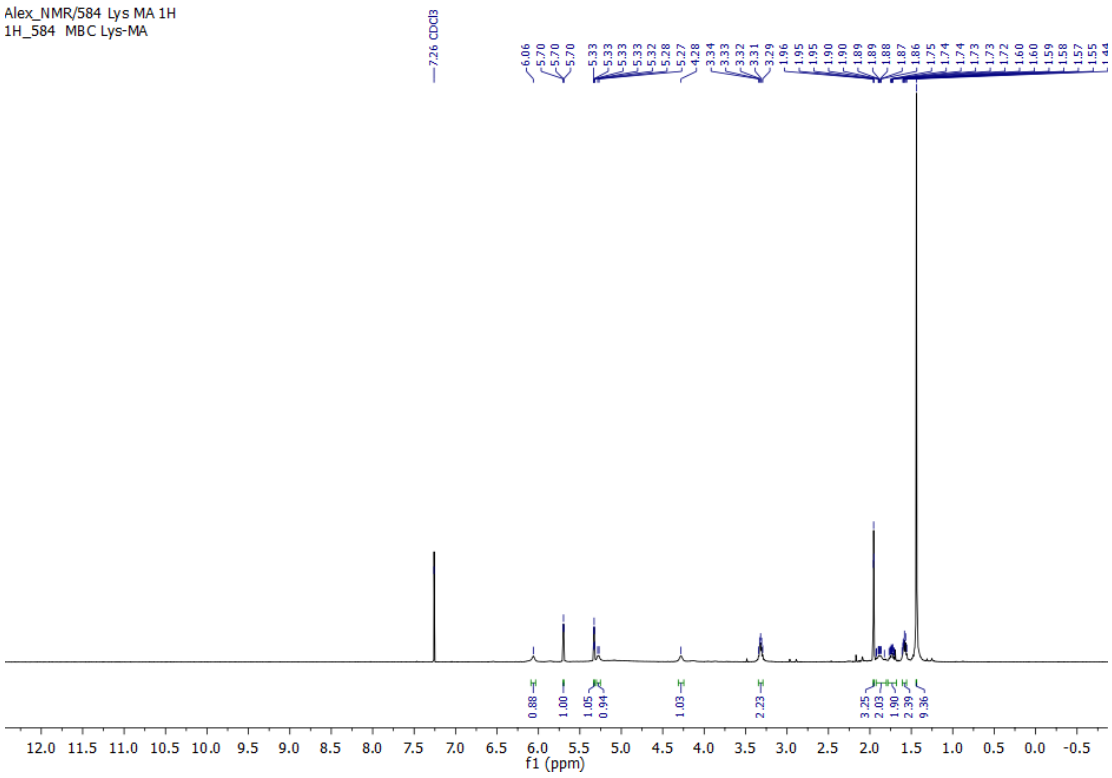

^{13}C NMR spectrum ($CDCl_3$, 126 MHz)

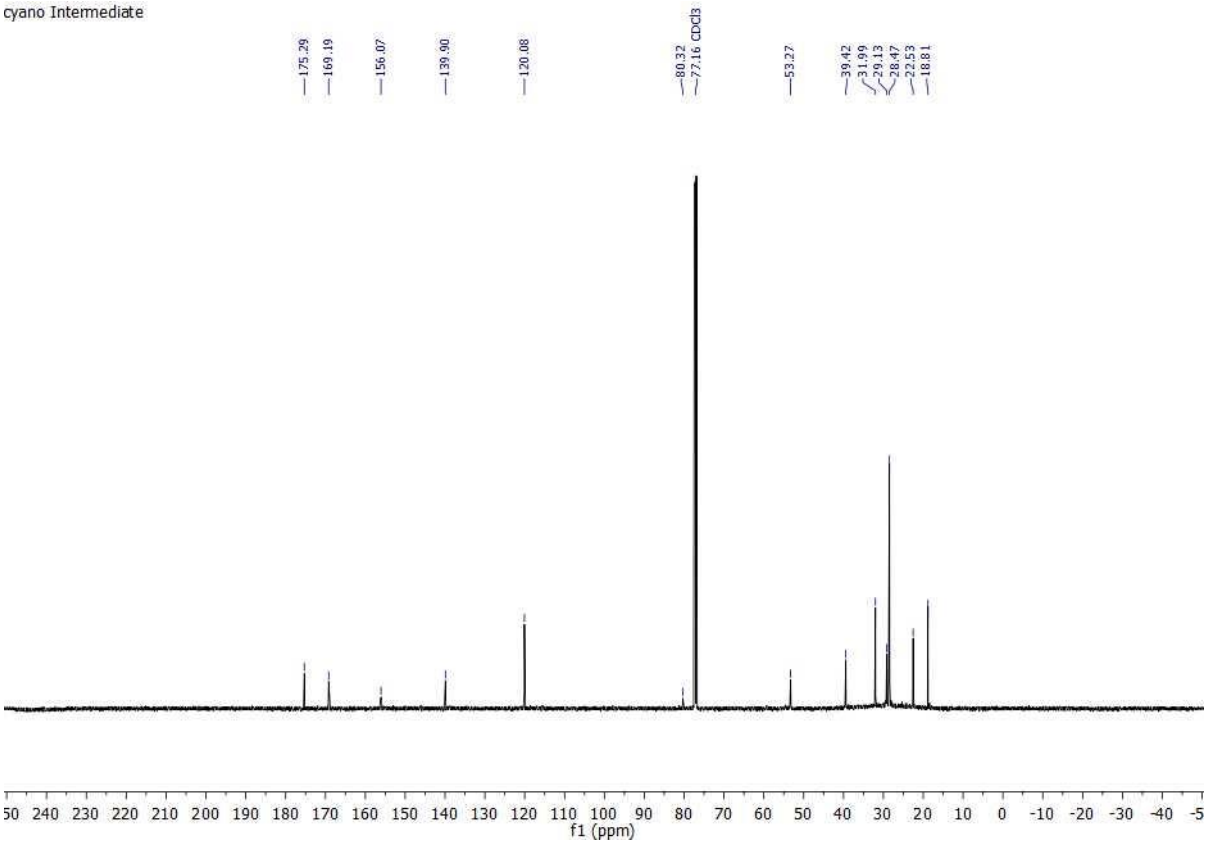

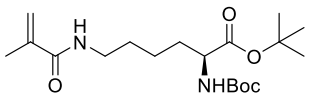

Compound **3-17**

^{1}H NMR spectrum ($CDCl_3$, 500 MHz)

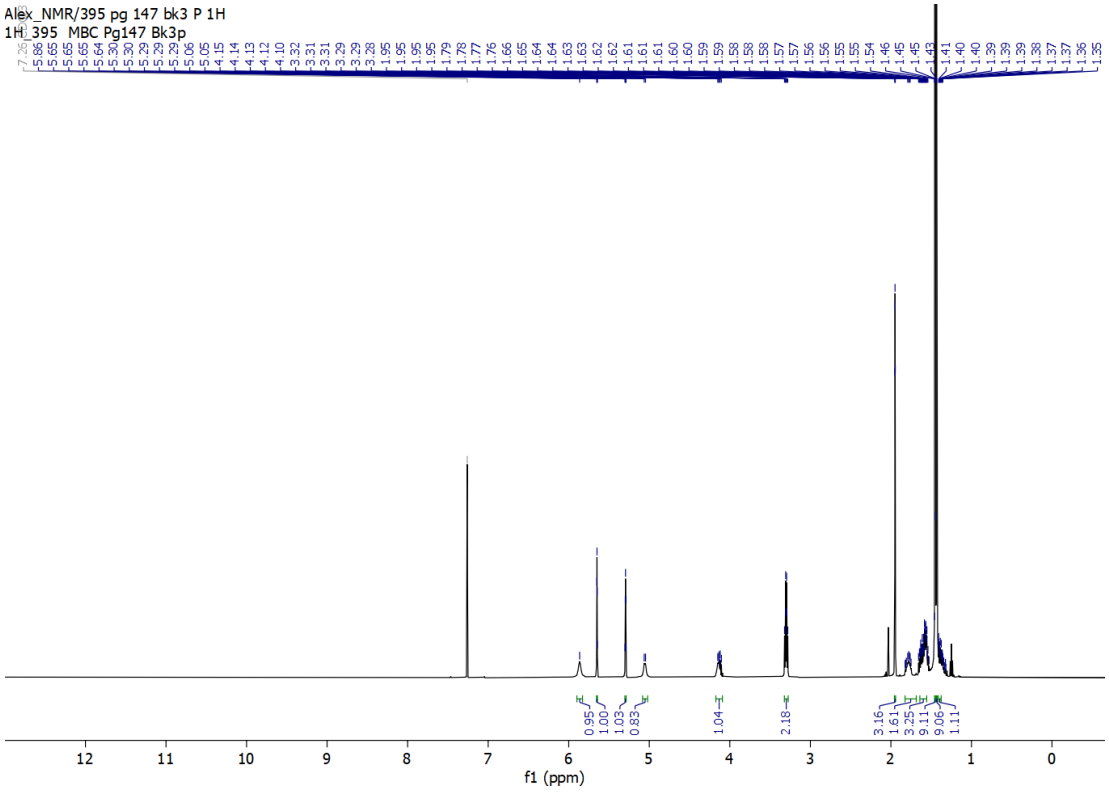

^{13}C NMR spectrum ($CDCl_3$, 126 MHz)

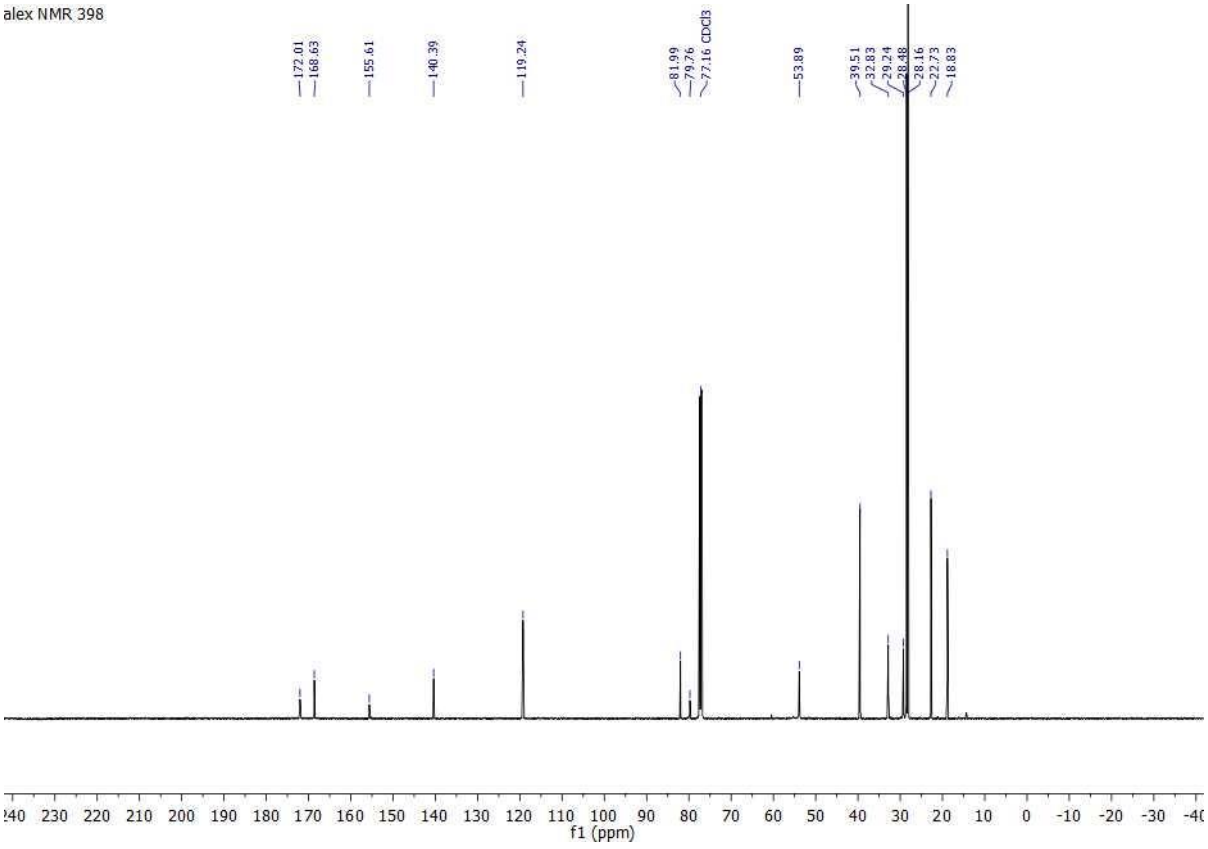

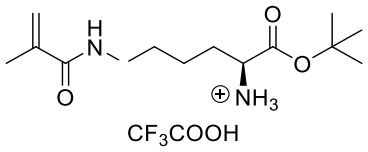

Compound **3-18**

^{1}H NMR spectrum (MeOD, 500 MHz)

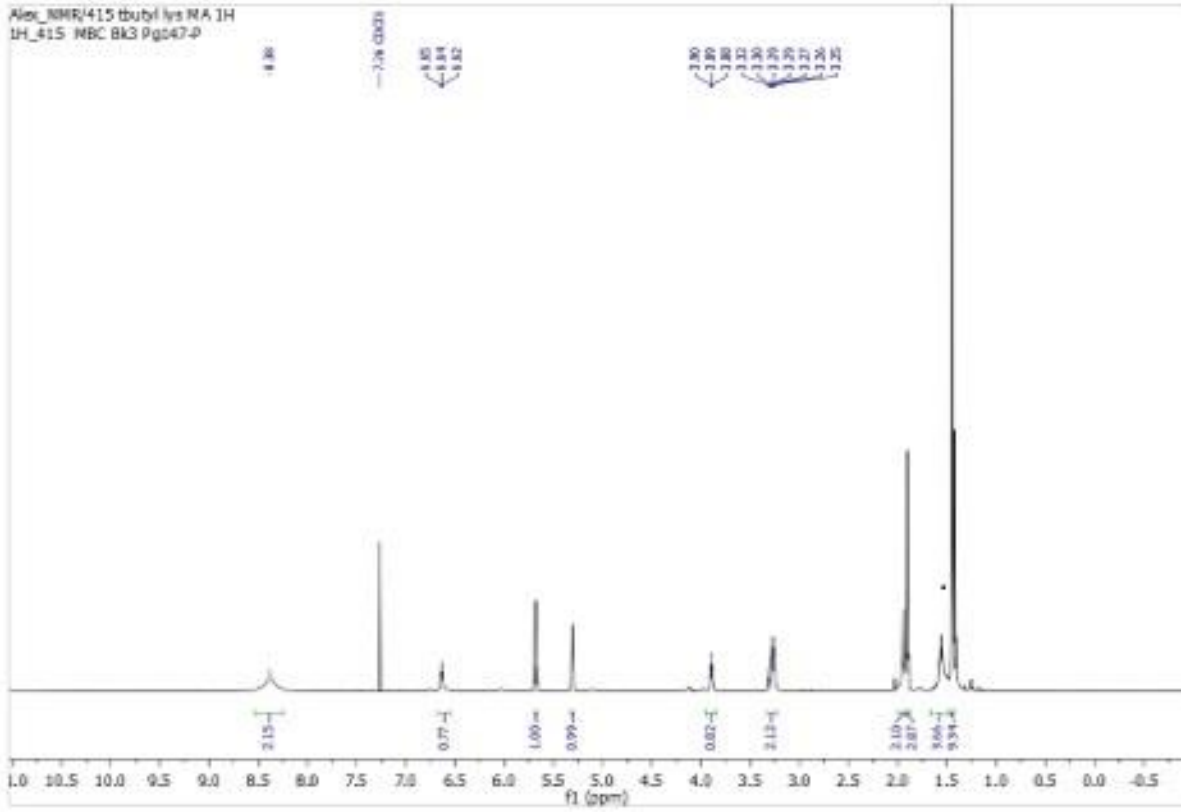

^{13}C NMR spectrum (MeOD, 126 MHz)

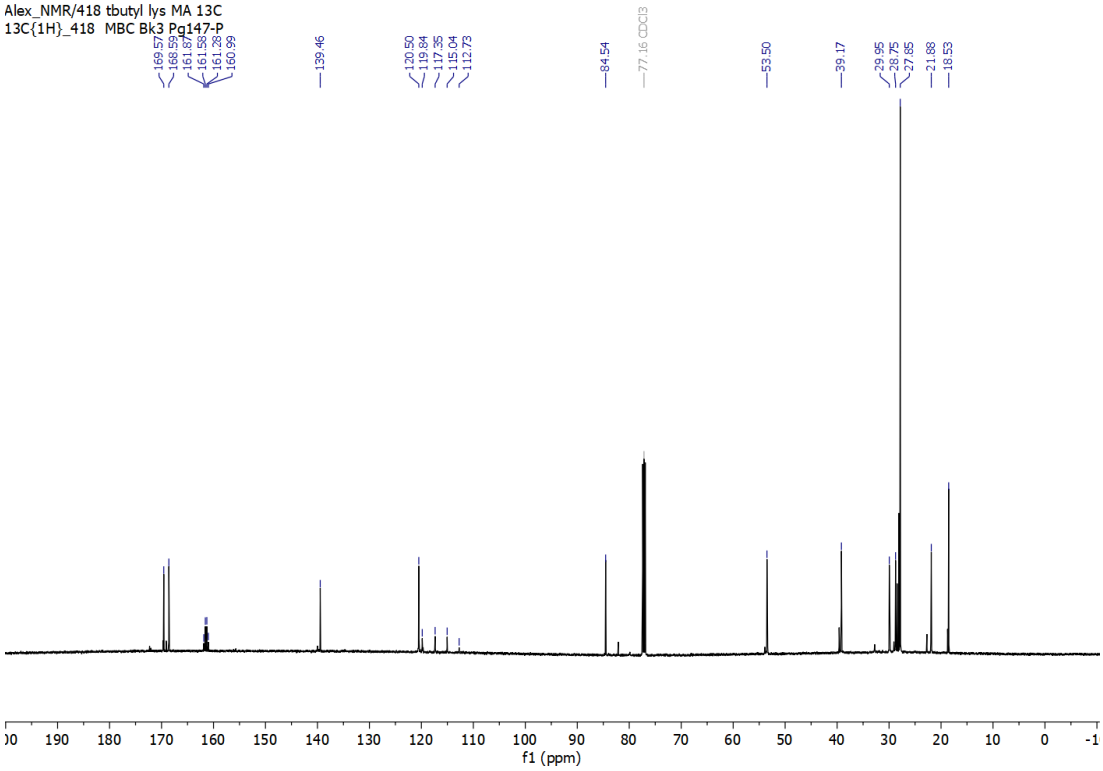

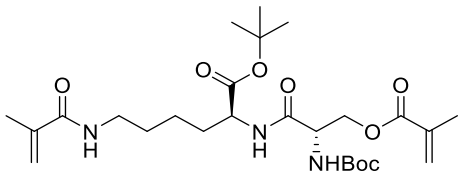

Compound **3-22**

^{1}H NMR spectrum ($CDCl_3$, 500 MHz)

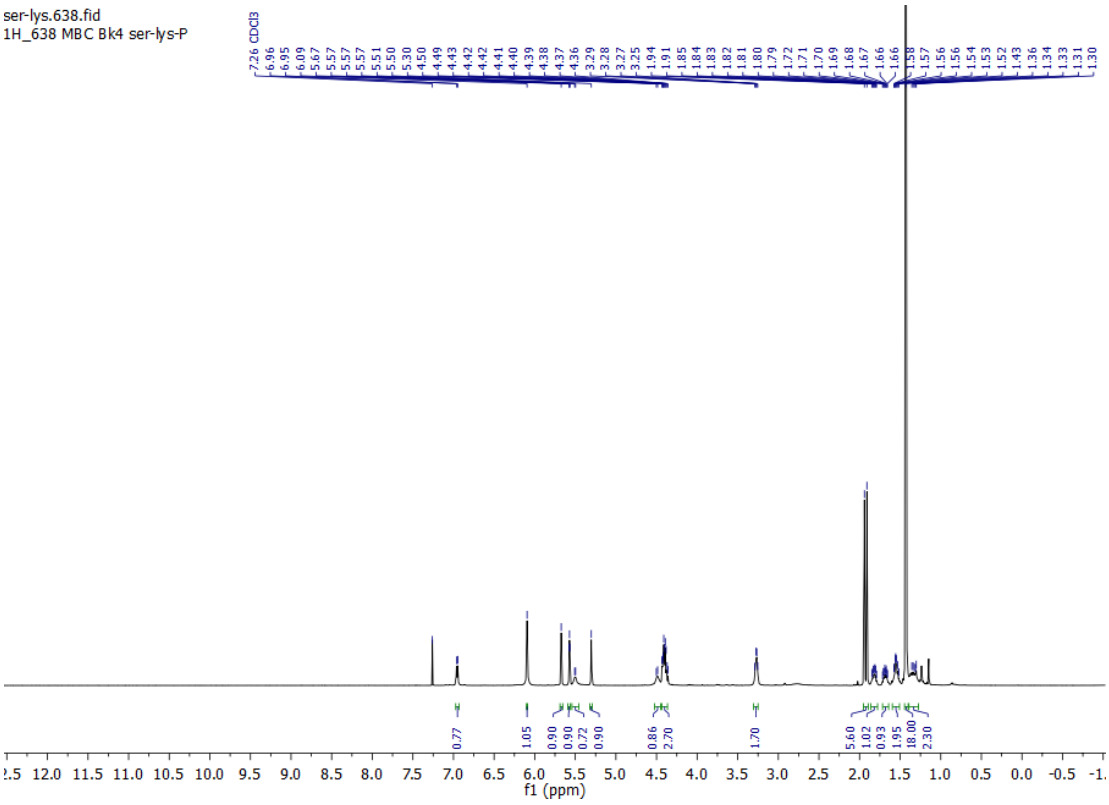

^{13}C NMR spectrum ($CDCl_3$, 126 MHz)

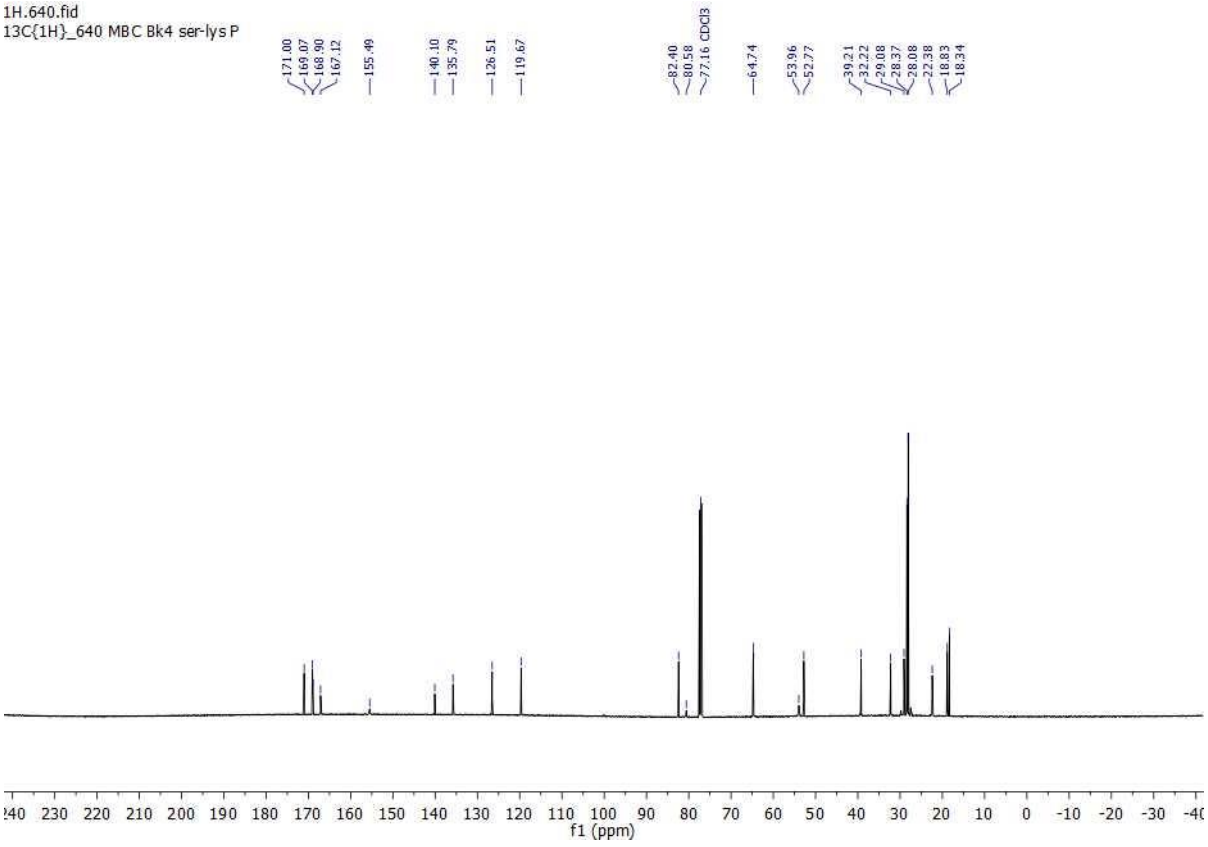

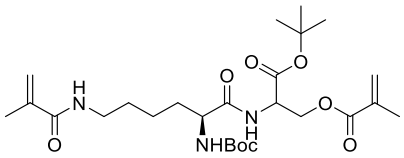

Compound **3-23**

^{1}H NMR spectrum ($CDCl_3$, 500 MHz)

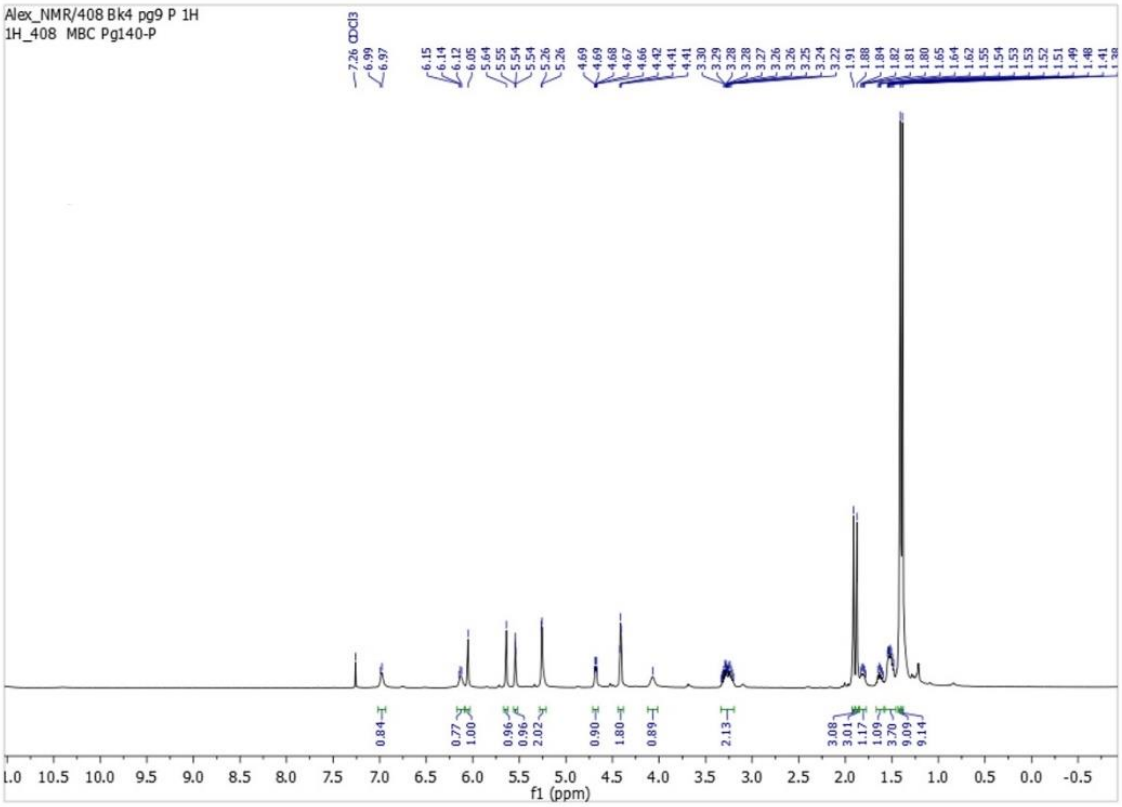

^{13}C NMR spectrum ($CDCl_3$, 126 MHz)

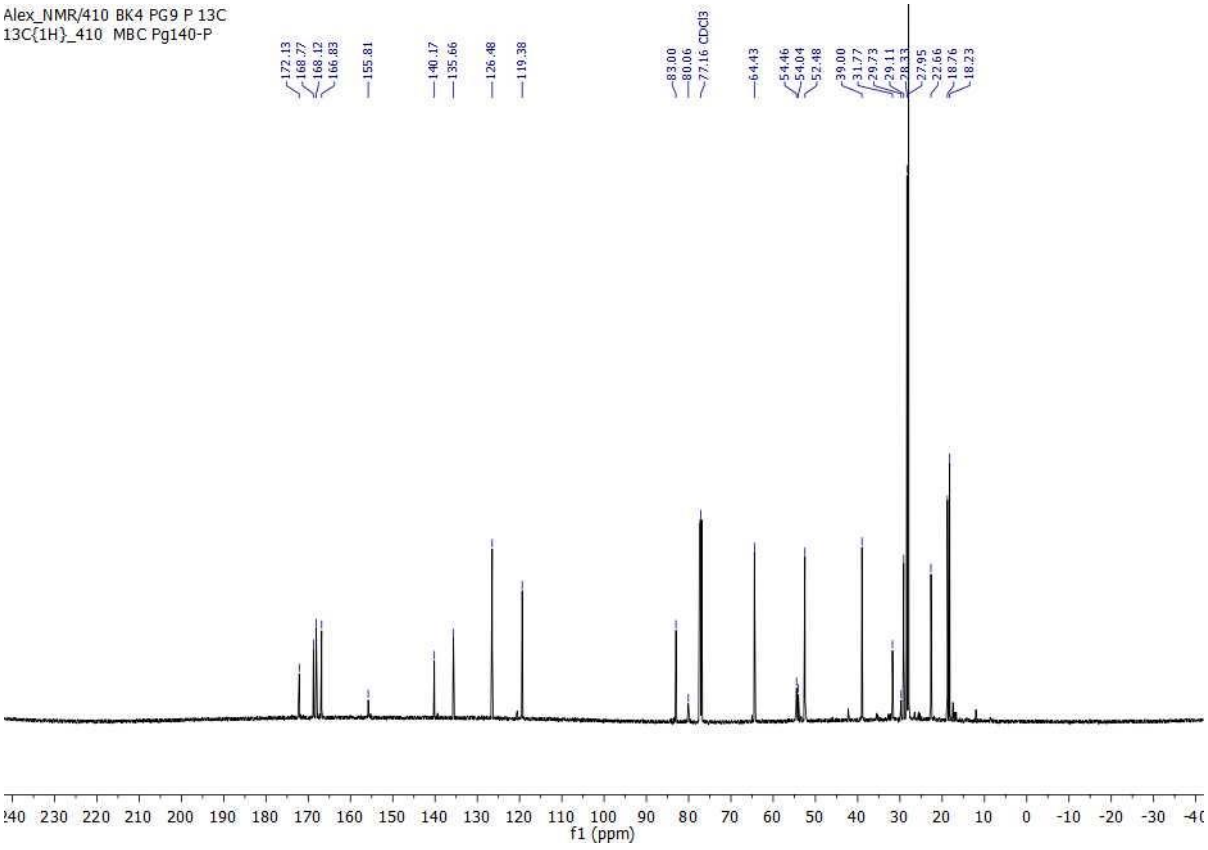

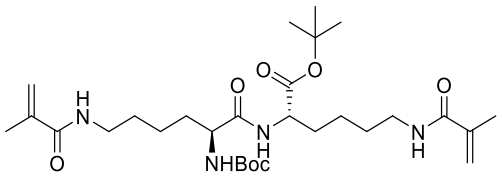

Compound **3-21**

^{1}H NMR spectrum ($CDCl_3$, 500 MHz)

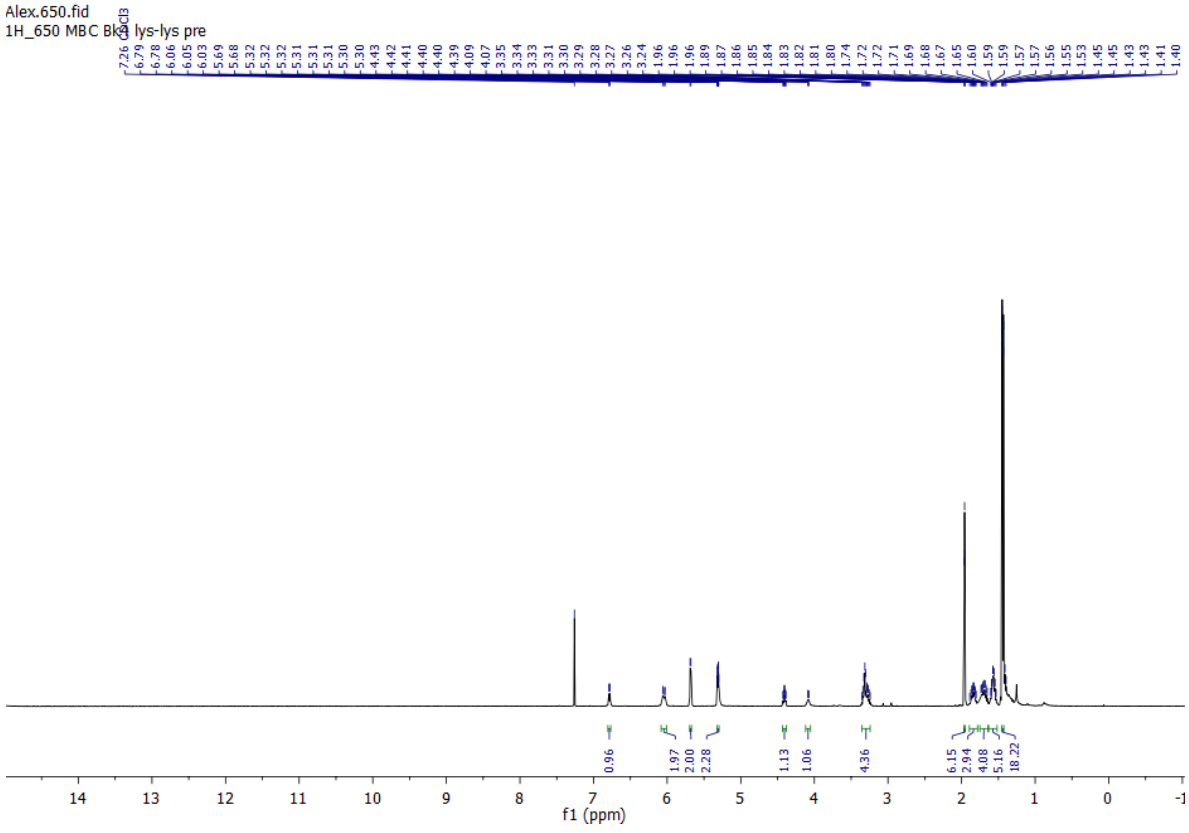

^{13}C NMR spectrum ($CDCl_3$, 126 MHz)

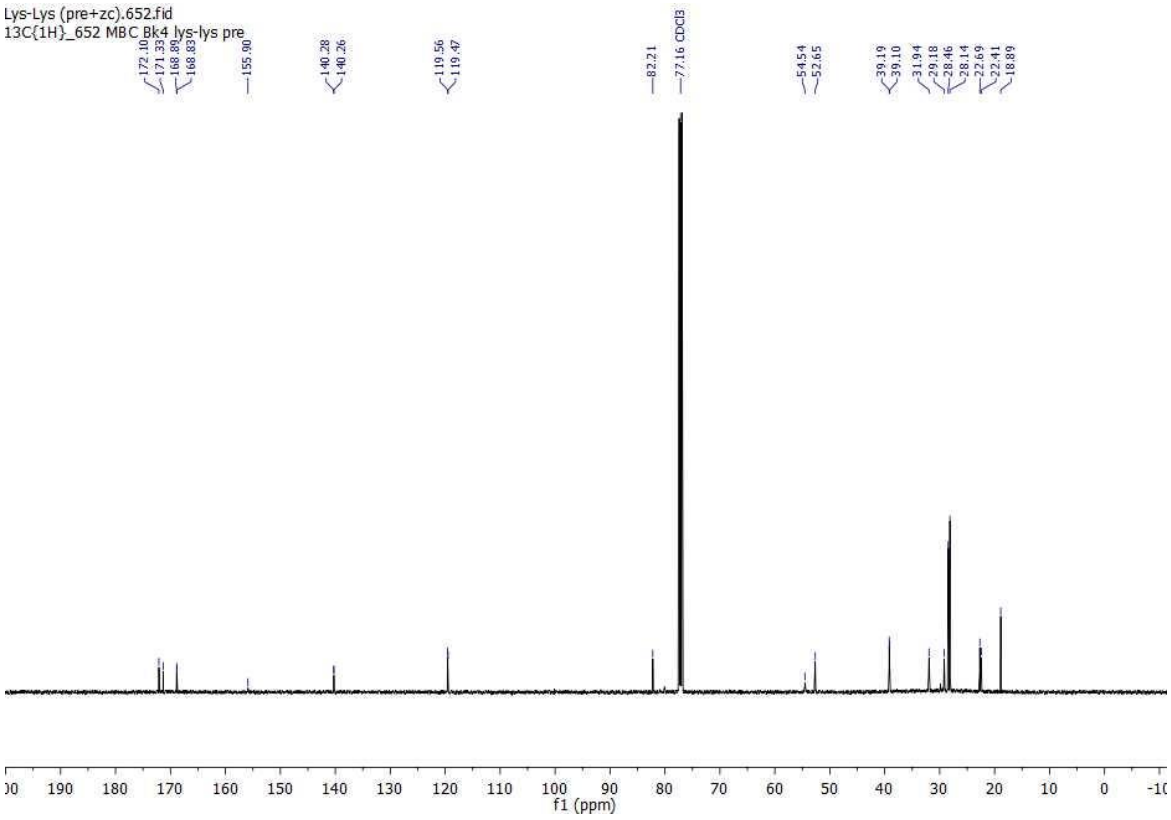

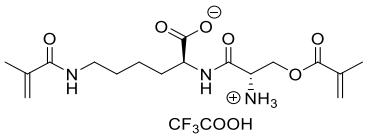

Compound **3-12**

^{1}H NMR spectrum (MeOD, 500 MHz)

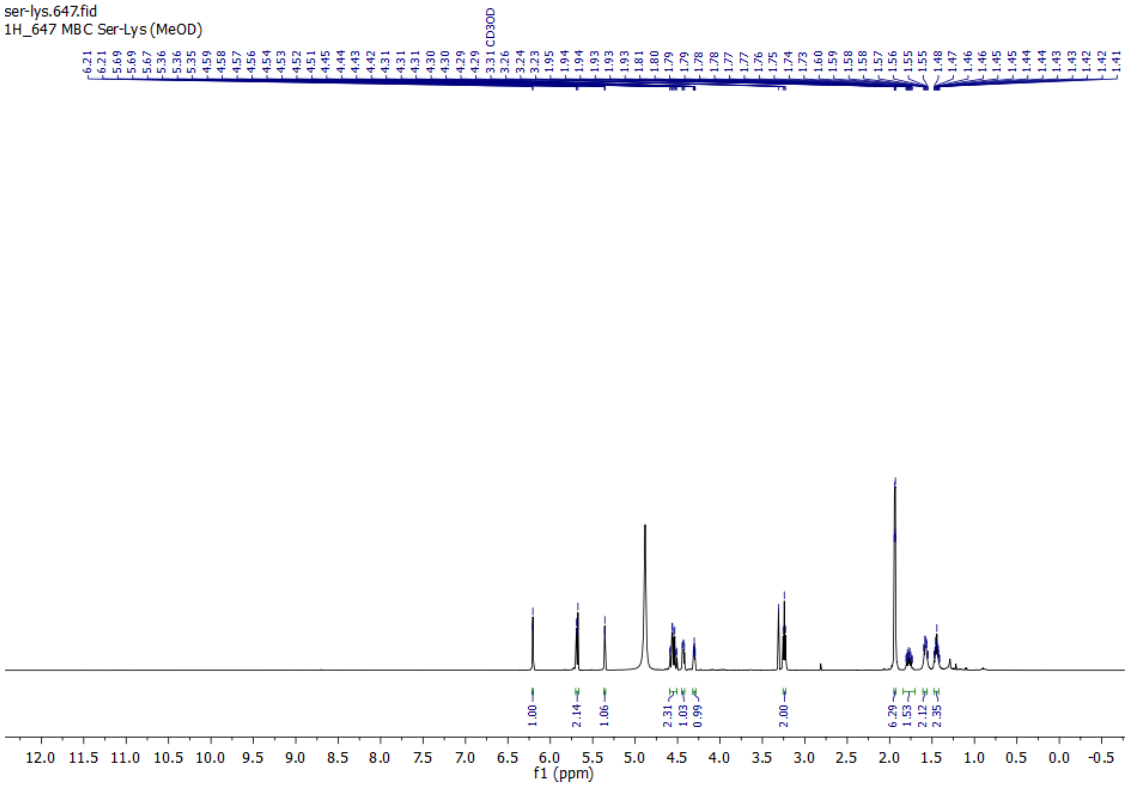

^{13}C NMR spectrum (MeOD, 126 MHz)

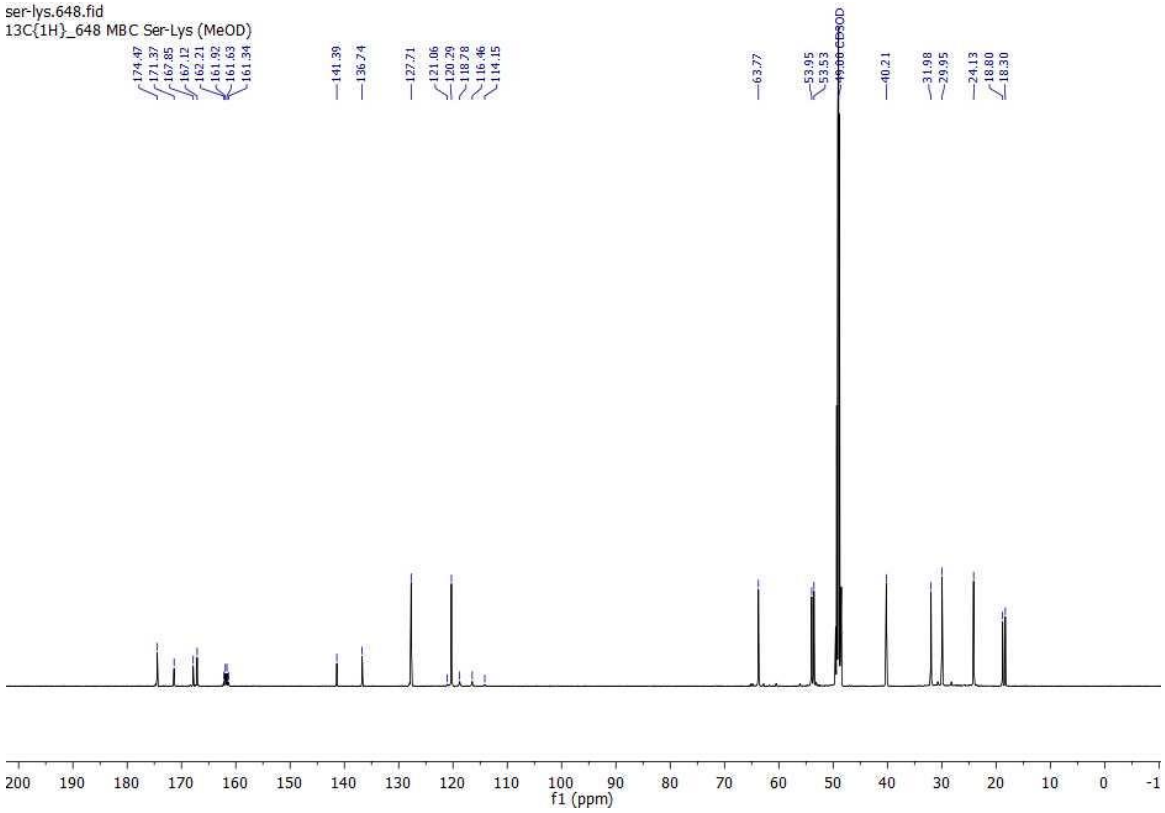

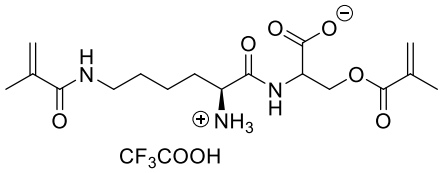

Compound **3-13**

^{1}H NMR spectrum (MeOD, 500 MHz)

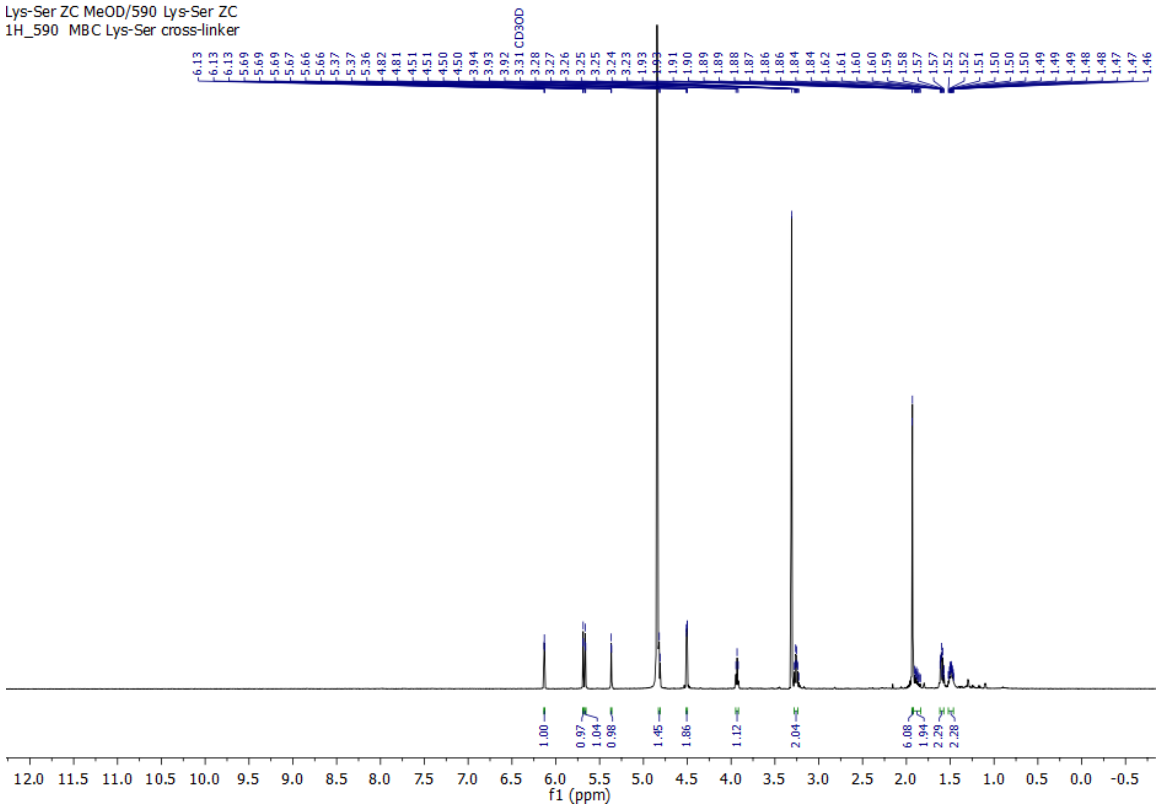

^{13}C NMR spectrum (MeOD, 126 MHz)

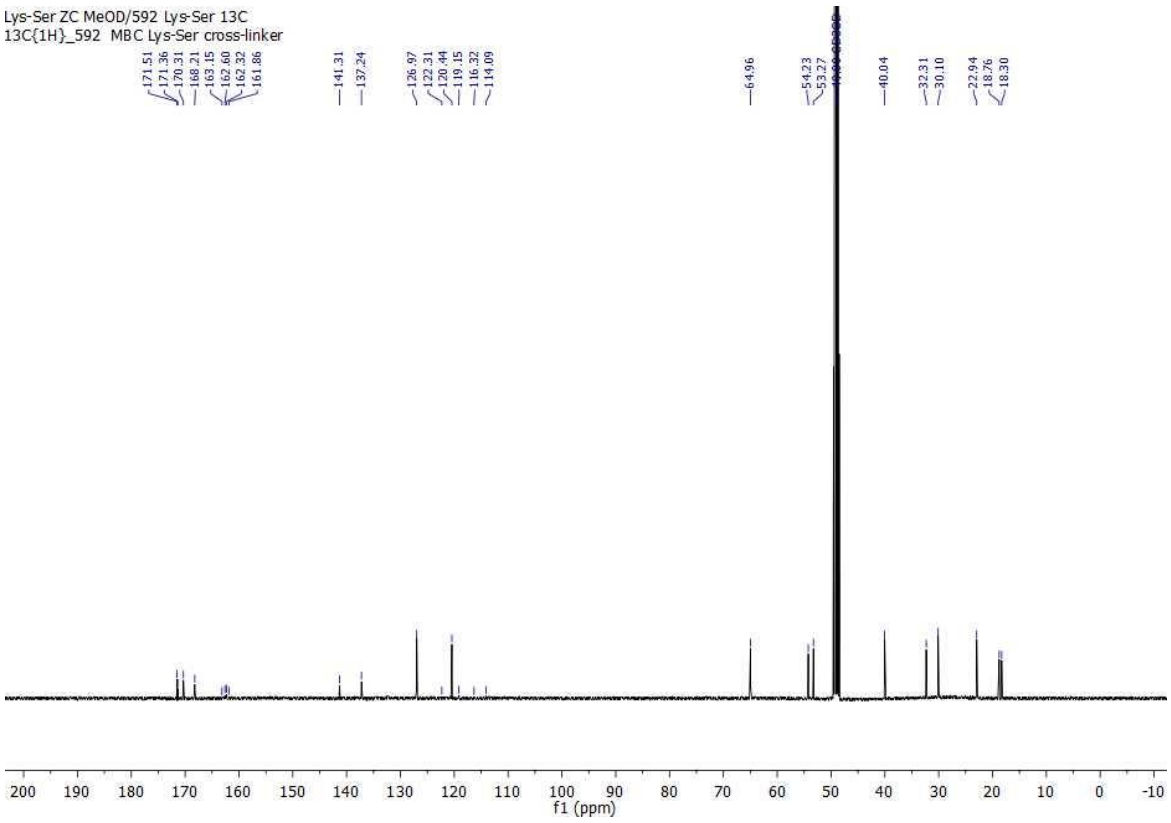

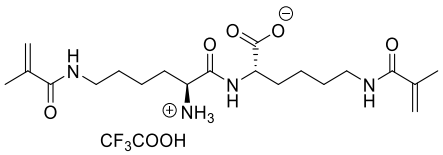

Compound **3-11**

^{1}H NMR spectrum (MeOD, 500 MHz)

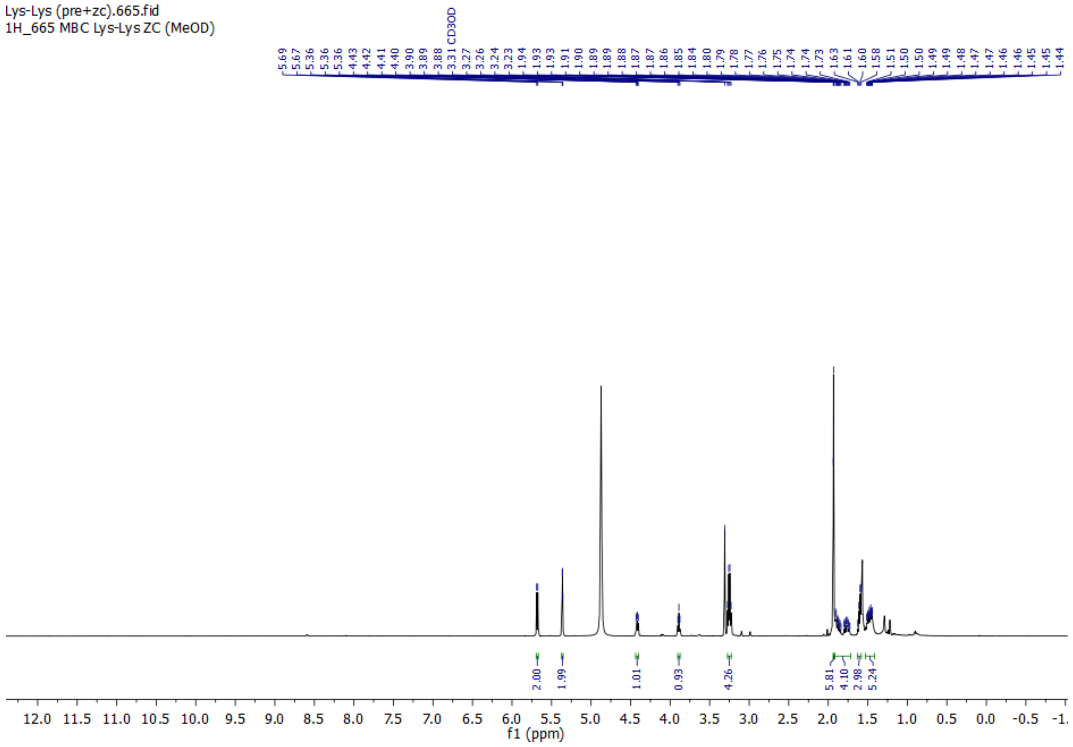

^{13}C NMR spectrum (MeOD, 126 MHz)

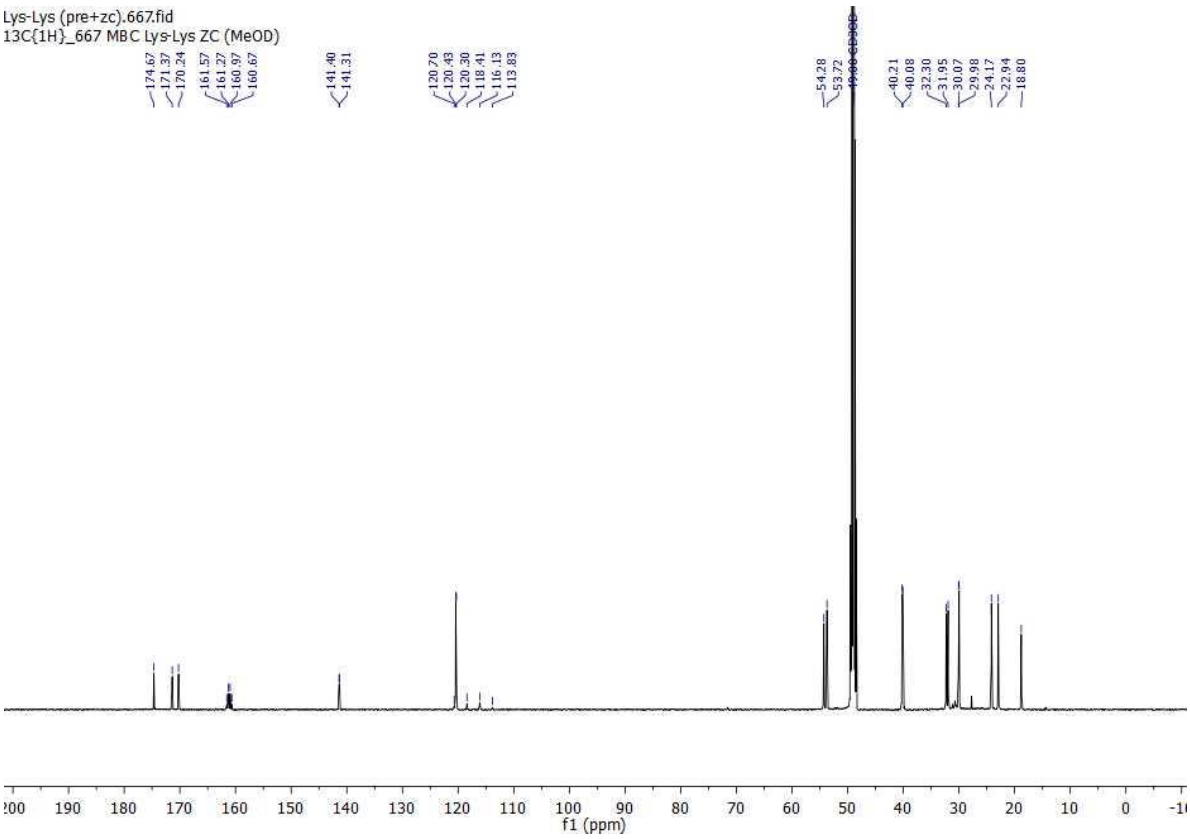

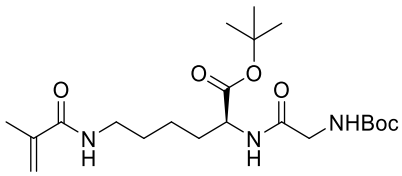

Compound **3-24**

^{1}H NMR spectrum ($CDCl_3$, 500 MHz)

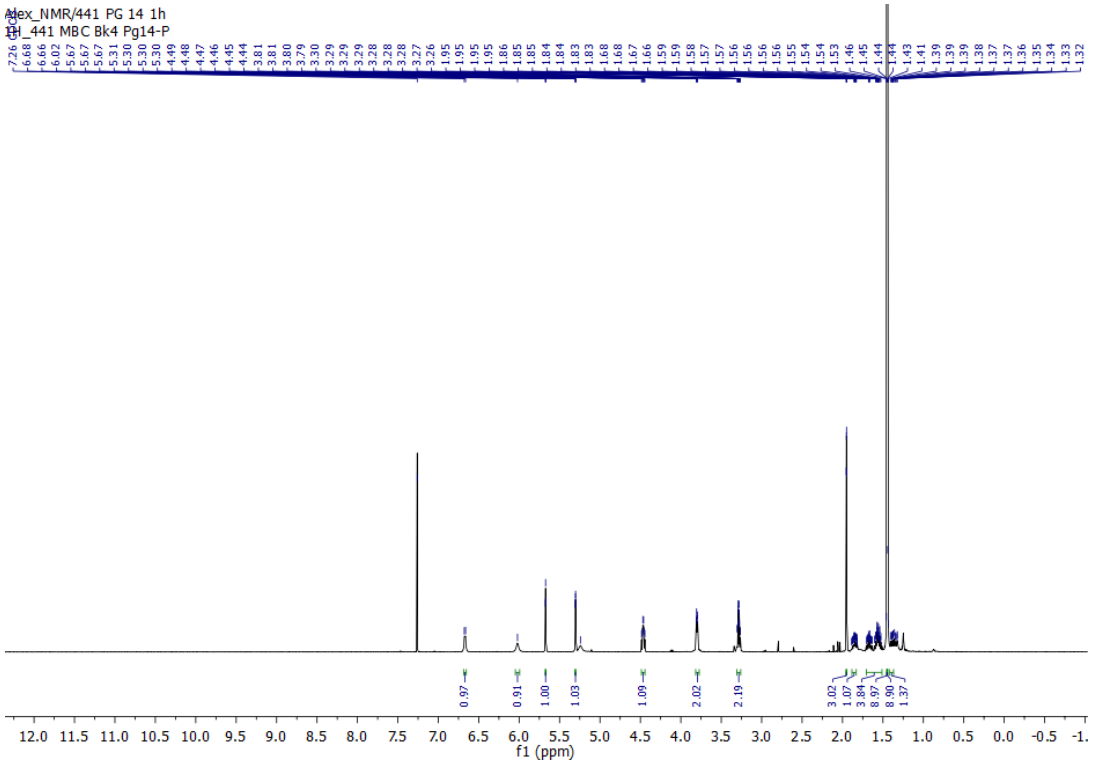

^{13}C NMR spectrum ($CDCl_3$, 126 MHz)

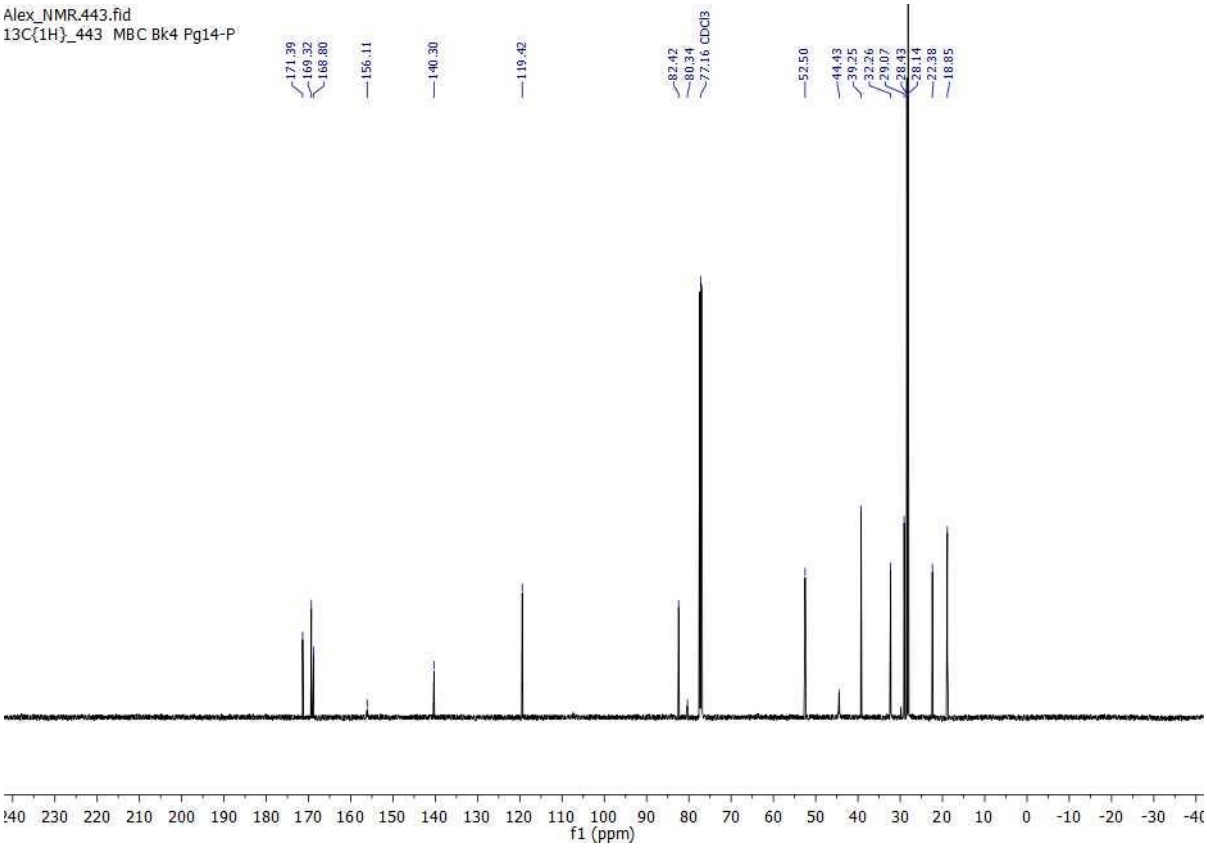

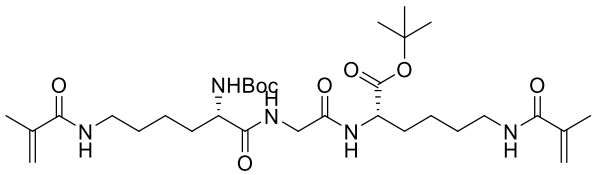

Compound **3-25**

^{1}H NMR spectrum ($CDCl_3$, 500 MHz)

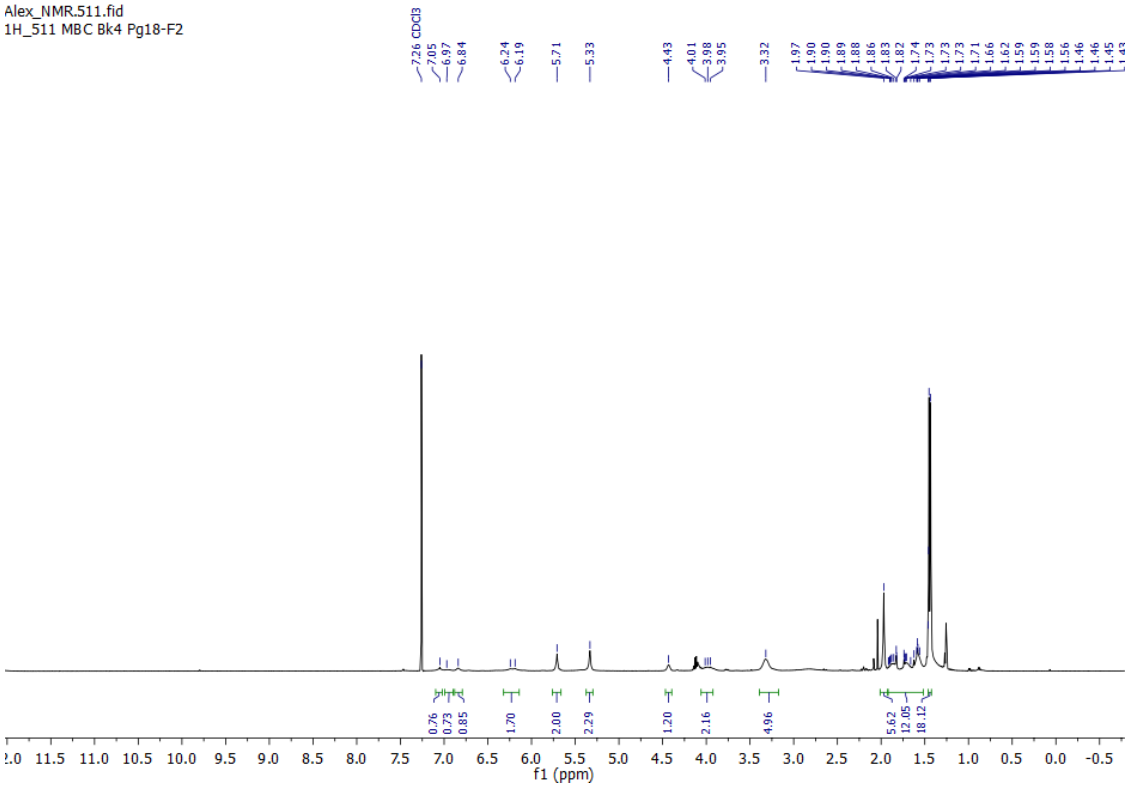

^{13}C NMR spectrum ($CDCl_3$, 126 MHz)

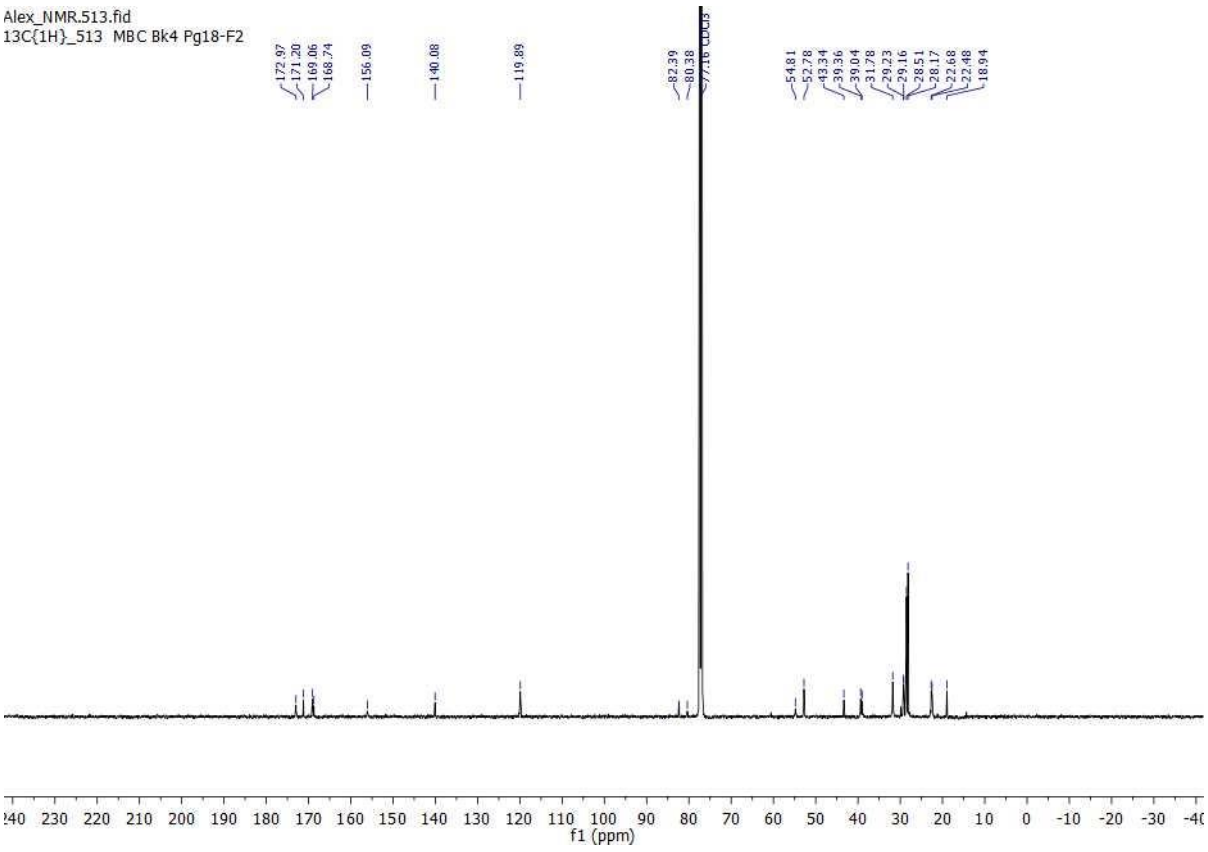

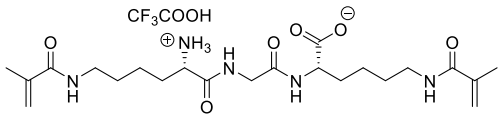

Compound **3-15**

^{1}H NMR spectrum (MeOD, 500 MHz)

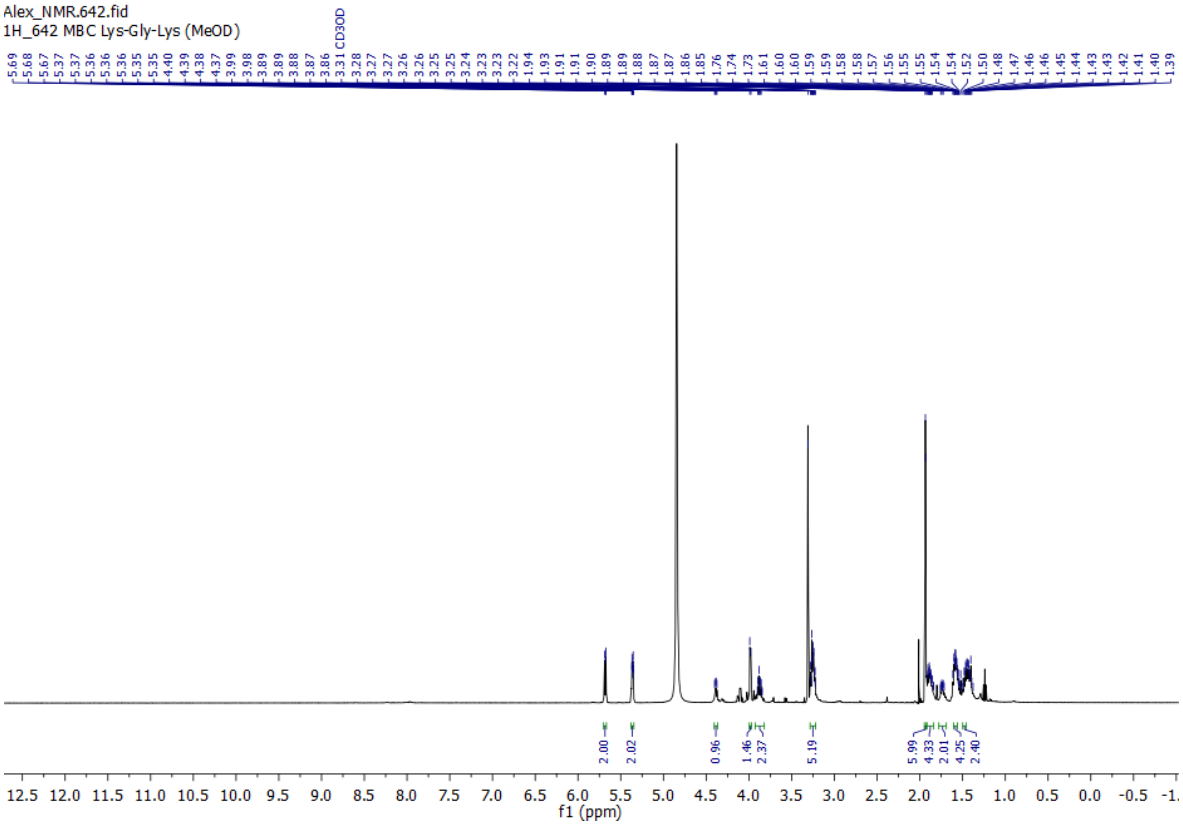

^{13}C NMR spectrum (MeOD, 126 MHz)

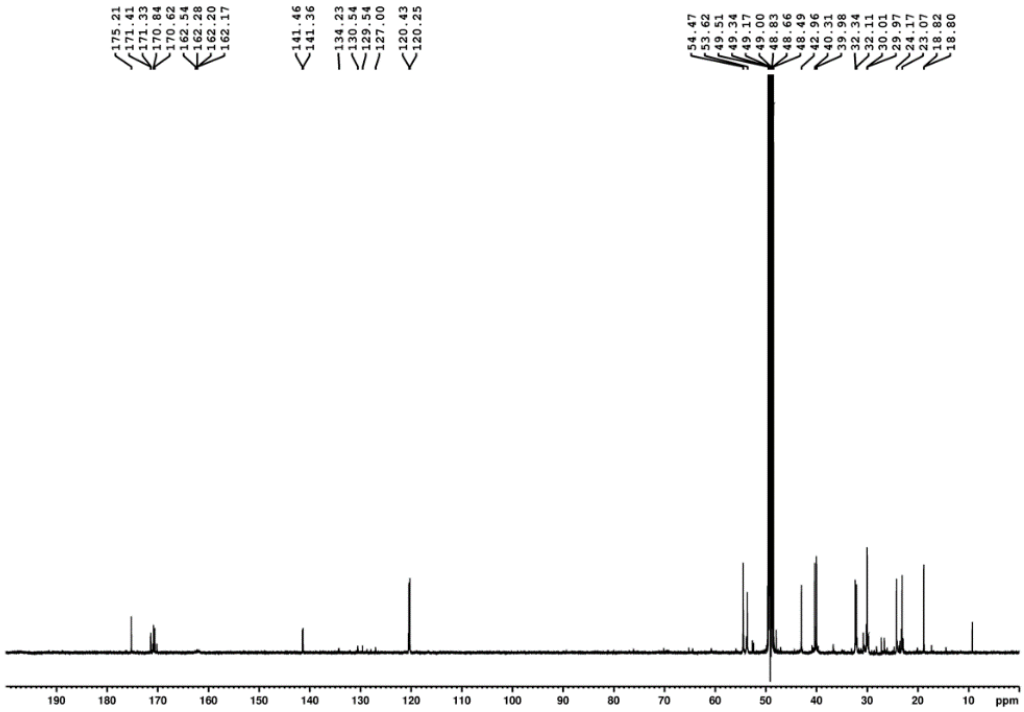

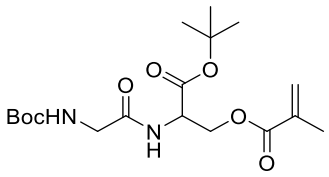

Compound **3-27**

^{1}H NMR spectrum ($CDCl_3$, 500 MHz)

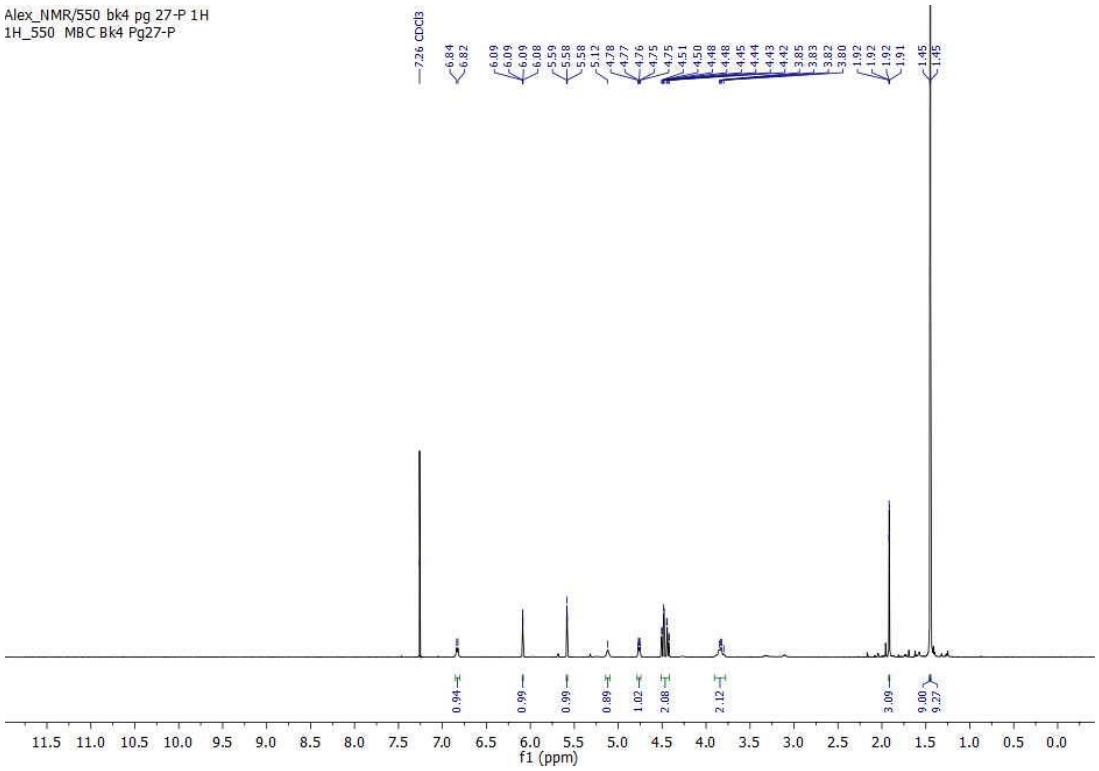

^{13}C NMR spectrum ($CDCl_3$, 126 MHz)

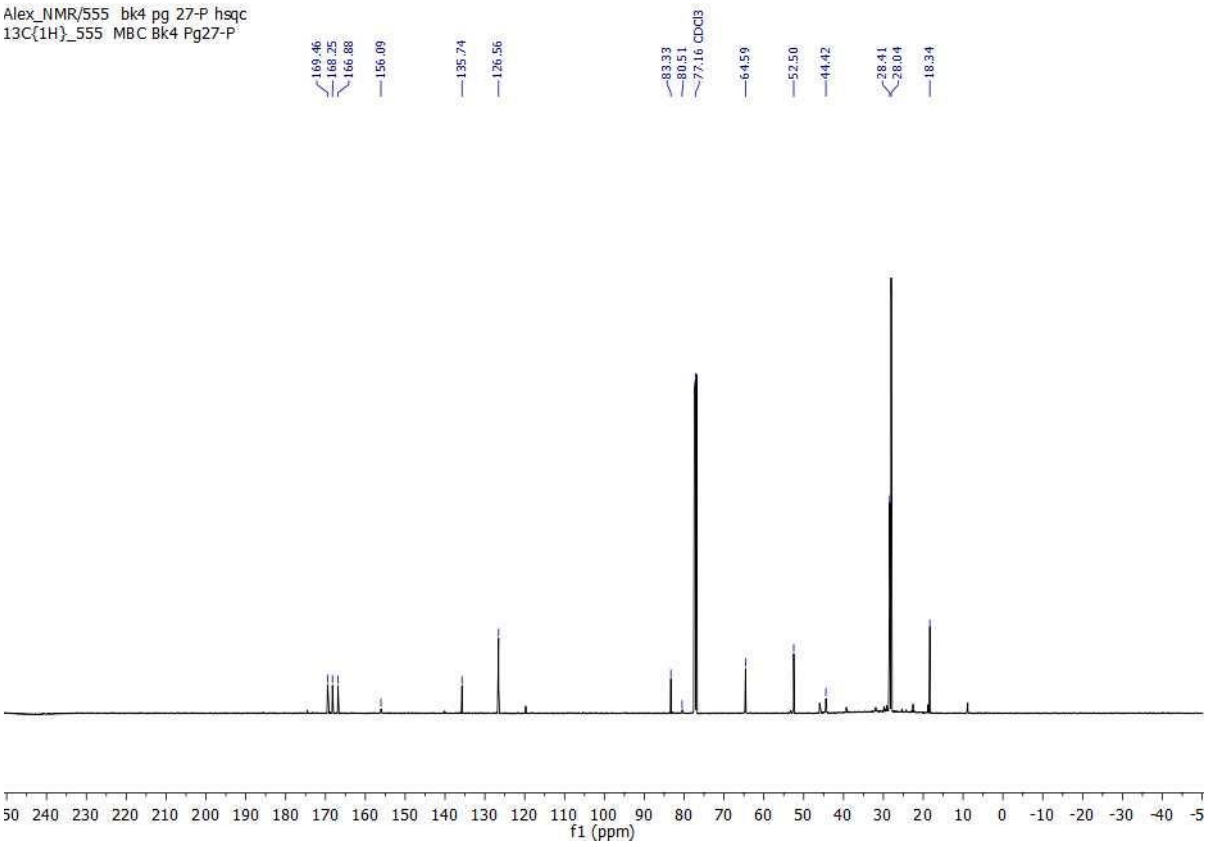

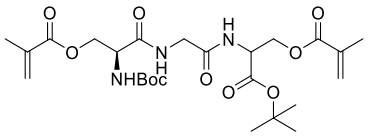

Compound **3-27a**

^{1}H NMR spectrum ($CDCl_3$, 500 MHz)

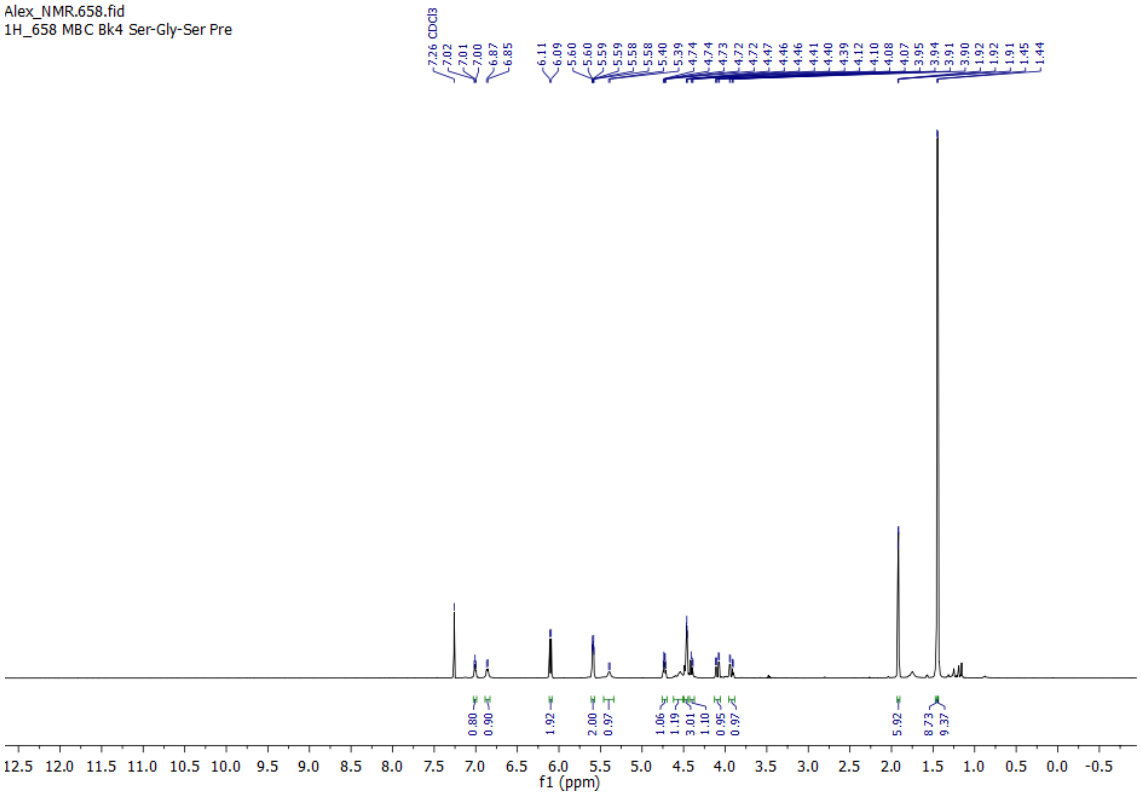

^{13}C NMR spectrum ($CDCl_3$, 126 MHz)

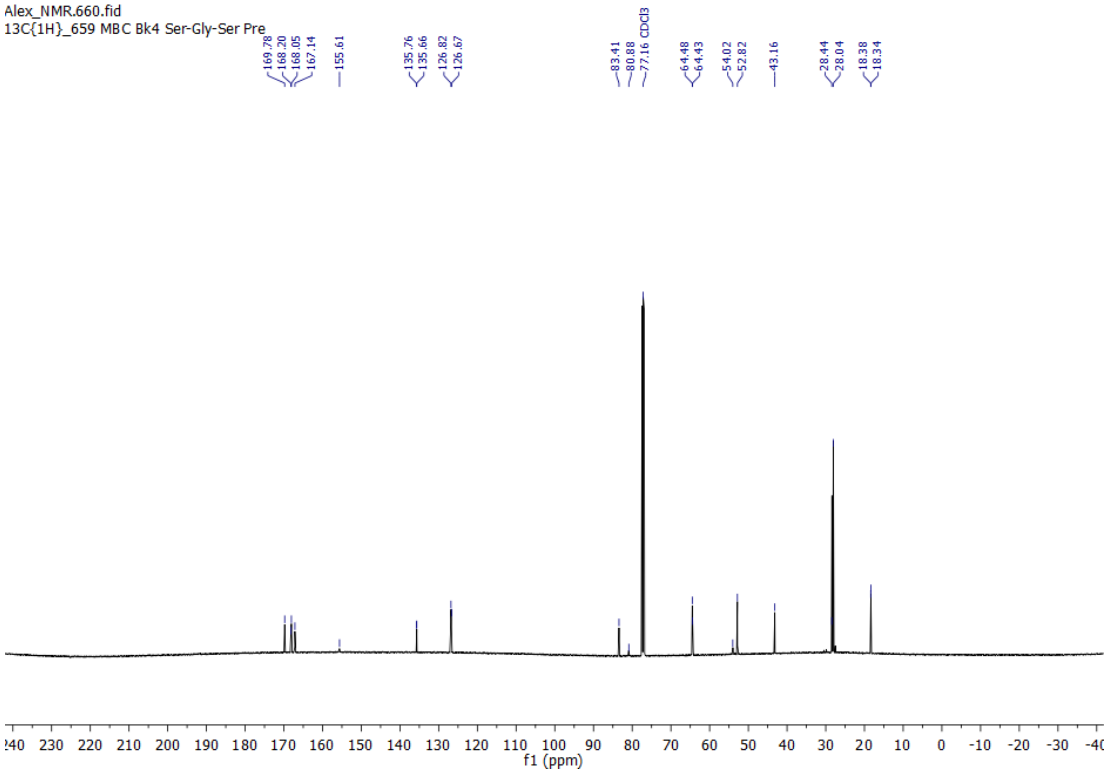

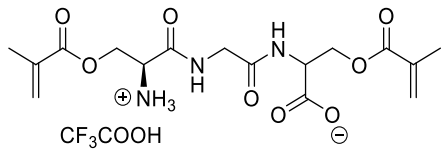

Compound **3-14**

^{1}H NMR spectrum (MeOD, 500 MHz)

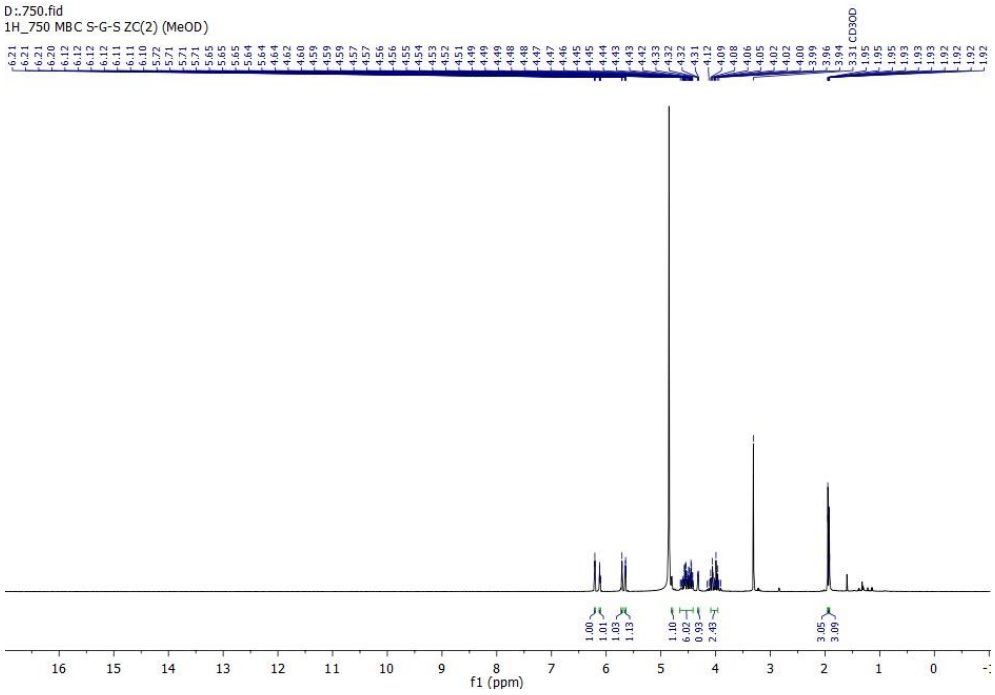

^{13}C NMR spectrum (MeOD, 126 MHz)

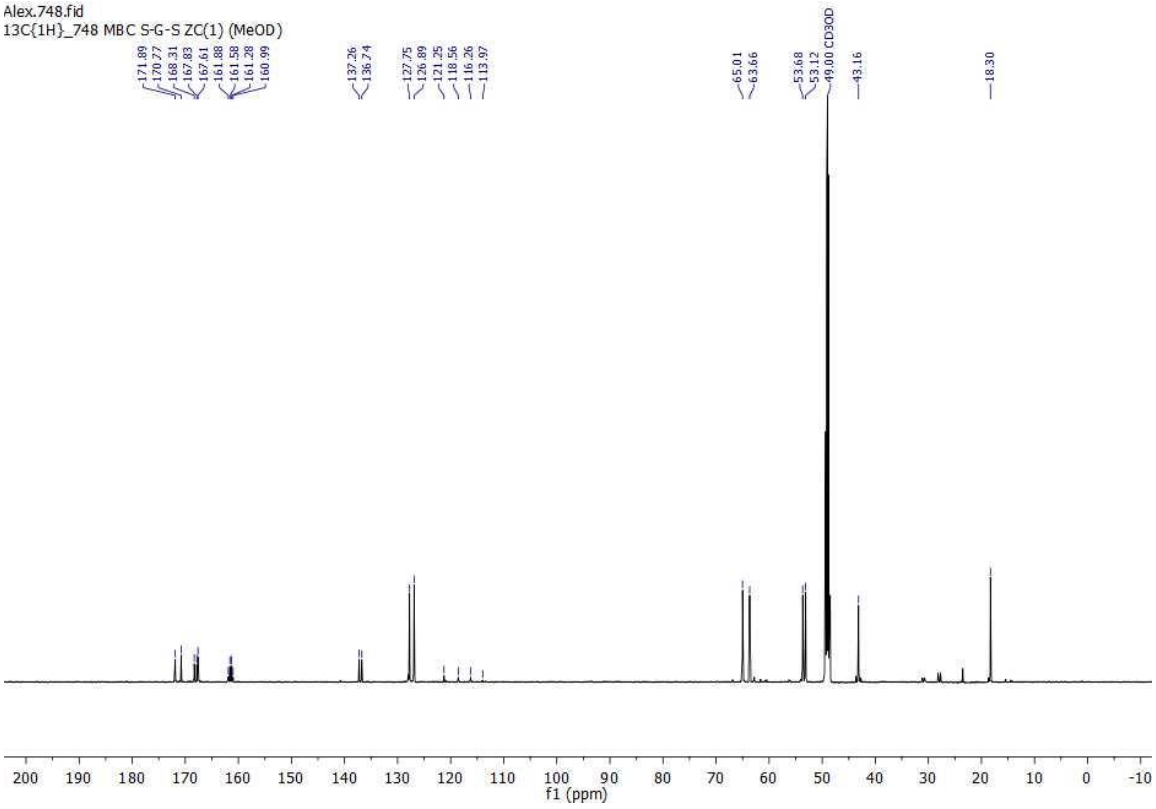

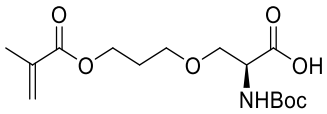

Compound **4-28**

^{1}H NMR spectrum ($CDCl_3$, 500 MHz)

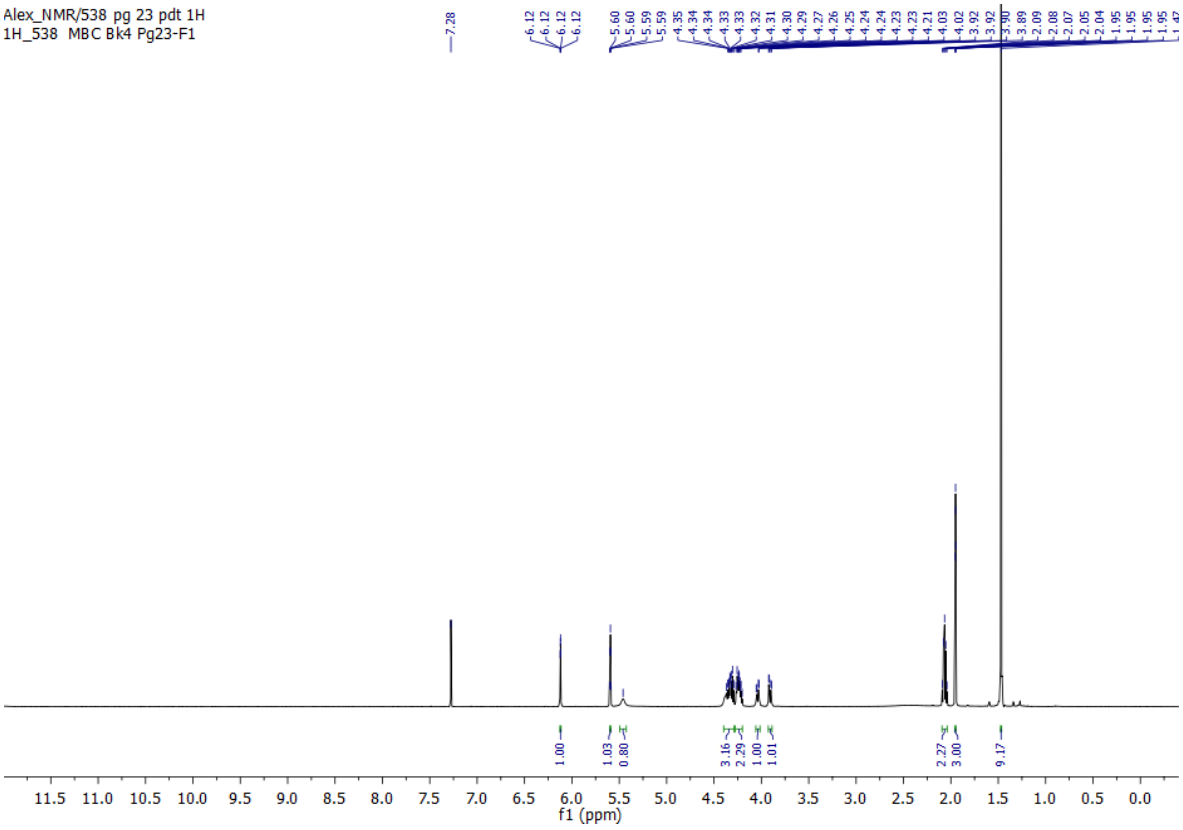

^{13}C NMR spectrum ($CDCl_3$, 126 MHz)

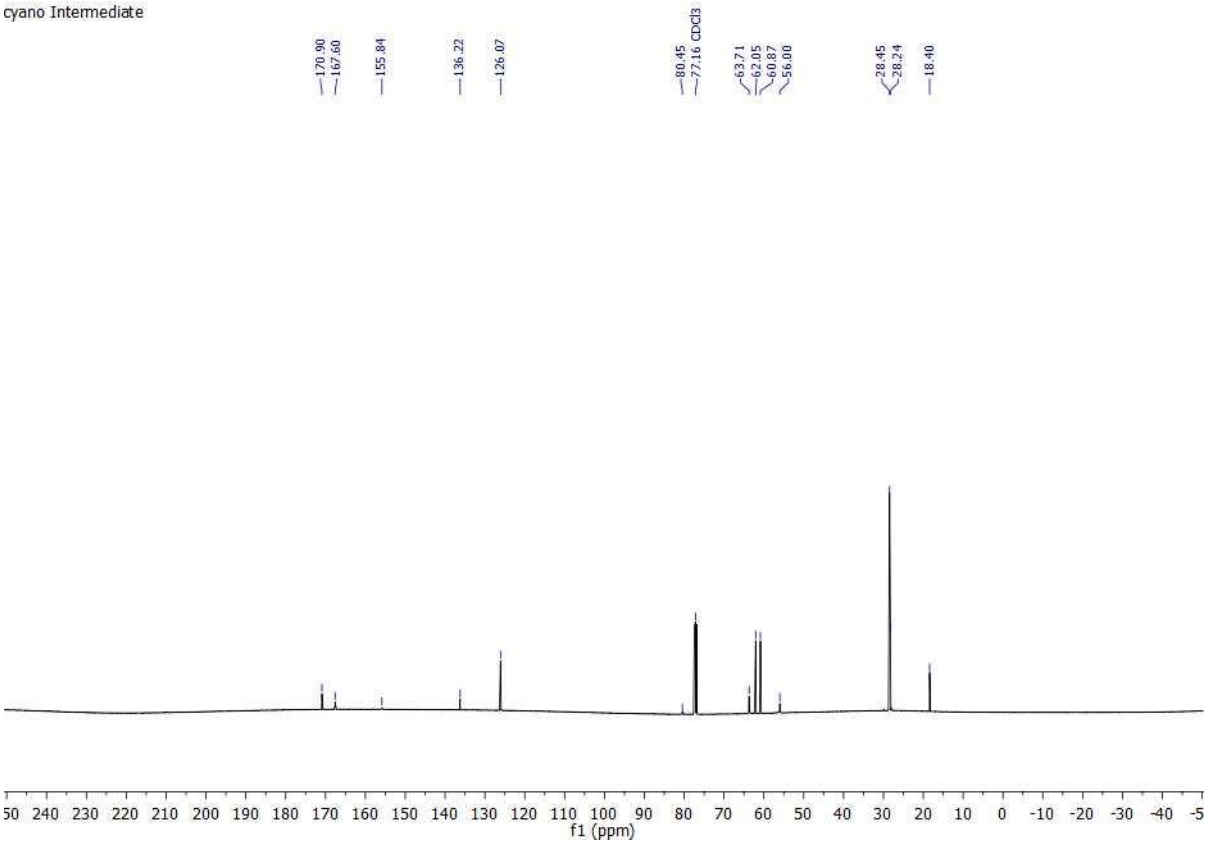

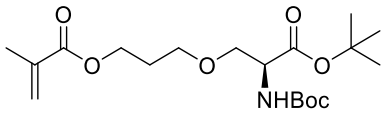

Compound **4-29**

^{1}H NMR spectrum ($CDCl_3$, 500 MHz)

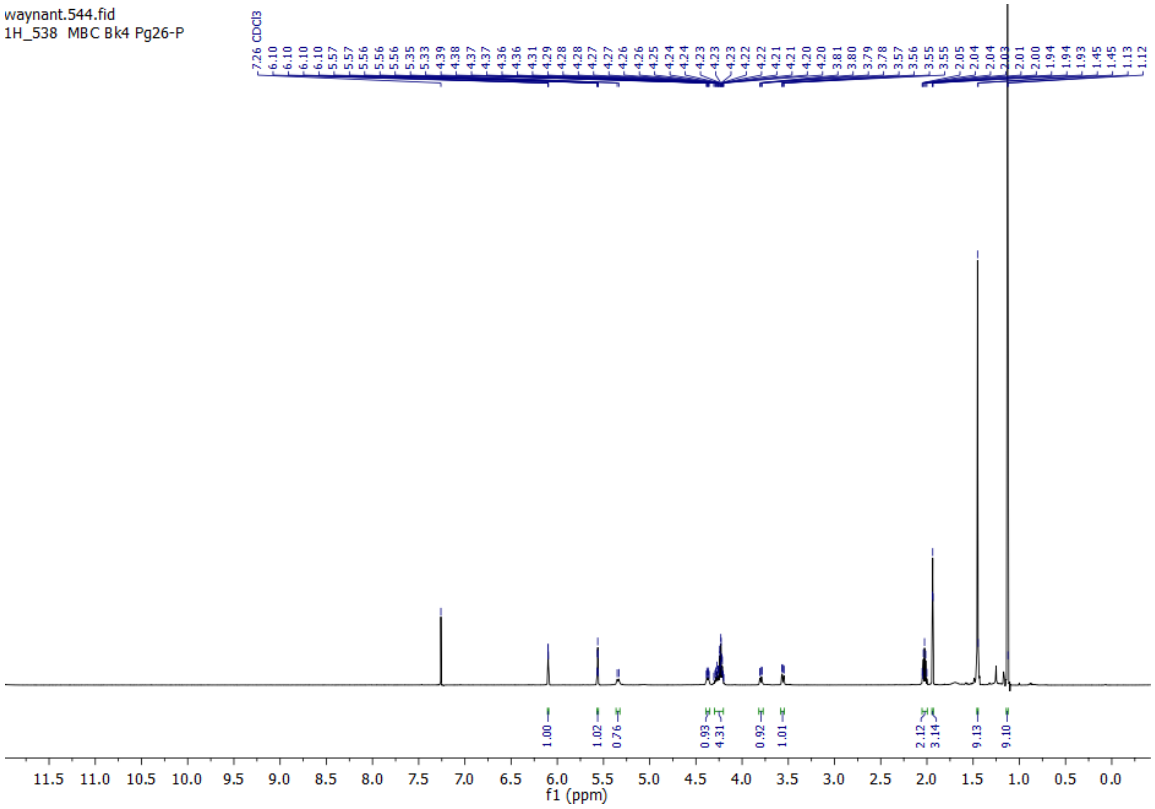

^{13}C NMR spectrum ($CDCl_3$, 126 MHz)

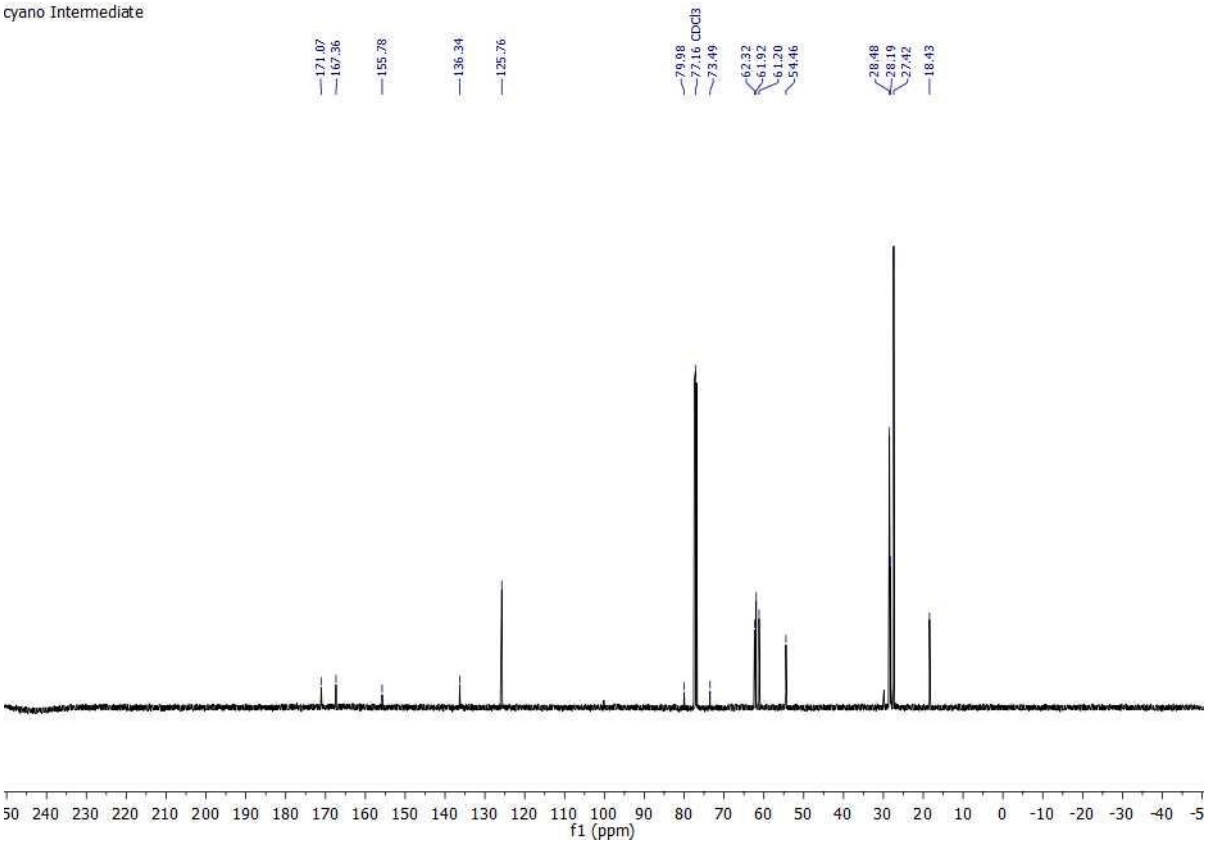

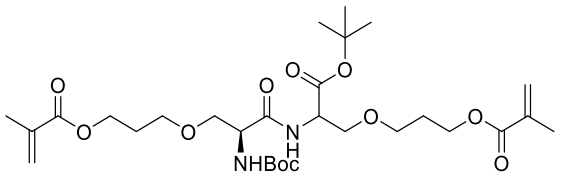

Compound **4-31**

^{1}H NMR spectrum ($CDCl_3$, 500 MHz)

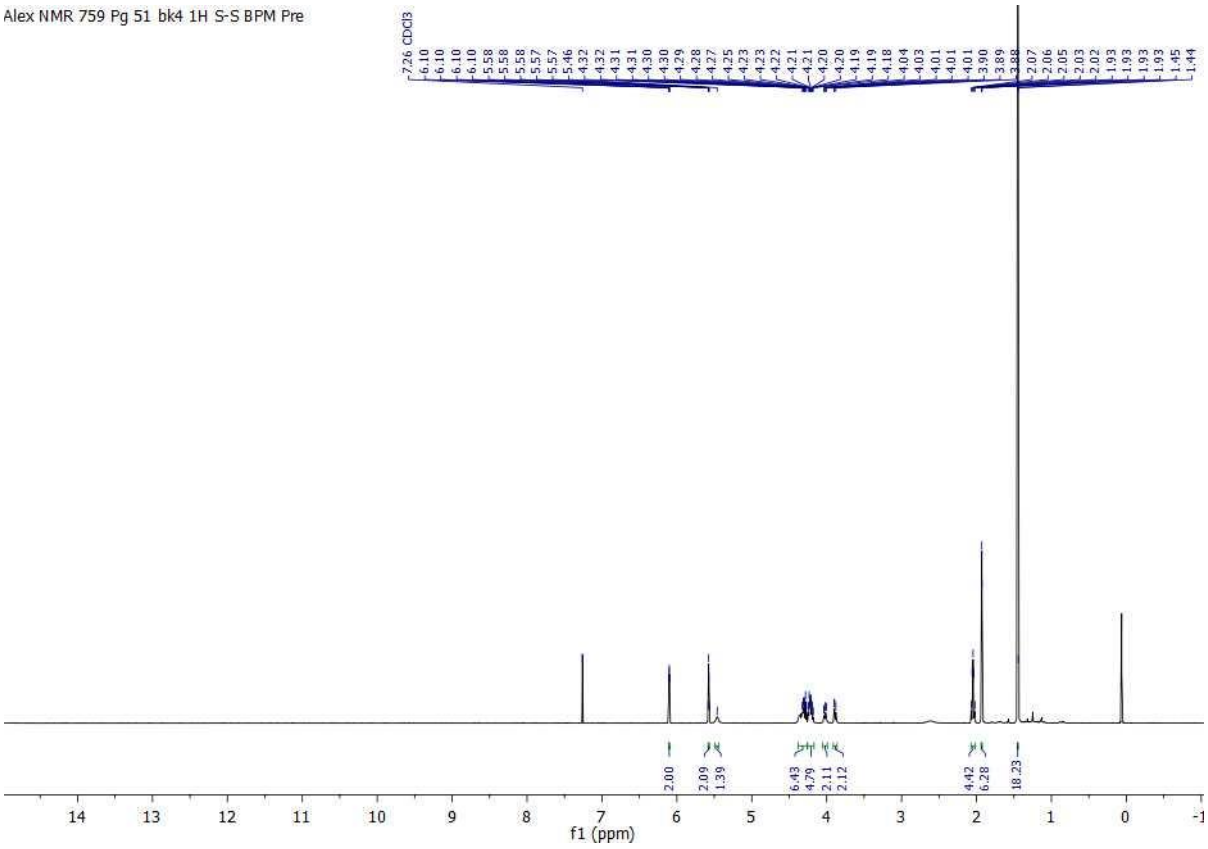

^{13}C NMR spectrum ($CDCl_3$, 126 MHz)

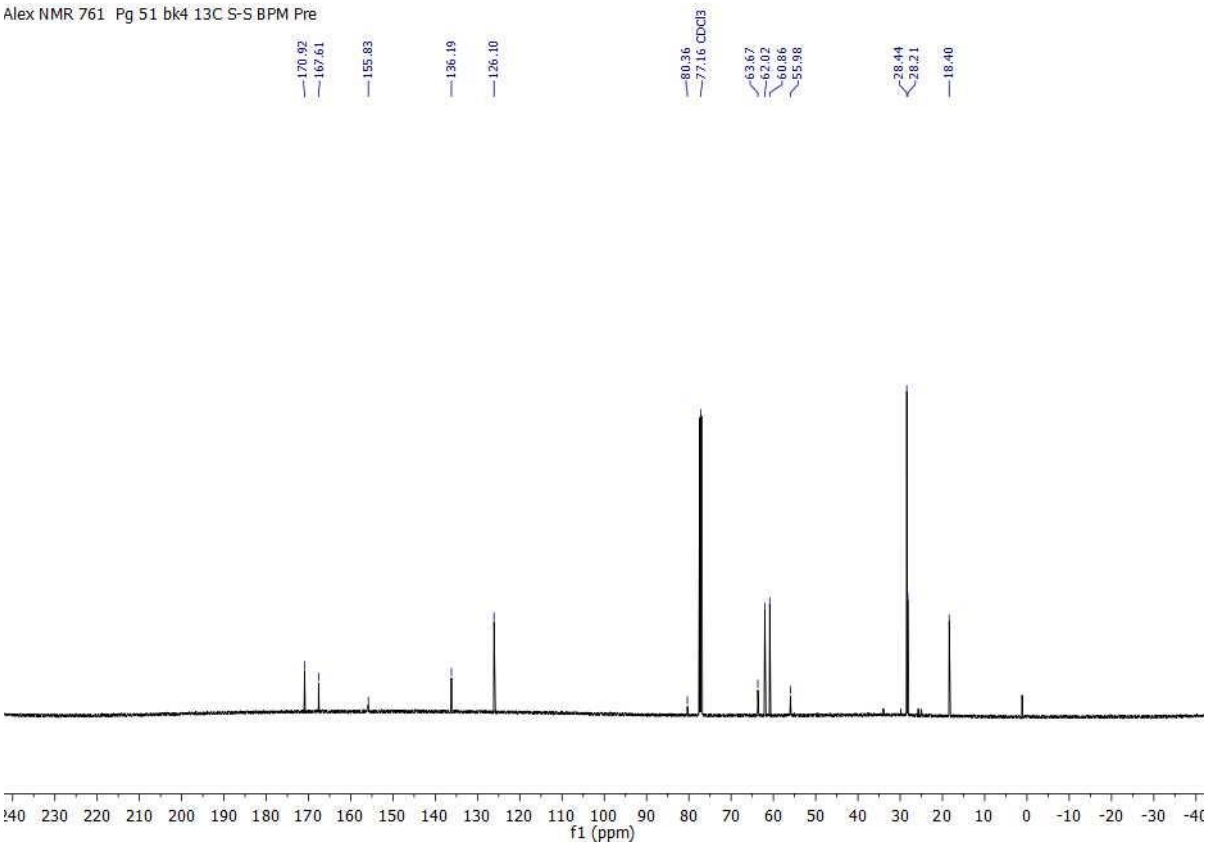

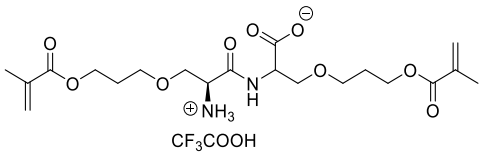

Compound **4-32**

^{1}H NMR spectrum (MeOD, 500 MHz)

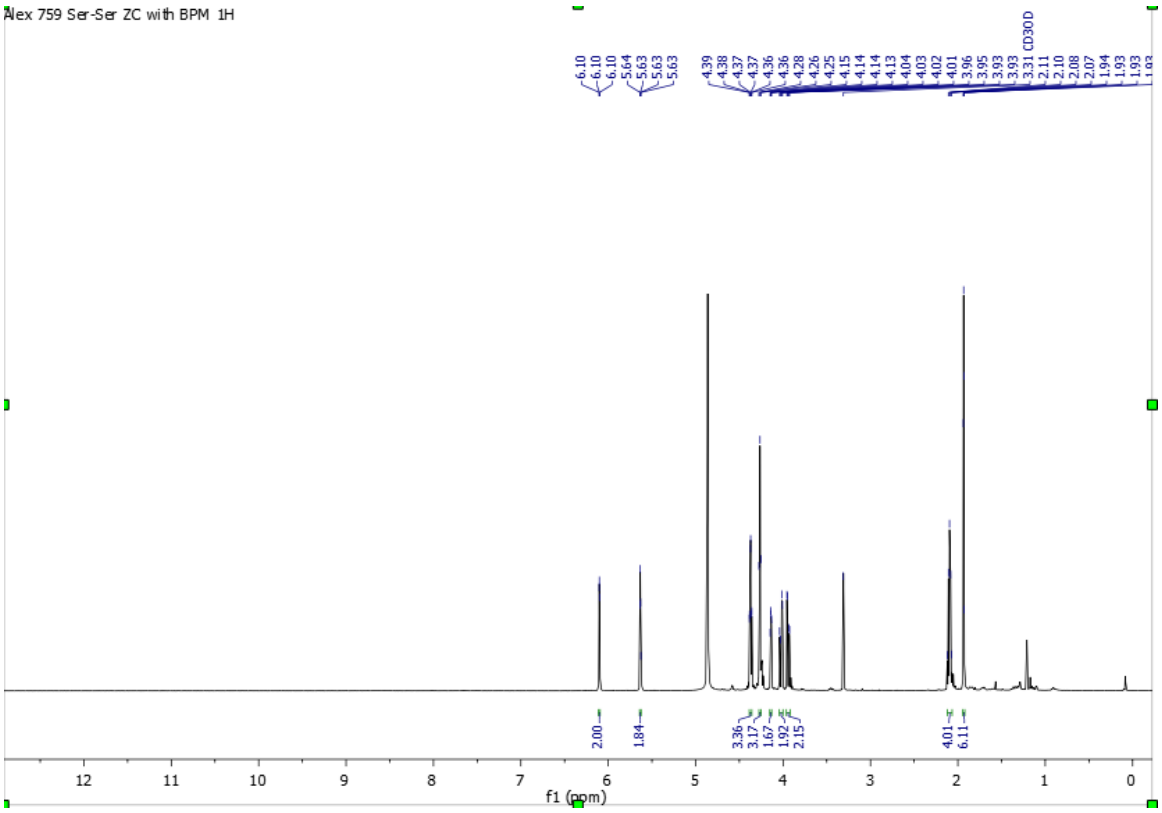

^{13}C NMR spectrum (MeOD, 126 MHz)

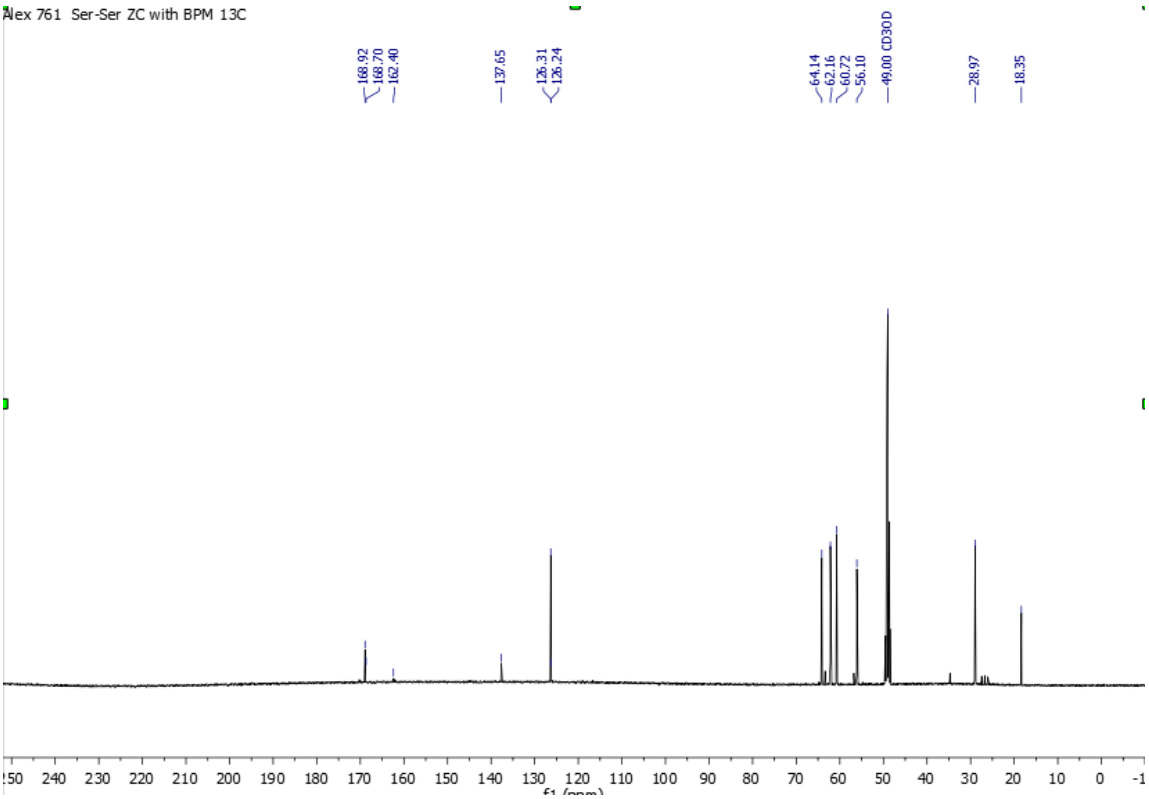

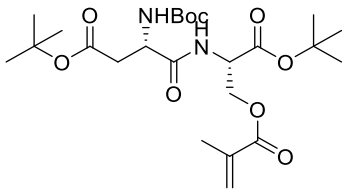

Compound **4-34**

^{1}H NMR spectrum ($CDCl_3$, 500 MHz)

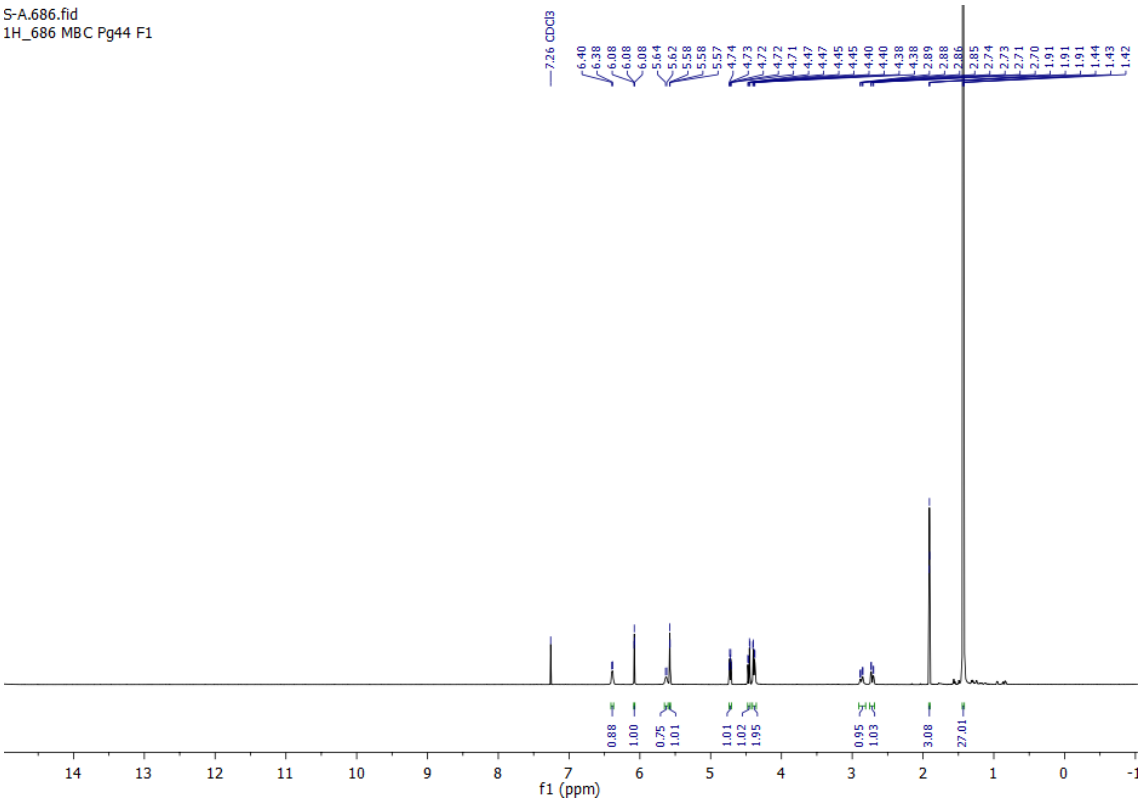

^{13}C NMR spectrum ($CDCl_3$, 126 MHz)

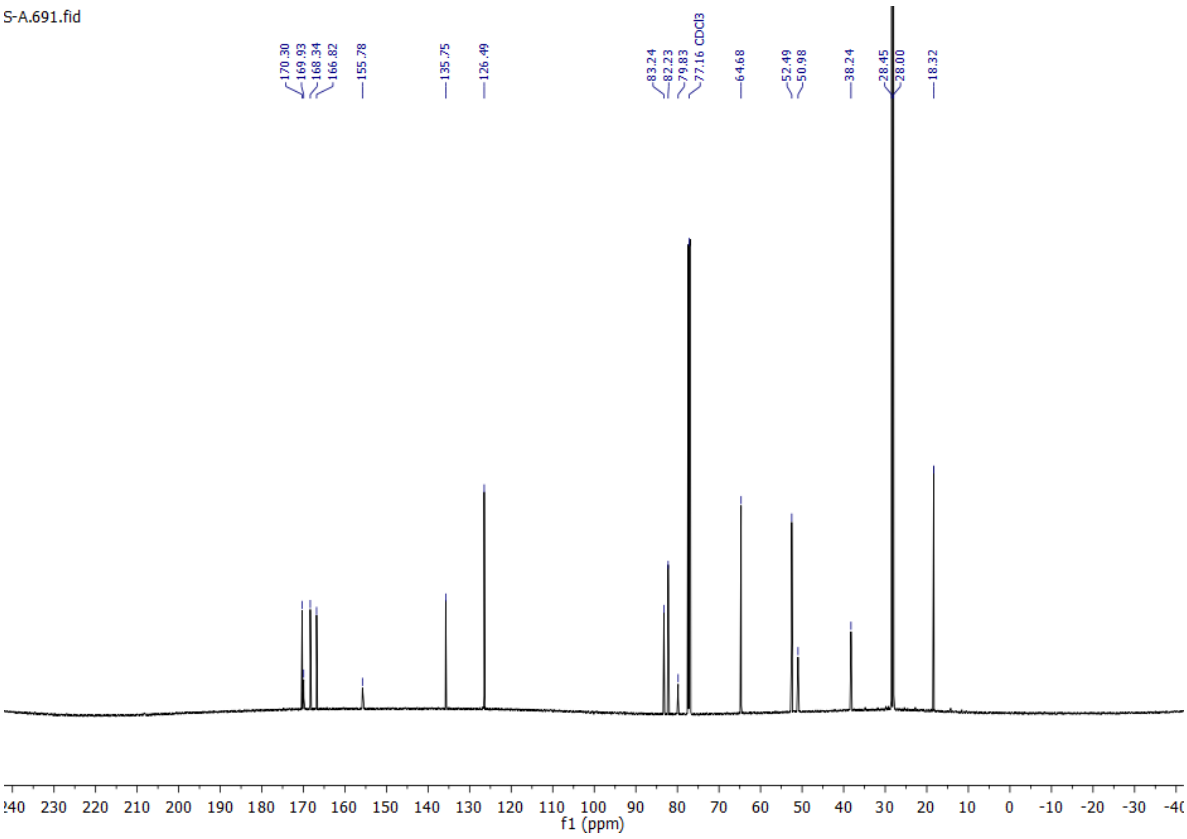

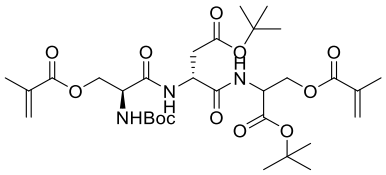

Compound **4-36**

^{1}H NMR spectrum ($CDCl_3$, 500 MHz)

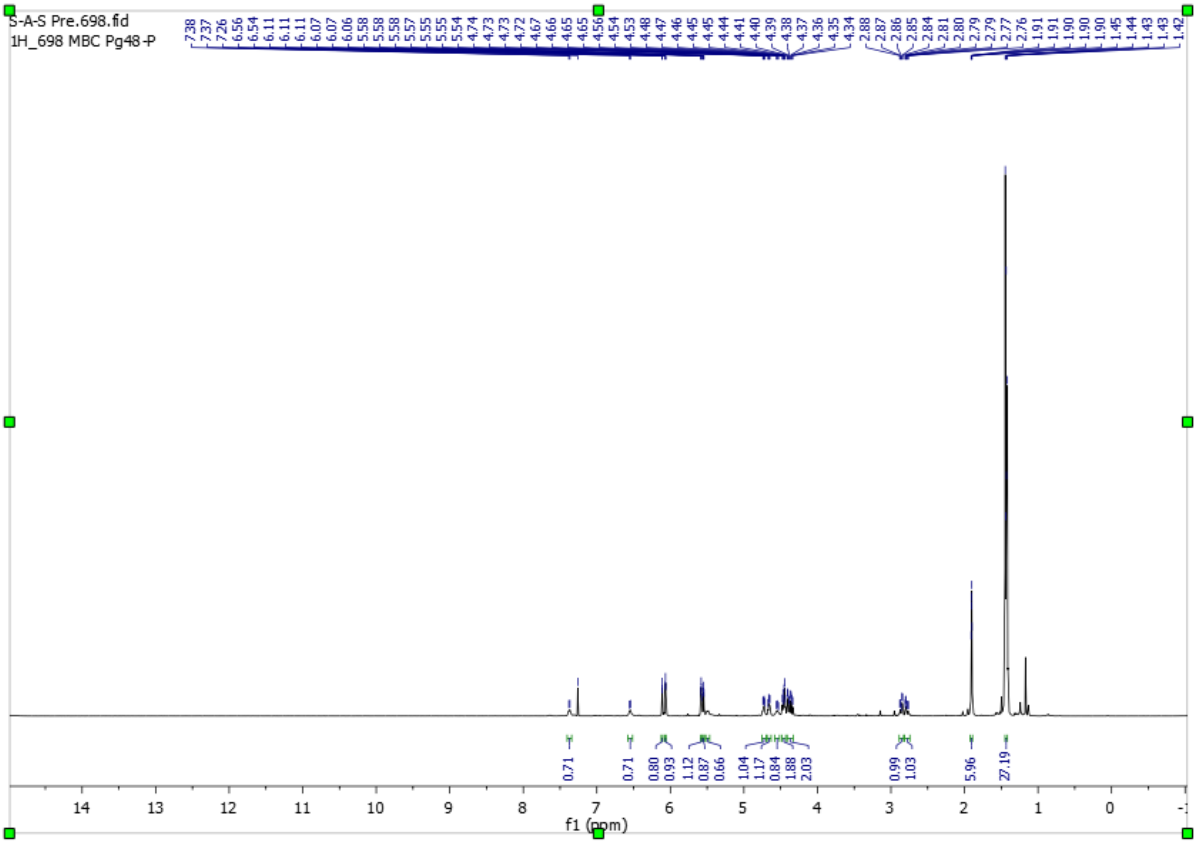

^{13}C NMR spectrum ($CDCl_3$, 126 MHz)

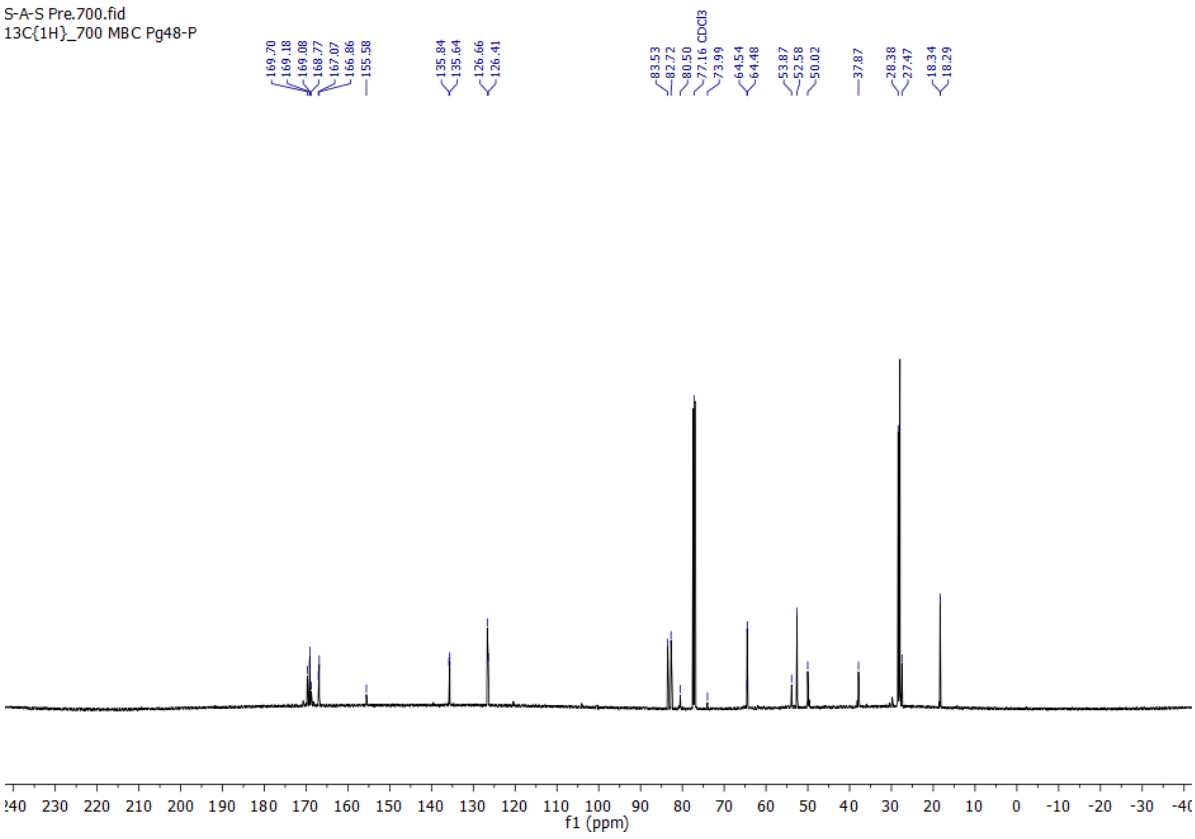

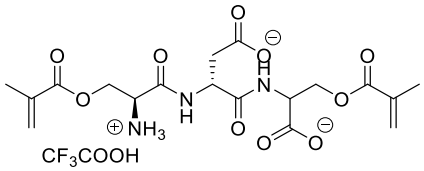

Compound **4-37**

^{1}H NMR spectrum (MeOD, 500 MHz)

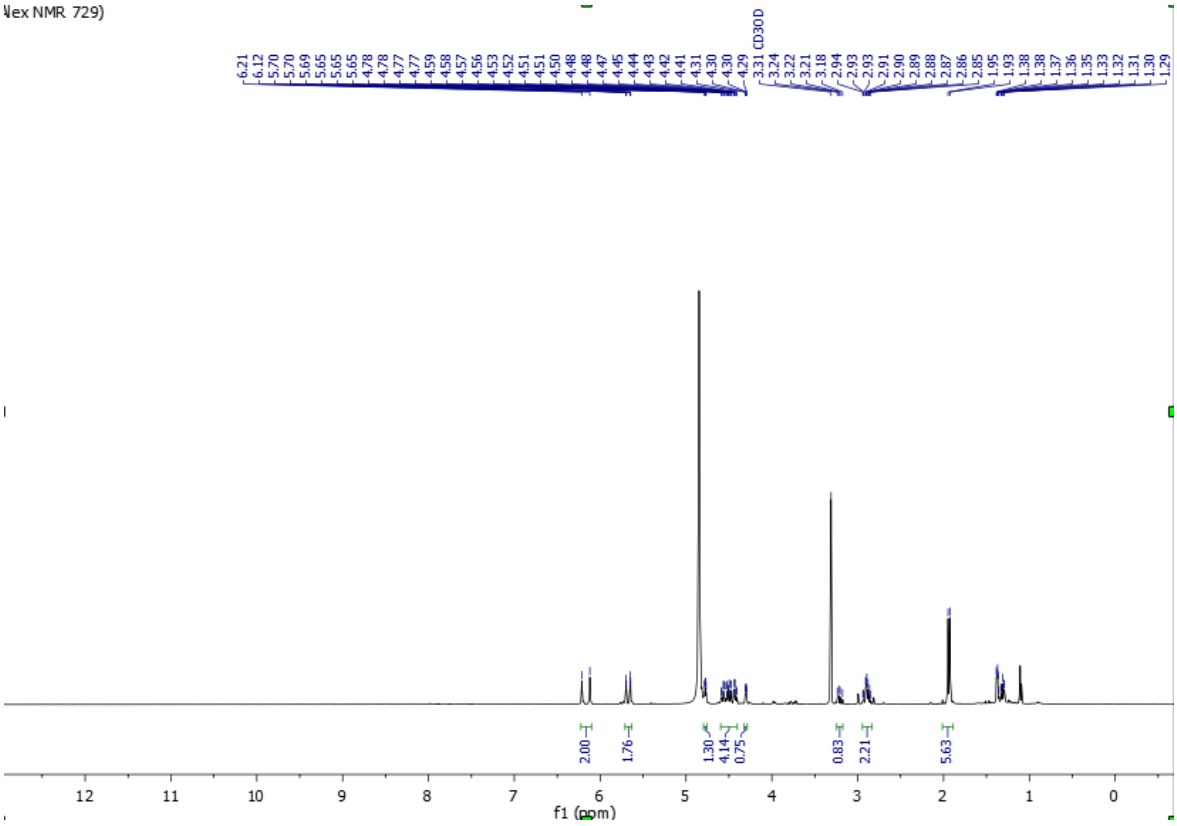

^{13}C NMR spectrum (MeOD, 126 MHz)